View Article Online
View Journal

Environmental Science Nano

Accepted Manuscript

This article can be cited before page numbers have been issued, to do this please use: I. Gregorovic, N. Lotfian, R. Khajavian, S. Maity, M. Mirzaei, S. S. Mal, M. Aureliano and A. Rompel, *Environ. Sci.: Nano*, 2026, DOI: 10.1039/D5EN00964B.

ROYAL SOCIETY OF CHEMISTRY

rsc.li/es-nano

View Article Online
DOI: 10.1039/D5EN00964B

This comprehensive review covers remediation, sensing, and energy storage, inspiring sustainable polyoxometalate innovations.

Polyoxometalates (POMs) are metal-oxide complexes with exceptional redox tunability, pseudocapacitive charge storage, and great structural versatility, making them ideal nanomaterials for environmental remediation. This review analyses the POM-based technologies for detection and treatment of air/water pollutants, surpassing conventional technologies that require harsh conditions for hard-to-remove contaminants such as refractory sulfur compounds.

Global pollution includes refractory sulfur compounds from fossil fuels, toxic gases in air, and heavy metals, dyes, and emerging contaminants in water, driving acid rain, smog, antibiotic resistance and ecosystem toxicity. POMs provide efficient oxidative desulfurization, photocatalytic dye/heavy metal removal, and multipollutant adsorption in POM-based hybrid materials. POM structures enable visible-light mineralization in low-input environments with less energy; benefits include scalable low-toxicity remediation, while metal leaching risks under extreme pH are mitigated by heterogenization.

View Article Online
DOI: 10.1039/D5EN00964B

ARTICLE

Polyoxometalates in Environmental Remediation and Energy Storage

Received 00th January 20xx,
Accepted 00th January 20xx

DOI: 10.1039/x0xx00000x

Ingrid Gregorovic[a,b], Nahid Lotfian[c], Ruhollah Khajavian[c], Sukanya Maity[d,e], Masoud Mirzaei[c]*, Sib Sankar Mal[e]*, Manuel Aureliano[f,g]* and Annette Rompel[a,b]*

Over recent decades, while environmental awareness and pollution control efforts have yielded localized improvements, ongoing industrial growth, rapid global population expansion, and escalating energy demands continue to drive significant global environmental pollution challenges. Polyoxometalates, a remarkable class of metal-oxide complexes, have recently emerged as promising compounds in the development of multifunctional materials for environmental pollutant removal, energy conversion and storage, and sensing. This review critically examines current research on their use for the removal of common toxic gases – such as H_2S, NO_x, and volatile organic compounds (VOCs) – from polluted air, as well as the elimination of various organic dyes, heavy metals, and pharmaceutical contaminants from wastewater. POMs have also gained recognition as adaptable redox-active materials suitable for next-generation energy storage systems. Their high electron-transfer capacity, structural flexibility, and remarkable chemical stability make them ideal candidates for various applications. POMs can facilitate multi-electron redox processes, allowing for their application in batteries, supercapacitors, and hybrid devices, which results in improved energy density and cycling performance. Recent developments in POM-based composites and electrode designs are further discussed for innovative, sustainable, and scalable energy storage solutions. Additionally, their tunable electrical and magnetic properties make them effective sensors for detecting various environmental pollutants.

1 Introduction

In recent times, rapid industrial and technological development has caused a significant increase in energy demand and environmental pollution (EP).[1,2-3] The Encyclopaedia Britannica defines environmental pollution as the addition of any substance (solid, liquid, or gas) or any form of energy (such as heat, sound, or radioactivity) to the environment at a rate faster than it can be removed from the environment or stored in a harmless form. It further categorizes environmental pollution based on the affected medium into air, water, and land pollution.[4] Increasing attention has been paid to the development of new methods for the removal of potential environmental pollutants[1-3] during industrial processes and clean energy production.[5] Although industrial development has brought many positive aspects to everyday life (e.g. new technology, better food safety and supply, medicines, etc.), it has also increased consumption and pollution of natural resources (water, soil and air)[3,6], which has become both an environmental problem and a health threat for the entire human population.[7]

The global shortage of clean water and the pollution of water resources pose critical health, economic[8], and environmental challenges.[9–11] Especially in many underdeveloped and currently developing parts of the world, sewage wastewater and wastewater from different factories are discharged directly into the environment, causing catastrophic water pollution (Section 2; **Figure 1**) with hard-to-remove toxic chemicals – inorganic pollutants (Section 2.2) such as heavy metals (Section 2.2.1) and organic pollutants[12] (Section 2.3) such as organic dyes[13] and solvents.[14]

The most prominent classes of health emerging pollutants (EPs)[15-17] (Section 3; **Figure 1**) are pharmaceuticals[18] (Section 3.1), pesticides and herbicides[19] (Section 3.2), cosmetics[20,21], industrial and household products[22], metals[13] (Section 2.2), dyes[13] and aromatic hydrocarbons (Section 2.3.2).[23] The presence of EPs in wastewater has been associated with the development of bacterial resistance[20,24], and mutagenicity and toxicity in aquatic organisms[21,25] and humans.[22,25]

Pesticides and herbicides (for their removal, see Section 3.2) are an inevitable part of the modern agricultural industry and food production.[26] However, in addition to ensuring yields and

[a] Universität Wien, Fakultät für Chemie, Institut für Biophysikalische Chemie, Josef-Holaubek-Platz 2, 1090 Wien, Austria. E-mail: annette.rompel@univie.ac.at
[b] Vienna Doctoral School in Chemistry (DoSChem), Universität Wien, Währinger Straße 42, 1090 Vienna (Austria)
[c] Department of Chemistry, Faculty of Science, Ferdowsi University of Mashhad, Mashhad 9177948974, Iran. E-mail: mirzaeesh@um.ac.ir
[d] Department of Physics, Chemistry and Biology (IFM), Linköping University, 58183 Linköping, Sweden
[e] Department of Chemistry, National Institute of Technology Karnatka, Surathkal, Mangalore-575025, India. E-mail: malss@nitk.edu.in
[f] Faculdade de Ciências e Tecnologia (FCT), Campus de Gambelas, Universidade do Algarve, 8005-139 Faro, Portugal
[g] Centro de Ciências do Mar do Algarve (CCMAR/CIMAR LA), Campus de Gambelas, Universidade do Algarve, 8005-139 Faro, Portugal. E-mail: maalves@ualg.pt

Supplementary Information available: [details of any supplementary information available should be included here]. See DOI: 10.1039/x0xx00000x

View Article Online
DOI: 10.1039/D5EN00964B

protecting crops from pests, the widespread use of these chemicals also affects soil enzymes and microorganisms[26] crucial for many essential biological processes, such as N_2-fixation in plants by rhizobacteria.[27] The excessive use of pesticides also impacts wildlife, with a scientific focus on bees, birds, fish and small mammals.[28-30] Human health is also affected by pesticide residues in the environment and food[31] causing various health problems, such as cancer,[32,33] endocrine disruption,[34] obesity,[35,36] reproductive health issues, and birth defects.[37] Therefore, many Western countries (e.g. EU, USA) have introduced stricter controls and limitations[38] on the use and allowable levels of pesticide residues in food, water and soil.[31]

Fossil fuels continue to be one of the primary energy sources in today's world.[39] Their combustion (Section 4.1) produces various toxic refractory sulfur-containing compounds (dibenzothiophenes, DBTs)[40,41] and gases (hydrogen sulfide[42] (Section 4.2.1), nitrogen oxides (Section 4.2.2), and sulfur oxides (Section 4.2.2)[43], which cause different severe environmental issues such as global warming,[40] smog[44] and acid rains.[45] Toxic gases generated from traffic and flue gases from the industry have made poor air quality an important factor in causing respiratory[46–48] and cardiovascular health[49] issues in urban areas.[50] Air purification (Section 4; **Figure 1**) using adsorption processes[51] (Section 4.2) and desulfurization of fossil fuels[52] (Section 4.1) is currently a logical approach to decreasing air pollution.

Global environmental pollution has escalated to crisis levels, driven significantly by fossil fuel combustion that releases refractory sulfur compounds such as dibenzothiophenes (DBTs), toxic gases including H_2S, NO_x, and SO_2, and emerging contaminants resistant to conventional treatment methods. These pollutants contribute directly to the formation of acid rain, smog, and severe health crises that impact billions worldwide.[52,53–59] Conventional technologies like hydrodesulfurization (HDS) are ineffective against sterically hindered DBTs and require extreme conditions (300-400 °C, 30-100 bar H_2), while amine scrubbing and selective catalytic reduction (SCR) systems[60] face limitations in capacity, cost-efficiency, and simultaneous multi-pollutant management for air purification.[53,61] Water faces persistent heavy metals, dyes, pharmaceuticals, and microplastics that evade standard filtration and oxidation.[15,16,17,20,22,24,25] POMs offer a powerful, direct solution to these multifaceted challenges via mild-condition oxidative desulfurization achieving over 99% removal of refractory sulfur, versatile multi-pollutant adsorption and catalysis, and photocatalytic mineralization.[62,63] Their uniquely tunable redox properties and acidity provide sustainable remediation options precisely where traditional technologies are insufficient.[53,62]

The first step in combating pollution is building a good system to monitor and detect various harmful compounds present in the environment. In this regard, various materials have been extensively researched and designed to develop new chemical[64], electrochemical[65], and biosensors[66] (Section 5; **Figure 1**) for environmental monitoring. For example, metal or metal oxide nanoparticles are widely used to develop various electrochemical sensors.[67–69]

New efficient technologies for energy conversion and storage need to be developed (Section 6; **Figure 1**) because renewable energy sources such as wind, hydroelectric, and solar power alone cannot meet the world's current energy demands.[70] In addition, the growing popularity and use of various portable electronic devices in everyday life have led to intensive research and development of new efficient battery technologies such as lithium-ion[71], sodium-ion[72], and redox-flow batteries.[73] Rechargeable Li-ion batteries and supercapacitors have been commercially utilized due to their ability to hold high energy with power density for various applications (e.g., electric vehicles, power tools, or portable/wearable electronic devices).[74–76]

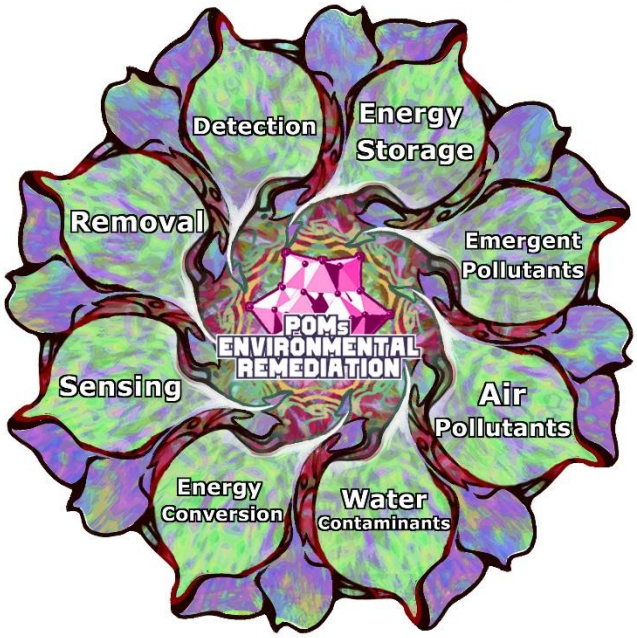

Figure 1. Schematic illustration of the main roles of polyoxometalates (POMs) in environmental remediation and energy storage. The central part emphasizes POM-based environmental remediation, while the surrounding segments shows key applications, including pollutants detection, removal, sensing, treatment of (health) emerging pollutants, air pollutants and water contaminants, energy storage, energy conversion, and signalling.

1.1 Polyoxometalates

Polyoxometalates (POMs)[77] are a class of transition metal-oxide clusters, usually containing Mo or W ions in their highest oxidation states. They exhibit exciting and unique physical and chemical properties, such as controllable shape and size[77], oxo-enriched surfaces, photoactivity[78], molecular conductivity[79], excellent chemical stability, and redox properties[80]. These properties have led to their increasing use in diverse fields, including catalysis[81,82], magnetism[83], medicine[84,85], biotechnology[86], protein crystallography[87-89], and material science[90].

POMs are typically synthesized via controlled acidification and condensation of simple metal oxoanions such as $Mo^{VI}O_4^{2-}$, $W^{VI}O_4^{2-}$, or $V^{V}O_4^{3-}$, which allows the precise formation of diverse structural archetypes, including some of the most common POM archetypes like Keggin (**Figure 1.F**), Wells-Dawson (**Figure 1.H**), and Anderson-Evans (**Figure**

View Article Online
DOI: 10.1039/D5EN00548B

1.I).[76,77,91,92,93] Their functionality in pollutant removal is often enhanced by immobilization or hybridization[94], where POMs are incorporated into different solid supports like metal-organic frameworks (MOFs)[95–105], porous silica[106,107], graphene oxide (GO_x)[108,109], or polymeric supports[94,110,111], improving POM stability and catalytic efficiency.[94,101,112] Ion exchange with organic or inorganic cations[113,114,115], surface modifications[94], or doping with lanthanide ions[116] further tailor their physicochemical properties. Such synthetic versatility enables customization of POM-based materials to optimize catalytic, adsorptive, and photocatalytic performance in environmental remediation.[94,101,117] The structural characteristics of polyoxometalates can be divided into two main general subgroups, isopolyoxometalates and heteropolyoxometalates.[76,77] The isopolyoxometalates, with the general formula $[M_xO_y]^{n-}$ (where M = Mo, W or V; **Figure 2.A–D**), contain only addenda metals and oxygen atoms in their structure, such as Lindqvist[118,119] ($[M_6O_{19}]^{2-}$; Figure 2.A), heptamolybdate[120,121] ($[Mo^{VI}_7O_{24}]^{6-}$; Figure 2.B), octamolybdate[122,123] ($[Mo^{VI}_8O_{26}]^{4-}$; **Figure 2.C**), decatungstate[124,125] ($[W^{VI}_{10}O_{32}]^{4-}$; **Figure 2.D**) and decavanadate[126,127] ($[V^{V}_{10}O_{28}]^{6-}$; **Figure 2.E**). Heteropolyoxo species have the general formula $[X_zM_xO_y]^{n-}$ (X = heteroion, M = Mo, W or V, z<x, y = number of oxygen atoms in the POM structure, n = overall anion charge), where different heteroions X are present alongside addenda ions M and oxygen atoms. This composition allows them to form a variety of structural types, including common ones such as Keggin[128,129] ($[XM_{12}O_{40}]^{n-}$; **Figure 2.F**), lacunary Keggin[130] ($[XM_{11}O_{39}]^{n-}$; **Figure 2.G**), Wells-Dawson[131,132] ($[X_2M_{18}O_{62}]^{n-}$; **Figure 2.H**), Anderson-Evans[133,134] ($[XM_6O_{24}]^{n-}$; **Figure 2.I**), Preyssler[135] ($[MP_5M_{30}O_{110}]^{(15-n)-}$; **Figure 2.J**), Strandberg[136,137] ($[X_2Mo^{VI}_5O_{23}]^{n-}$, (X = P^V, S^{VI}, As^V, Se^{VI}); **Figure 2.K**), Weakley[138,139] ($[M^{III}(M^{VI}_5O_{18})_2]^{n-}$; **Figure 2.L**) , among others. Moreover, if the POM solution is reduced, a unique class of giant molybdenum blue and molybdenum brown-type structures ({Mo_{154}} and {Mo_{132}}) are formed.[140] For more detailed information on POMs structures and general synthetic procedures, the reader is referred to the reviews in reference 91, 92, 93, 141, and 142.

Pure POMs exhibit different solution behaviors across the wide pH range; some, like Wells-Dawson-type structures, maintain their structural integrity, while others, such as Keggin-type POMs, undergo monolacunarization under acidic conditions relevant to environmental remediation.[143-145] Their high solubility in aqueous media presents significant challenges for their use in applications, including leaching during wastewater treatment and difficulties in catalyst recovery.[113] While pure POMs often dissolve in aqueous media[113], strategic heterogenization approaches[94], such as immobilization on mesoporous silica (SBA-15)[106,107,146], metal-organic frameworks (like UiO-66 and MIL-101)[95–101], and POM-supported ionic liquid phases (POM-SILPs)[147,112], address this issue. Such methods significantly reduce leaching to < 1 % after 10 cycles (Tables S1 and S2). These enable recyclability over 5–10 cycles with minimal activity loss (**Table S1**)[148–151]. Nevertheless, challenges remain including potential metal cation leaching from POM-composites under prolonged extreme pH exposure and the need for long-term stability studies under real environmental conditions. These heterogenized systems demonstrate > 95 % POM retention after multiple uses.[63]

Keggin-type POMs (**Figure 2.F–G**) are the most widely studied POM archetype, representing an average of 77.6 % of all published articles, particularly in applications targeting environmental pollutant removal (approximately 69 %). This predominance in environmental applications surpasses that of Wells-Dawson (**Figure 2.H**; ~9 %), Anderson-Evans (**Figure2.I**; ~9 %), Sandwich-type (**Figure 2.L**; ~5 %), isopolymolybdates (**Figure 2.A–E**; ~5 %), and other types of POMs (each ~5 %). In this review, Keggin-type POMs (**Figure 2.F–G**) are most frequently addressed in Section 3 (wastewater treatment, 75 %) and Section 4 (air pollutant removal, 85 %). Wells-Dawson type POMs (**Figure2.H**) rank second in environmental pollutant removal (average 16.9 %), with their primary use found in sensing (75 %, Section 5). Notably, Section 4.1. showcases the broadest diversity of structural archetypes for POM-mediated fossil fuel desulfurization.

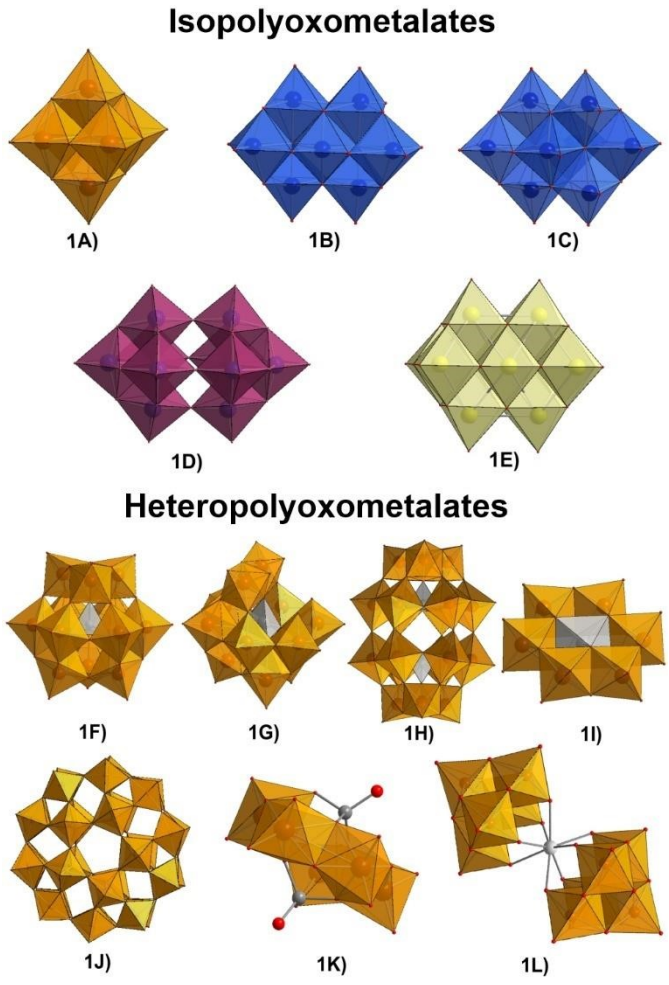

Figure 2. Structures of isopolyoxometalates and heteropolyoxometalates: 1A) Lindqvist ($[M^{VI}_6O_{19}]^{2-}$), 1B) heptamolybdate ($[Mo^{VI}_7O_{24}]^{6-}$), 1C) β-octamolybdate (β-$[Mo^{VI}_8O_{26}]^{4-}$), 1D) decatungstate ($[W^{VI}_{10}O_{32}]^{4-}$), 1E) decavanadate ($[V^{V}_{10}O_{28}]^{5-}$), 1F) Keggin ($[XM^{VI}_{12}O_{40}]^{n-}$), 1G) monolacunary Keggin ($[XM^{VI}_{11}O_{39}]^{n-}$), 1H) Wells-Dawson ($[X_2M^{VI}_{18}O_{62}]^{n-}$), 1I) Anderson-Evans ($[XM^{VI}_6O_{24}]^{n-}$), 1J) Preyssler ($[MP_5M^{VI}_{30}O_{110}]^{(15-n)-}$), 1K) Strandberg ($[X_2Mo^{VI}_5O_{23}]^{n-}$), and 1L) Weakley ($[M^{III}(M^{VI}_5O_{18})_2]^{n-}$). Color legend: orange = M (either Mo^{VI}, W^{VI} or V^V), blue = Mo^{VI}, purple = W^{VI}, yellow = V^V, gray = X (heteroion), white = M^{III}, and red = oxygen.

A literature search conducted on Web of Science in August 2025 (**Figure 3**) revealed that approximately 12 % (1928) of the

View Article Online
DOI: 10.1039/D5EN00964B

published articles on POMs related to the keyword "environment", out of a total of 15830 articles. As of August 14, 2025, the number of articles varies by specific subject: the combination of "polyoxometalate" and "degradation" yielded 1306 articles, while "polyoxometalates" and "dyes" yielded 910 articles. These numbers exceed those for "polyoxometalate" combined with "pollutants" (353), "waste" (258), "industrial chemicals" (134), and "wastewater" (215). Fewer articles were found for combinations with "antibiotics" (98), "pesticides" (48), "fossil fuels" (40), and "air pollution" (26). The number of publications related to "antibiotics" and "wastewater" has more than doubled over the past 2 years, reflecting a marked increase in research interest in these areas.

In fact, the importance of POMs in environmental science and their relationship to sustainable development and green chemistry is clearly increasing. POMs are crucial in environmental science for their roles as catalysts and adsorbents, aiding in the degradation of emerging pollutants such as dyes, plastics, and antibiotics, in addition to well-known organic and inorganic contaminants[152–160]. Moreover, POMs can act as novel antibacterial agents for water purification[161]. As described in the sections below, POMs are also fundamental for sustainable development by enabling energy applications such as solar hydrogen production and energy storage[70–76]. Recent studies further explore POMs as electrochemical sensors for the simultaneous detection of inorganic heavy metal ions and organic antibiotic contaminants in aquatic environments[162], and as triboelectric nanomaterials for gait monitoring[163].

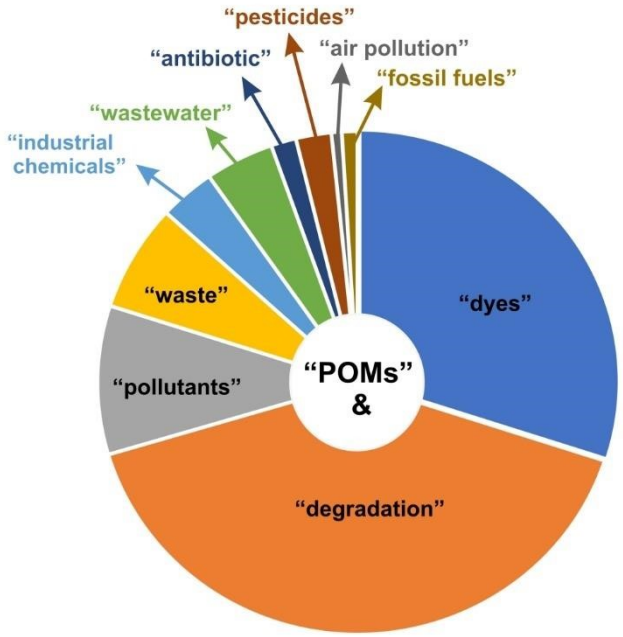

Figure 3. Number of articles containing the term "polyoxometalate" combined with keywords such as dyes, pollutants, industrial chemicals, wastewater, pesticides, and antibiotics, as of August 14, 2025.

2 Water decontamination by polyoxometalates

Inorganic contaminants (Section 2.2) enter the environment as inorganic salts, mineral acids, sulfates, cyanides, and metal ions, including heavy and radioactive metals. These contaminants are generally more persistent and more difficult to eliminate than organic ones.[164,165] On the other hand, organic contaminants (Section 2.3) represent a more diverse class, consisting of organic dyes, aromatic hydrocarbons, pesticides, and pharmaceuticals (see Section 3 for pharmaceutical and pesticide removal). Due to rapid industrial development, large amounts of industrial, sewage, and agricultural waste discharged into water bodies cause organic pollutants to become pseudo-persistent in the ecosystem.[166,167] Therefore, the removal of this class of contaminants requires careful consideration to move toward a sustainable ecosystem.

As discussed in Section 2.1, oxidation, catalysis, photocatalysis, ion-exchange, adsorption, and membranes are among the commonly used technologies for the removal of these pollutants due to their high efficiency, cleanliness, and simple operation. POMs have shown promise in mitigating the global water purification issue using the above-mentioned technologies. This section covers novel solutions by highlighting recent achievements in designing multi-component materials for use in water-purification systems.

2.1 Emerging pollution treatment technologies

Water treatment is a multi-stage process, comprising several stages with various technologies. Tertiary treatment is the final stage of the multi-stage wastewater treatment process. It is used after preliminary stages, and commonly used techniques utilized for the treatment include oxidation, photocatalysis, ion exchange, adsorption, and membranes technology (**Figure 4**).[168] Chemical oxidation is a cost-effective and simple technology for the decontamination of both organic and inorganic pollutants using an oxidizing agent such as chlorine, hydrogen peroxide, ozone, and molecular oxygen. In advanced oxidation processes (AOPs), POMs (especially iron-containing POMs) have been used as efficient catalysts for the decomposition of the oxidizing agent (H_2O_2) and removal of organic pollutants.[169] In particular, POMs can initiate the activation through electron transfer to H_2O_2 (originating from the redox property of the addenda atoms) or *via* formation of peroxo complexes.[147,170] This method, however, may produce secondary pollutants that are formed after the initial oxidation. This may cause a decrease in the catalyst selectivity, while increasing the costs.

In photocatalysis, the ability of the catalyst to harvest photons from a light source and to generate free radicals to undergo photocatalytic oxidation or reduction reactions is crucial. In this regard, POMs have shown promise since i) their band gap value can be adjusted by changing the heteroatoms or adjusting the valence states of addenda atoms, and ii) they can store multiple electrons in one molecule; thus they exhibit fast charge transfer properties.[171,172] Due to some drawbacks associated with pure POMs (*e.g.*, limited light absorption, high solubility), they are often employed in the form of hybrids or composites.[112] In these structures, the intermolecular interactions between two species can improve the stability and promote the lifetime of photogenerated charge carriers. In this regard, the incorporation of noble

View Article Online
DOI: 10.1039/D5EN00964B

metals,[173,174] metals from the lanthanide series,[175] metal oxides,[176] metal-organic frameworks[177] and metal-free species[110] have been reported to be effective.

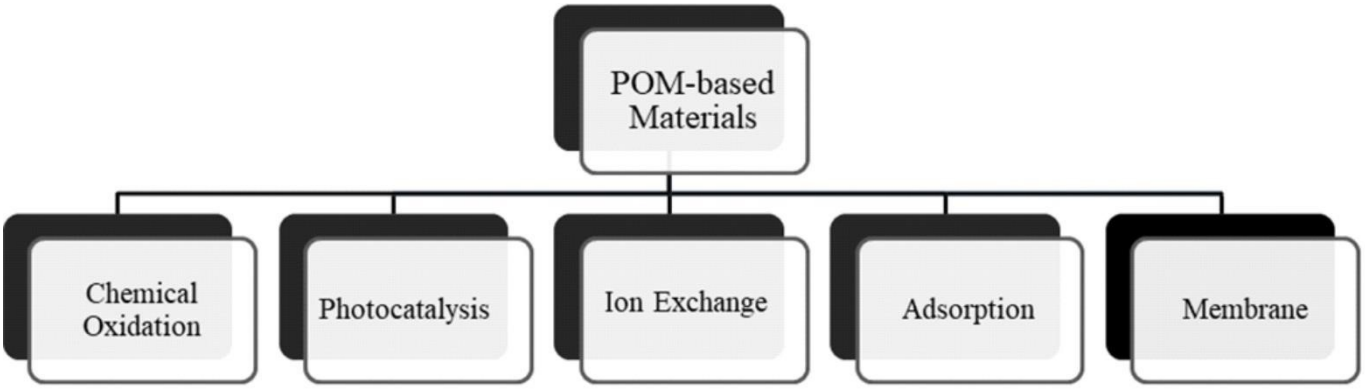

Figure 4. Summary of tertiary treatment technologies used against inorganic and organic pollutants for water purification.

Ion exchange water purification technology relies on the availability of exchange surfaces with accessible specific surface area and the ability to reversibly uptake/release ions from water. POMs can fulfill some of these requirements. For example, their diverse topology, high negative charge, and redox properties of POMs have turned them into potential candidates for cation (heavy metal) uptake and exchange. However, POMs lack a high surface area that is problematic.[113] Adsorption-based protocols have been extensively used for wastewater treatment on the account of cost, simplicity, and energy considerations. The concept of this approach is based on removing pollutants by promoting their adsorption on the adsorbent surface *via* physical or chemical interactions.[178] In this context, some intrinsic properties of POMs (*e.g.,* high negative charge, strongly basic oxygen surfaces) are advantageous for the physi/chemisorption of adsorbate molecules. However, when considering POMs as water purifiers, some limitations such as their high solubility and the low surface area must be taken into consideration. The heterogenization of POMs by inorganic substrates[106,107,179] or organic matrices[111,179,180] is the common approach to solve their solubility issue and low specific surface area. In heterogenization with organic matrices, the surface chemistry of the matrix plays an important role. Along with the degree of POM dispersion and matrix morphology, it can enhance the physicochemical properties and improve the membrane's performance. Heterogenization by porous coordination polymers (MOFs) is another successful strategy that combines both the merits of POMs and MOFs (*e.g.* recyclability and porosity).[95–101] This strategy is commonly used for the adsorptive removal of cationic dyes.[102–105] However, the catalytic activity of POM composites greatly depends on their structural properties. In some cases, as for POM@MOF composites, the activity is mainly governed by pore-dependent diffusion limitation, where the match of pore aperture and POM diameter is essential.[139] Meanwhile, each individual structural component can also induce different electron transfer kinetics due to its unique electron-storage/transfer capacity.[181,182]

Controlled deposition of POMs on substrates is another concept that enables the fabrication of POM-based functional devices for water purification.[94] Techniques such as layer-by-layer assembly, casting, and dip-coating have been recently reported.[183–185]

Membrane filtration is a reliable, and environmentally friendly process with relatively low cost and simple operation, which has been widely used for water purification. Catalytic membranes represent a new generation of membranes created by incorporating inorganic particles, such as POMs, into a polymer matrix to enhance the membrane's (photo)catalytic properties.[186–189] As a convincing demonstration of this approach, Yao *et al*. designed and fabricated an amine-functionalized APTMS-treated PEI membrane for dye removal from wastewater. $[PV^{V}_{2}Mo^{VI}_{12}O_{40}]^{5-}$ was incorporated into the matrix *via* a simple sol-gel protocol. The presence of $[PV^{V}_{2}Mo^{VI}_{12}O_{40}]^{5-}$ in the membrane not only enhanced the mechanical strength of PEI but also catalyzed the degradation of RB5 in the presence of a diluted solution of an oxidant (**Figure 5**).[190] The presence of different POM species was reported to be necessary for the self-cleaning property of the membrane.[183]

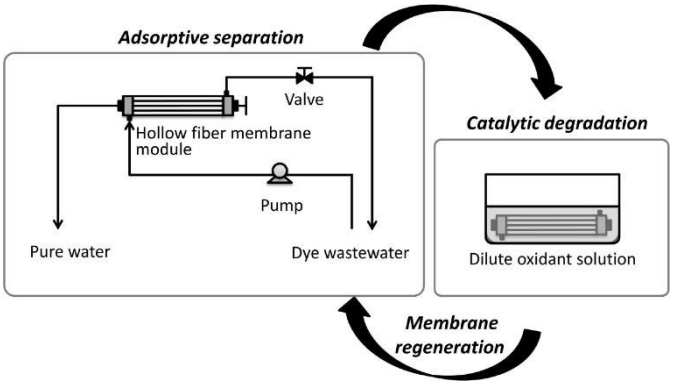

Figure 5. Illustration of a POM-integrated catalytic membrane for organic dye decontamination from water. Reproduced from Ref. 190 with permission from Elsevier, Copyright 2016.

2.2 Removal of inorganic pollutants

2.2.1 Removal of heavy metals. Catalysis and photocatalysis are appropriate strategies for removing reductive toxic metal ions

View Article Online DOI: 10.1039/D5EN00964B

from water.[108,191,192] Gong *et al*. demonstrated that different highly reduced molybdophosphate hybrid materials such as $\{Co^{II}[P^{V}_4Mo^{V}_6X_{31}]_2\}^{n-}$ (X = O or OH)[193] or $\{Mn^{II}[P^{V}_4Mo^{V}_6O_{31}]_2\}$[194] clusters could act as efficient heterogeneous catalysts for the reduction of toxic Cr(VI) to nontoxic Cr(III) in the presence of formic acid as the reducing agent under mild conditions. These noble metal-free POM catalysts have great potential to replace high-priced Pt/Pd catalysts for the elimination of Cr(VI) from water.

POMs or their modified derivatives, acting as electron reservoirs, have demonstrated efficiency in photoactivity, especially in visible light photocatalysis. Therefore, there is continuous effort to design a POM-based photocatalyst that can utilize solar energy for the reduction of highly toxic Cr(VI). Due to the good photocatalytic response of Ag-based photocatalysts, Wang's group heterogenized $H_3[PMo^{VI}_{12}O_{40}]$ with Ag^+ counter cations.[195] $Ag/Ag_xH_{3-x}PMo^{VI}_{12}O_{40}$ nanowires were synthesized by a facile solid-state reaction route and in situ photodeposited method. The resulting $Ag/Ag_x[H_{3-x}PMo^{VI}_{12}O_{40}]$ ($Ag/AgHPMo_{12}$) nanowires, where x denotes the irradiation time (x = 2, 4, 6, 8 h, respectively), showed higher stability and photocatalytic activity than traditional Ag-based photocatalysts (*e.g.* Ag/AgX (X = Cl, Br, I), $AgPO_4$ or $AgVO_3$)[196–199] for Cr(VI) reduction. This is attributed to their good visible-light absorption and reversible redox properties of the Keggin-type POM (**Figure 2.F**). In addition, a part of the Ag^+ in the nanowires was *in situ* photoreduced to Ag NPs under visible light irradiation, and these Ag NPs enhanced visible-light absorption and the charge separation of photogenerated electrons (e^-) and holes (h^+) in $Ag/[AgHPMo^{VI}_{12}]$. In order to improve the catalytic efficiency of $Ag/[Ag_xH_{3-x}PMo^{VI}_{12}O_{40}]$ nanowires, these Ag-loaded 1D silver POM nanowires were well dispersed on duplicated 2D graphite-like carbon nitride (g-C_3N_4) nanosheets.[200] The obtained $[Ag_xH_{3-x}PMo^{VI}_{12}O_{40}]/Ag/g\text{-}C_3N_4$ (x represents the irradiation time; x = 2, 4, and 6 h, respectively) 1D/2D Z-scheme heterojunction photocatalyst exhibited excellent and durable photocatalytic performance towards the reduction of Cr(VI), methyl orange (MO) and tetracycline (TCY) under visible light.[200]

In attempts to obtain efficient photocatalysts based on inorganic-organic hybrid POMs, a series of $[Ag_4(H_2O)(L)_3(SiW^{VI}_{12}O_{40})]$, $[Zn(L)(H_2O)]_2[SiW^{VI}_{12}O_{40}]\cdot 3H_2O$, $[Cu(L)(H_2O)]_2[SiW^{VI}_{12}O_{40}]$, and $[Cu_2(L)_2(HPW^{VI}_{10}W^{V}_{2}O_{40})]\cdot 4H_2O$ (L = 1,4-bis(3-(2-pyridyl)pyrazole)butane), have been synthesized.[201] Interestingly, $[Ag_4(H_2O)(L)_3(SiW^{VI}_{12}O_{40})]$ (1) hybrid was able to act as an efficient photocatalyst to reduce Cr(VI) using the scavenger isopropanol under visible light at ambient temperature. In comparison with $[Ag_4(H_2O)(L)_3(SiW^{VI}_{12}O_{40})]$, the three other POM hybrids showed relatively weak photocatalytic activity. In a possible reduction mechanism of Cr(VI) to Cr(III), first, the $[Ag_4(H_2O)(L)_3]^{4+}$ unit was excited under visible light, and the excited state electrons on the organic ligand were inclined to transfer to the $[Ag_4(H_2O)(L)_3(SiW^{VI}_{12}O_{40})]$ POM. Simultaneously, the isopropanol on the surface of the hybrid yielded reducing radicals and captured the photoinduced holes produced by the hybrid photocatalyst. Finally, the isopropanol scavenged the photoinduced holes and formed CO_2, H_2O, and other products. This charge transfer maintains the recombination of holes and electrons. The electrons accumulated on $[Ag_4(H_2O)(L)_3(SiW^{VI}_{12}O_{40})]$ were responsible for reducing Cr(VI). It was concluded that the much larger $[Ag_4(H_2O)(L)_3]^{4+}$ metal-organic unit, in comparison to the other metal-organic units presented in other above-mentioned inorganic-organic hybrids, is probably responsible for the higher photocatalytic activity of the $[Ag_4(H_2O)(L)_3(SiW^{VI}_{12}O_{40})]$ compared to the other three compounds.[201] Adsorption is the other most used purification technique to remove heavy metals from wastewater. In order to prepare a multi-functional composite, Herrmann *et al*.[63] used a combination of lacunary Keggin anions $[\alpha\text{-}SiW^{VI}_{11}O_{39}]^{8-}$ and tetra-n-alkyl ammonium cations ($(n\text{-}C_6H_{13})_4N^+$ and $(n\text{-}C_7H_{15})_4N^+$) to prepare a highly viscous, lipophilic POM-IL complex, which was then immobilized on porous silica to give POM-SILP.[165] Each component of the POM-SILP composite contributed to the removal of a specific type of water contaminant. The lacunary Keggin tungstate anions (**Figure 2.G**) were responsible for metal-ion binding, whereas the long-chain quaternary organo-ammonium cations[202] acted as an antimicrobial. In addition, the POM-IL lipophilicity enabled the adsorption of organic contaminants, and the silica support bound radionuclides. Thus, using the water-insoluble POM-SILP composite in filtration columns allowed the simultaneous removal of toxic heavy metals (as Ni^{2+}, Pb^{2+}, Cu^{2+}, Cr^{3+} and Co^{2+}), microbes (*E. coli*), organic aromatics (trityl dye), and nuclear waste (UO_2^{+}) from water (**Figure 6**).[63]

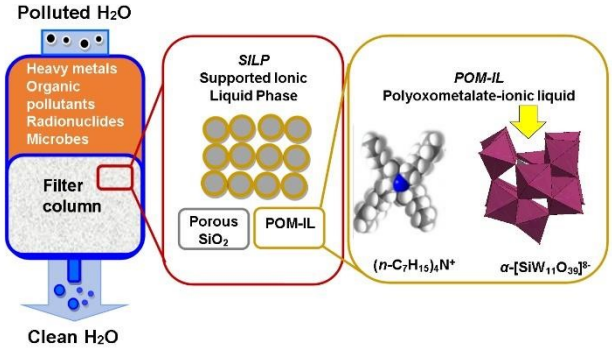

Figure 6. Water purification using POM-SLIPs: the POM-SLIP column filter removes toxic heavy metals (e.g. Ni(II), Pb(II), UO_2(II)), microbes (*E.coli*), and aromatic organic pollutants (e.g. trityl dyes) due to the presence of lacunary polyoxometalate anions with specific metal-binding sites (yellow arrow) and antimicrobial tetra-alkyl ammonium cations. Reproduced from Ref. 63 with permission form Wiley-VCH, Copyright 2017.

The highly hydrophobic nature of POM-IL leads to surface heterogeneity and thus facilitates biphasic removal of metal ions from aqueous solutions. At the same time, the negative charge present on the POM units is the driving force for the removal of metal ions with a positive charge. In order to increase the removal of heavy metals from water by POM-IL, Shakeela and Rao synthesized a series of Keggin-based ionic liquids by reacting in situ generated first-row transition-metal ion (Mn^{2+}, Fe^{3+}, Co^{2+}, Ni^{2+}, Cu^{2+}, and Zn^{2+}) substituted monolacunary Keggin with tetraoctylammonium (TOA) cations.[203] Metal-substituted lacunary POMs carried a relatively higher negative charge which facilitated the absorption of metal cations. Thus, all these thermoreversible POM-ILs effectively

View Article Online DOI: 10.1039/D5EN00964B

removed Cd^{2+} and Pb^{2+} metal ions from the aqueous phase.[203] Embedding POM-ILs with tri-lacunary Keggin $[\alpha\text{-}PW^{VI}_9O_{34}]^{9-}$ featuring coordinative binding of up to six metal cations into 3D printed organic polymers[204] has been shown to produce a highly porous organic-inorganic composite for effective transition-metal removal (**Figure 7**).[205]

Cation exchange is another process for the removal of various metal cations from water. Synthetic inorganic ion exchangers with well-defined chemical and phase compositions appear to be the most suitable ones compared to organic ion exchangers due to higher thermal and chemical stability and higher exchange capacity and selectivity for a wide range of metal ions.[113] For example, Cronin's group designed an inorganic open framework nanocube-based $K_{18}Li_6[Mn^{II}_8(H_2O)_{48}P_8W^{VI}_{48}O_{184}]\cdot 108H_2O$, from highly anionic crown-type POM ($[P_8W^{VI}_{48}O_{184}]^{40-}$) and Mn^{II} as linkers to accommodate Cu^{II} cations from a solution into the network of channels and cavities. The cation-exchange capacity and rate are controlled by oxidizing the Mn linkers from +II to +III.[206] In some cases, POM-IL systems exhibited greater efficiency than conventional ion-exchange resins.[207]

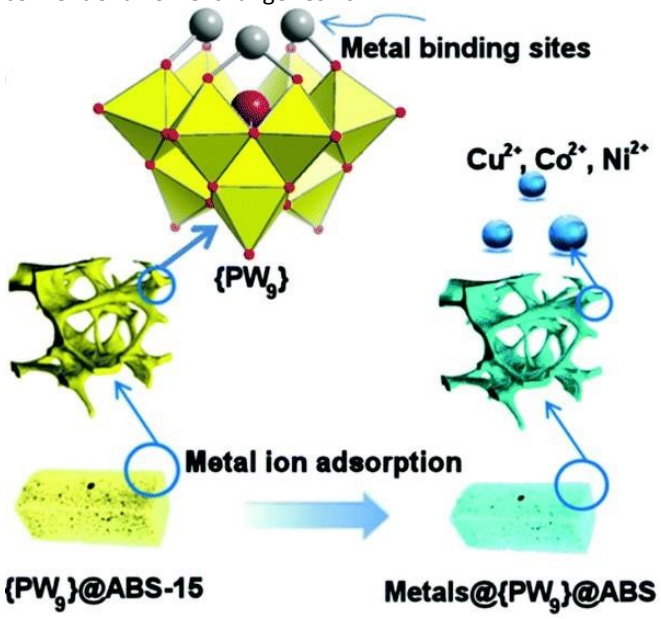

Figure 7. Schematic illustration of the POM-modified 3D-printed copolymer substrates used for transition-metal removal by the cation binding sites of the lacunary $[\alpha\text{-}PW^{VI}_9O_{34}]^{9-}$. Reproduced from Ref. 205 with permission from The Royal Society of Chemistry, Copyright 2018.

2.2.2 Removal of radioactive metals. Although metal-organic frameworks (MOFs) initially exhibited a unique performance for the adsorptive removal of metal ions, most of these materials have low stability in aquatic media, which has limited their applications for water purification. To improve the stability of MOFs, Zou *et al*. functionalized HKUST-1 MOF with Keggin-type POM $[H_3PW^{VI}_{12}O_{40}]$ POM (**Figure 2.F**) to form HKUST-1@$[H_3PW^{VI}_{12}O_{40}]$ under microwave conditions. It was proposed that the improved water stability of HKUST-1@$[H_3PW^{VI}_{12}O_{40}]$ was the result of POMs being encapsulated into HKUST-1 pores. The HKUST-1@$[H_3PW^{VI}_{12}O_{40}]$ showed high adsorption affinity and capacity towards selective adsorption of heavy metal ions (highly selective for Pb^{2+} and Cd^{2+}, but no adsorption of Hg^{2+}) from contaminated water.[208] Studies on HKUST-1@$[H_3PW^{VI}_{12}O_{40}]$ adsorption ability to remove U(VI) from wastewater showed that it could selectively adsorb U(VI) from low concentration uranium solutions in the presence of other metal ions.[209] The adsorption capacity of HKUST-1@$[H_3PW^{VI}_{12}O_{40}]$ was strongly pH dependent and did not significantly decrease after three adsorption-desorption cycles. The presence of phosphate groups in the adsorbent structure has a great affinity for radioactive U(VI) ions in an aqueous solution.[210,211] In this regard, a ship-type nano-cage POM $\{[C_5NH_5]_9[H_{31}Mo^{VI}V^{V}_{12}O_{24}Co^{II}_{12}(PO_4)_{23}(H_2O)_4]\}^{2-}$ (Co-POM) with 23 $\{PO_4\}$ groups was designed and synthesized. The high adsorption capacity of this POM-based inorganic framework for U(VI) ions in aqueous solution was mainly ascribed to coordination interaction between U(VI) and O in the phosphate groups on Co-POM which was proved by FT-IR and XPS analyses.[212] Composites of POMs ($H_3PW^{VI}_{12}O_{40}$) with graphene oxide also exhibited a significant potential for uranyl uptake from wastewater.[113]

The cation exchange studies by POMs have been widely used to separate radioactive metal ions from radioactive wastes.[109] Kortz's group worked on a cyclic K^+-templated POM, $[K\subset\{(\beta\text{-}As^{III}W_8O_{30})(W^{VI}O(H_2O))\}_3]^{14-}$, which showed high selectivity to Rb^+, due to the relatively large size of the central cavity for K^+ (**Figure 8**).[114] Uchida's group combined the Keggin cluster $[SiMo^{VI}_{12}O_{40}]^{4-}$ anions with a cationic oxo-centered trinuclear complex, to produce ionic crystals with isolated pores, $(etpyH)_2[Cr_3O(OOCH)_6(etpy)_3]_2[SiMo^{VI}_{12}O_{40}]\cdot 3H_2O$ (etpy = 4-ethylpyridine), which selectively adsorbed Cs^+ among alkali and alkaline earth metals *via* reduction of the Keggin $[SiMo^{VI}_{12}O_{40}]$ with ascorbic acid.[213] The previously reported ionic crystal, $(mepyH)[Cr_3O(OOCH)_6(mepy)_3]_2[PMo^{VI}_{12}O_{40}]\cdot 5H_2O$ (mepy = 4-methylpyridine, $mepyH^+$ = 4-methylpyridinium ion), with 1D open channels, was able to incorporate Na^+ as well as Cs^+ by the reduction-induced cation exchange processes.[115] The authors concluded that the high selectivity towards Cs^+ is due to the existence of closed pores rather than open channels. Despite the high selectivity towards Cs^+ however, several disadvantages such as the requirement of heating (343 K) and slow adsorption kinetics (12 h to reach equilibrium) limited the widespread application of $(mepyH)[Cr_3O(OOCH)_6(mepy)_3]_2[PMo^{VI}_{12}O_{40}]\cdot 5H_2O$. Later, this group overcame disadvantages by utilizing the large-molecular size and easily reducible Wells-Dawson-type of POMs $[P_2M^{VI}_{18}O_{62}]^{6-}$ (M = Mo, W).[214] In comparison with the Keggin-type POM, the larger molecular size and higher reduction potential of Dawson-type POM increased the pore volume and facilitated the reduction-induced Cs^+ exchange. As expected, the capacity and rate of Cs^+ uptake increased significantly (with only 1 h to reach equilibrium at room temperature), demonstrating the potential application of these adsorbents for radioactive Cs^+ (Cs-137) removal.[214]

View Article Online
DOI: 10.1039/DEN00054A

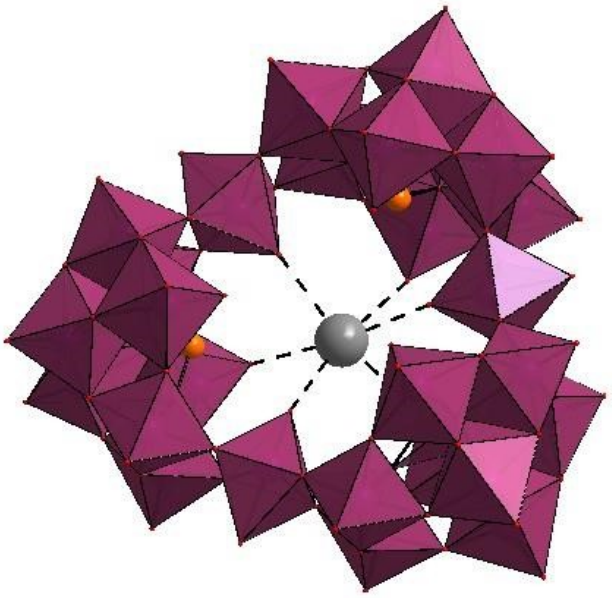

Figure 8. Structure of $[M\subset\{(\beta\text{-}As^{III}W_9O_{30})(WO(H_2O))\}_3]^{14-}$ with the central guest being either K^+ or Rb^+. Color code: WO_6 (violet octahedra), As (orange), K/Rb (grey). [114]

2.3 Removal of organic pollutants

2.3.1 Removal of organic dyes. As shown in **Table S2** (Supporting Information), the decontamination mechanisms, in the case of organic pollutants, are similar to previously discussed methods for inorganic ones. Adsorption of dye molecules, especially cationic ones, by POMs is strongly governed by solution pH. The selective adsorption of methylene blue (MB) in the presence of methyl orange (MO) over $[P_2W^{VI}_{18}]$/MOF-5 catalyst is spontaneous and endothermic. In addition, the pH value of dye solution should also be carefully controlled to obtain maximum adsorption capacity, because the surface charge of the adsorbent is strongly affected by the pH (pH_{PZC}; PZC = point-of-zero charge).[215] Furthermore, olation and oxolation processes are responsible for the high negative charge on the POM surface at lower pH values.[216]

In a generally accepted approach, photooxidation of dye molecules occurs through generation of free $OH^{\bullet}$. The proposed mechanism is based on the photoexcitation of $Cs_4SiW^{VI}_{12}O_{40}$ POM and a subsequent hydrogen abstraction reaction which results in the homolytic bond cleavage of H_2O. The photocatalytic activity of POMs, such as $[SiW^{VI}_{12}O_{40}]^{4-}$, can be enhanced in the presence of semiconductors. In fact, in such heterojunction structures with suitable energy band alignment, photogenerated carriers could be separated more efficiently.[217] Dye sensitization is another mechanism that may contribute to dye degradation in photocatalytic reactions. Due to the visible-light absorption abilities of the sensitizers, dye-sensitized POM photocatalysts can be excited upon visible-light irradiations. In these cases, the oxidation of dye proceeds through electron transfer between the excited dye (*e.g.*, thionine, phthalocyanine) and LUMO of Keggin ($[PW^{VI}_{12}O_{40}]^{3-}$)[218,219] or Wells-Dawson-type ($[\alpha\text{-}P_2W^{VI}_{18}O_{62}]^{6-}$ (P_2W_{18}) and $[\alpha\text{-}P_2W^{VI}_{17}O_{61}]^{10-}$)[218] type POMs.[218,219]

As an interesting example of membrane filtration technology, Yao *et al.*[179] incorporated surfactant-encapsulated POM microparticles into a PVDF matrix as a microfiltration membrane for the adsorptive removal of the anionic dye Reactive Black 5 (RB5). The authors prepared spherical microparticles through an ion exchange reaction between a cationic surfactant (DODA·Br) and $[PV^{V}_{2}Mo^{VI}_{10}O_{40}]^{5-}$. This architecture enhanced the flow rate of the system and dye removal efficiency reached up to 97.5 % within 120 min.[179] A similar concept has been applied in the case of surface-active ionic-liquid-encapsulated POMs.[220] Ion exchange reaction has also been used to replace small anions in the structure of layered double hydroxides (LDHs) with large polyanions. By this method the surface area of the resulting composite can be enhanced, since the interlayer distances of LDH increase. These composites have been used for the removal of cationic dyes from water; however, the instability of LDH in acidic media may limit their application.[221,222] In 2005 Zhao and co-workers suggested that an active peroxo species is responsible in the photo-Fenton oxidation of Rhodamine B (RhB) under visible light irradiation. The authors proposed that the active species is formed upon the interaction of reduced POM with H_2O_2.[223] Similarly, in Fenton systems the active species is formed by the coordination of iron to $[PW^{VI}_{12}O_{40}]^{3-}$ POM.[224] In Fenton-like systems the iron species is replaced with different POMs, like mentioned Keggin[224] or $[HPW^{V}_{4}W^{VI}_{8}O_{40}]^{6-}$ POMs.[225] The radical-based pathways, however, can enhance apparent degradation rate if not properly identified or controlled.

Among different transition metals (Co, Ni, Cu), Co-substituted Wells-Dawson anions $[\alpha_2P_2W^{VI}_{17}CoO_{61}]^{8-}$ exhibited higher catalytic performance.[226] Li's group prepared two POMCPs, $[Ag_4(H_2pyttz\text{-}I)(H_2pyttz\text{-}II)(Hpyttz\text{-}II)][HSiW^{VI}_{12}O_{40}]\cdot4H_2O$ (H_2pyttz-I = 3-(pyrid-2-yl)-5-(1H-1,2,4-triazol-3-yl)-1,2,4-triazolyl) and $[Ag_4(H_2pyttz\text{-}II)(Hpyttz\text{-}II)_2][H_2SiW^{VI}_{12}O_{40}]\cdot3H_2O$ (H_2pyttz-II = 3-(pyrid-4-yl)-5-(1H-1,2,4-triazol-3-yl)-1,2,4-triazolyl) with similar structure and different tunnels (**Figure 9a**). The photocatalytic degradation of methylene blue (MB) demonstrated that the structure of the hybrids influences the photocatalytic properties. The larger cavities in the compound and $[Ag_4(H_2pyttz\text{-}II)(Hpyttz\text{-}II)_2][H_2SiW^{VI}_{12}O_{40}]\cdot3H_2O$ increase the contact area between catalysts and crude materials and promote more active sites to participate in the reactions process. Thus, the photocatalytic properties of $Ag_4(H_2pyttz\text{-}II)(Hpyttz\text{-}II)_2][H_2SiW^{VI}_{12}O_{40}]\cdot3H_2O$ were improved. The proposed mechanism for enhanced photocatalytic activity in these hybrids is shown in **Figure 9b**. This mechanism includes LMCT from the HOMO to the LUMO, which was facilitated by Ag–O bridging units. In addition to this, Ag-pyttz acted as photosensitizers and promoted the transition of electrons onto $[SiMo^{VI}_{12}O_{40}]^{4-}$ POMs. Therefore, the $[SiMo^{VI}_{12}O_{40}]^{4-}$ POMs had

View Article Online
DOI: 10.1039/D5EN00964B

a higher charge density and exhibited a considerable impact on the photocatalytic degradation of RhB.[227]

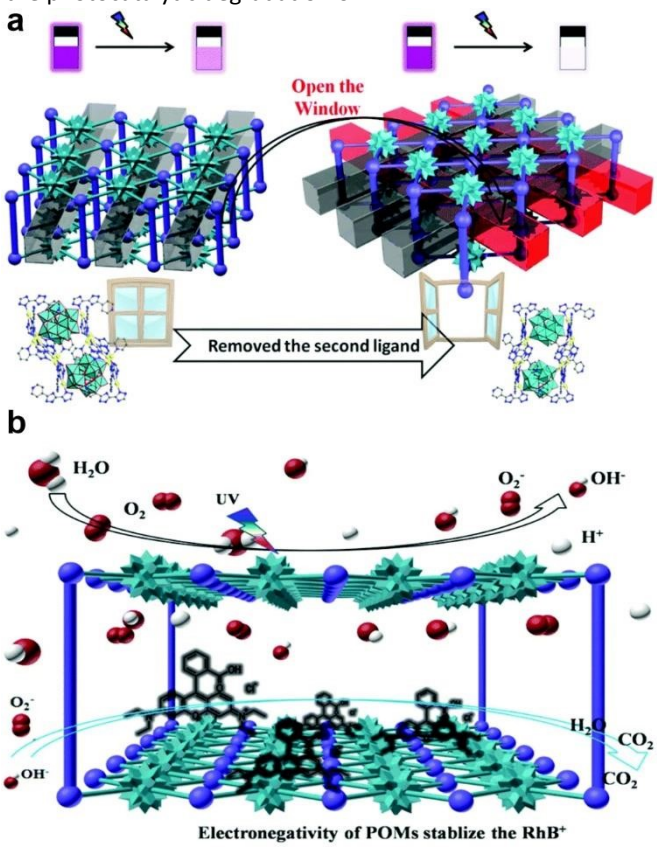

Figure 9. a) Representation of the $[Ag_4(H_2pyttz\text{-}I)(H_2pyttz\text{-}II)(Hpyttz\text{-}II)][HSiW_{12}O_{40}]$ and $[Ag_4(H_2pyttz\text{-}II)(Hpyttz\text{-}II)_2][H_2SiW_{12}O_{40}]$ compounds ((H2pyttz-I = 3-(pyrid-2-yl)-5-(1H-1,2,4-triazol-3-yl)-1,2,4-triazolyl) and H2pyttz-II = 3-(pyrid-4-yl)-5-(1H-1,2,4-triazol-3-yl)-1,2,4-triazolyl) with similar underlying frameworks and different tunnels. **b)** Representation of the photocatalytic mechanisms for POMCPs. Reproduced from Ref. 227 with permission from The Royal Society of Chemistry, Copyright 2015.

2.3.2 Removal of aromatic hydrocarbons. The oxidative potential of POMs has been broadly used in AOPs for phenol oxidation.[227] For example, $[PW_{11}O_{39}Fe^{III}(H_2O)]^{4-}$ can degrade chlorophenol (CP) compounds only if H_2O_2 is added to the solution. No photocatalytic activity was observed in aerated aqueous solution. In addition, the reaction rate was influenced by the initial concentration of the catalyst or H_2O_2 and the number of chlorines in the aromatic ring of CP.[168] Iron-containing POMs have also been used to construct heterojunction photocatalysts by grafting Fe-POM nanoclusters onto oxygen-deficient TiO_2. The synergistic effect between photocatalysis and Fenton-like reactions resulted in efficient degradation of sulfosalicylic acid (SSA).[228] Deposition of Au NPs on the surface of POM/TiO_2 is another strategy to improve light absorption and activity of the catalyst. A 4.6-fold increase was observed in photocatalytic degradation of nitrobenzene (NBZ).[229] Zhang *et al*. prepared a ferrocene-containing silicotungstate catalyst *via* a co-precipitation method for the photocatalytic oxidation of 4-chlorophenol (4-CP). It was suggested that the synergism between ferrocene and silicotungstate leads to the charge-transition from ferrocene to the POM unit, which ultimately contributes to the oxidation of the organic pollutant through a Fenton-like mechanism.[230] In another study, $[Cs_3PMo^{VI}_{12}O_{40}]$ was used as a modifier of the semiconductor Bi_2O_3. The experimental results indicated that the $[Cs_3PMo^{VI}_{12}O_{40}]$ generated on the surface of the semiconductor creates a P–N heterojunction photocatalyst with visible-light activity in the degradation of phenol. The best photocatalytic performance was observed when 2.5 % (mol) of $[Cs_3PMo^{VI}_{12}O_{40}]$ was added to the semiconductor. Also, trapping experiments showed that the major active species involved in the degradation process are superoxide and hydroxyl radicals.[231] Heterogenization of POMs with graphene aerogels (GA) has also shown promise in the adsorptive removal of a series of organic compounds from water.[232] A more comprehensive analysis of the studies from the past 5 years is provided in **Table S2** in Supporting Information.

2.4 Summary of water treatment technologies by polyoxometalates

Although the literature review shows promising evidence on how POM-based materials have attracted considerable attention for water treatment, like any emerging technology, they also have their own set of challenges and limitations. As tabulated in **Table S2**, POM-based materials have often been utilized as photocatalysts with high removal efficiencies. A key negative result that is rarely reported, but likely exists, is the structural instability of POM-based photocatalysts under realistic water matrices (containing chloride, carbonate, or natural organic matter). Such components can significantly suppress the photocatalytic activity or even partially decompose the structure, yet these effects are often not disclosed. Acknowledging this limitation is important for assessing the practical applicability of POM materials. For their broad implementation, they must also maintain the cost of processed water as low as possible. In this regard, substantial costs associated with synthesizing POMs and their composites remain as a significant challenge. In terms of the technology itself, other economically beneficial methods such as adsorption and ion exchange should also be considered, as they tend to provide more affordable solutions for water purification.

3 Removal of emerging health pollutants

Some of the most prominent classes of emerging health pollutants (EPs) are pharmaceuticals (antibiotics, antifungals, antidepressants, synthetic hormones)[12,13,18,27,28,233] plant protection products (pesticides, biocides)[31,234], and microplastics.[234,236,237] Excessive use of antibiotics and cosmetic products, *e.g.*, disinfectants and cleaning products, has led to the development of bacterial resistance through DNA mutations of bacterial cells, which have resulted in the adaptation and resistance of bacteria to these products.[24,25,238] In addition, bacterial resistance also occurs through the horizontal gene transfer mechanism from resistant bacteria to non-resistant bacteria through transformation, transduction, or conjugation.[25] Moreover, water bodies containing EPs play an essential role in this horizontal gene transfer mechanism by facilitating the horizontal gene transfer from pathogenic to non-

View Article Online
DOI: 10.1039/D5EN00964B

pathogenic microorganisms. In addition to contributing to the development of antibiotic resistance, pollutants such as UV filters from sunscreens have been shown to harm marine life significantly. These compounds accumulate in aquatic environments and negatively affect organisms, including phytoplankton, corals, microalgae, and sea urchins, by disrupting their physiology and ecosystem functions.[24,239]

A study, conducted over two consecutive years (2015 and 2016), on the final effluents from wastewater treatment plants in Europe, revealed high average concentrations of antibiotics in wastewater, especially in countries such as Portugal, Spain, and Ireland. The study identified that the most commonly found antibiotics, ciprofloxacin, azithromycin, and cephalexin, have a potentially significant impact on aquatic systems and the development of antibiotic resistance.[24,240]

Ciprofloxacin, a fluoroquinolone antibiotic, and erythromycin have also been detected in effluents and surface waters in other studies[24], and are included, along with the macrolides azithromycin and clarithromycin, as well as the penicillin-type antibiotic amoxicillin, in the surface water Watch List under the European Water Framework Directive.[17,240,241] More recently, this report has been updated to include other pharmaceutical products such as the antibacterials sulfamethoxazole and trimethoprim, the antifungal clotrimazole, fluconazole, and miconazole, the antidepressant venlafaxine, and the synthetic hormone norethisterone (**Figure 10**).[240,241] In addition to the aforementioned pharmaceuticals, such as proton pump inhibitors (PPIs), lansoprazole and omeprazole,[242,243] have been proposed as potential Watch List candidates due to their recently discovered possible mutagenic and toxic effects on aquatic organisms.[17,25,240]

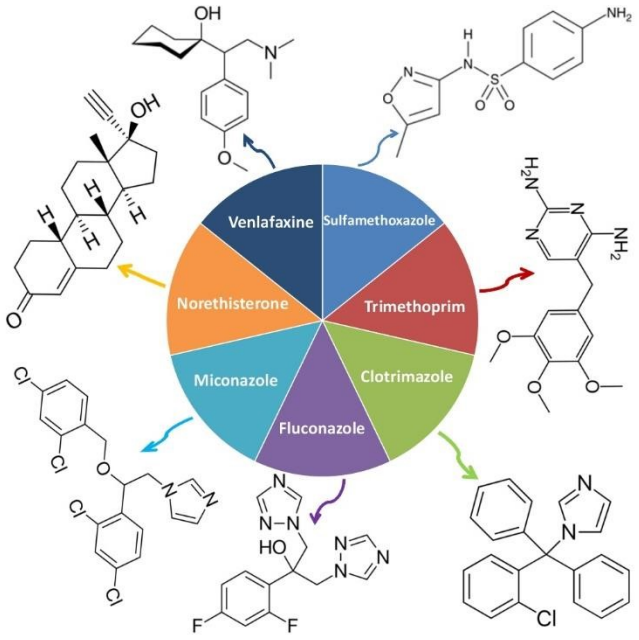

Figure 10. Emergent pharmaceuticals pollutants included in the updated 4th water watch list under the European Water Framework Directive: the antibacterial sulfamethaxazole and trimethoprim; the anti-fungus clotrimazole, flucozanole and miconazole; the antidepressant venlafaxine and the synthetic hormone norethisterone.[17]

Herein, we focus on the POMs' ability to degrade priority pharmaceuticals, mainly antibiotics, pesticides, microplastics, and dyes, to identify POMs with higher removal efficiency and kinetics, thus facilitating the development of more environmentally friendly POM materials.[244,245]

3.1 Removal of pharmaceutical pollutants

Every day, humans release pharmaceutical products into the environment in different forms and under different circumstances. This behavior of humanity has a major impact on health and economy and has a profound effect on our lives. It is therefore of great importance to conduct environmental protection in an effective and inexpensive manner to combat emerging health pollutants. Some of the most prominent classes of emerging pharmaceutical pollutants are the antimicrobial pharmaceuticals (antibiotics, antifungals) and other pharmaceuticals (antidepressants, synthetic hormones). It has been described that contamination of the environment with these pharmaceutical products can lead to bacterial resistance, which is an emerging and growing phenomenon worldwide in the 21st century.[10,20,22,24,246] Nonconventional low-cost adsorbents for pharmaceutical removal from wastewater, pollutant removal mechanisms, and detection using nanodevices and polymer-based adsorbents, as well as using fungal treatments, were recently summarized.[12,13,18] POMs have also been used for the detection of several pharmaceuticals, such as drugs of abuse[247] and triclosan (TCS)[248], as well for the selective extraction of antidepressants in undiluted urine.[249] TCS, a diphenyl ether with antibacterial properties, is used as a disinfectant in antiseptic creams, toothpaste, hand soaps, deodorants, and even in plastics.[21,22] In Europe, TCS is one of the most frequently detected contaminants in wastewater. However, studies from the United States have reported that its concentration in wastewater can be up to five times higher.[22] TCS has already been detected in surface waters in several regions of the world, including in fish tissues. In fact, the methylated form of TCS (M-TCS) is bioaccumulative in tissues, due to its lipophilic properties and stability. Moreover, it has been described that contamination of the environment with TCS can lead to bacterial resistance to four antibiotics: chloramphenicol, tetracycline, ciprofloxacin, and colistin. This resistance poses potential risks to human health as well as aquaculture.[21,22]

Of the seventeen pharmaceutical pollutants mentioned above, only one study has referred to the removal of ciprofloxacin by POMs. He *et al*. immobilized three Keggin-type POMs $[H_3PMo^{VI}_{12}O_{40}]\cdot nH_2O$, $[H_3PW^{VI}_{12}O_{40}]\cdot nH_2O$, and $[H_3PW^{VI}_{12}O_{40}]\cdot nH_2O$ onto nitrogen-deficient carbon nitride nanosheets (g-C_3N_4) and successfully utilized all three POM-based composites (**Figure 11.A**) for the removal of ciprofloxacin within only five minutes under visible light irradiation with 93.1 %, 97.4 % and 95.6 % efficiency, respectively.[250] This type of POM-based hybrid material was further explored on g-C_3N_4/PW_{12}/TiO_2 composites (PW_{12} = $[H_3PW^{VI}_{12}O_{40}]$) (**Figure 11.A–B**)[250,251], which showed remarkable and stable photocatalytic performance under visible light irradiation, not only for the removal of TC but also for bisphenol A and Cr(VI).[251] Their removal properties and stability without any observed

View Article Online
DOI: 10.1039/D5EN00964B

structural changes in the photocatalyst were attributed to the enhanced adsorption under visible light irradiation, a high specific surface area, effective separation, and photoinduced charge transfer *via* g-C_3N_4 and PW_{12}.[251]

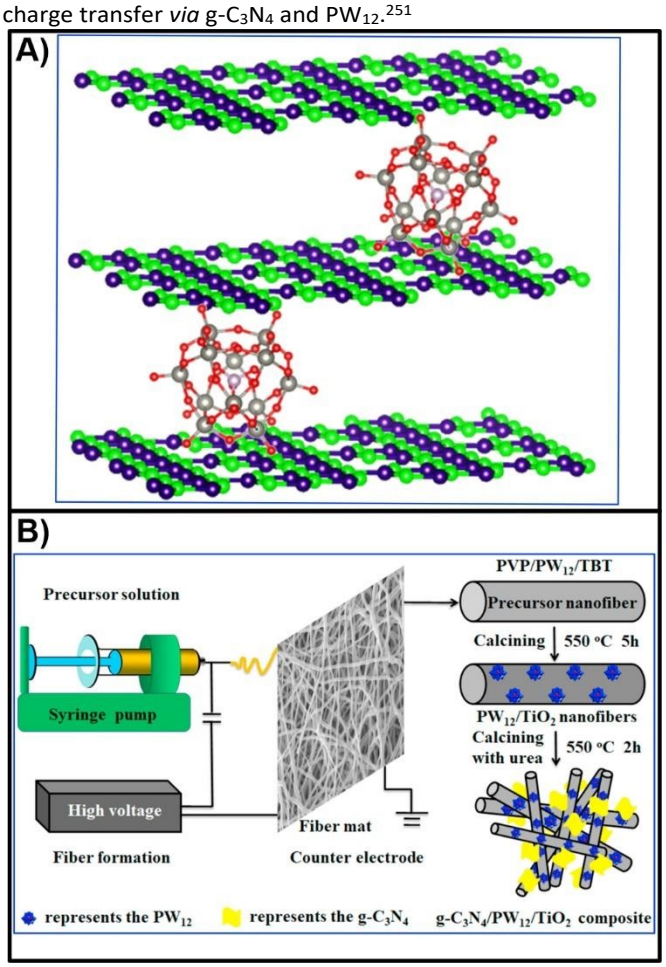

Figure 11. A) Nitrogen-deficient g-C_3N_x/POMs porous nanosheets (where x denotes N-deficiency) with P-N heterojunctions capable of photocatalytic degradation of drugs; Recreated from Ref. 250 with permission from The Royal Society of Chemistry. **B)** Fabrication of g-C_3N_4/PW_{12}/TiO_2 composite with enhanced photocatalytic performance under visible light; Reproduced from Ref. 251 with permission form Elsevier, Copyright 2021.

Moreover, Cheng *et al*.[252] have utilized the isopolyoxotungstate, decatungstate $[W^{VI}_{10}O_{32}]^{4-}$ (**Figure 2.D**) as a photocatalyst for the oxidation of sulfasalazine (SZZ)[253], an antibiotic commonly found in wastewater, and its human metabolite sulfapyridine (SPD). After 120 min in the presence of H_2O_2 and under UV irradiation, the metabolite SPD was more efficiently removed (75 %) by decatungstate than was the SZZ antibiotic (25 %). The proposed photocatalytic mechanism (**Figure 12**), which involves the generation and utilization of hydroxyl radicals (•OH) in the photocatalytic degradation of sulfasalazine[252], has attracted increasing attention over the past decades. This mechanism has been extensively studied in the ongoing research and development of novel pollution removal technologies.[254,255] Therefore, a similar strategy has been employed for the photodegradation of antibiotics such as nitrofurazone, tetracyclines and berberine under UV or visible light irradiation. This process utilizes H_2O_2 and the photoactive POM-based composite $[H_3PW^{VI}_{12}O_{40}]$@β-EDA-CD, as shown in **Figure 13.A**.[256]

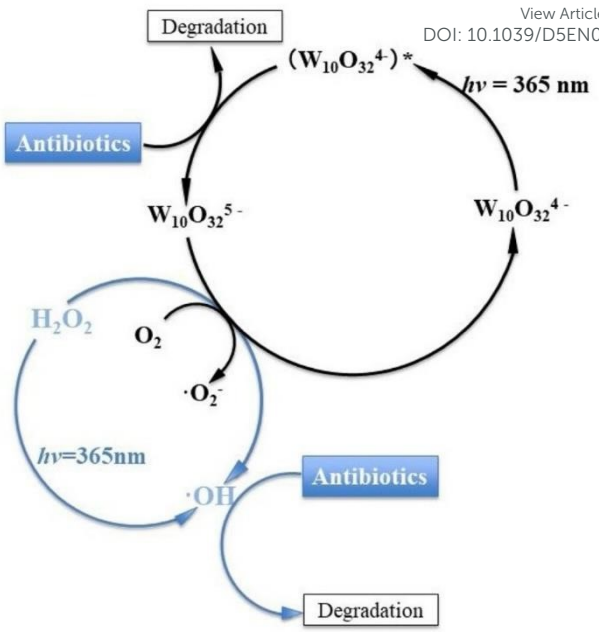

Figure 12. Cycle of photocatalysis and degradation of antibiotics (left) through the isopolyoxometalate decatungstate. Reproduced from Ref. 252 with permission from Elsevier, Copyright 2002

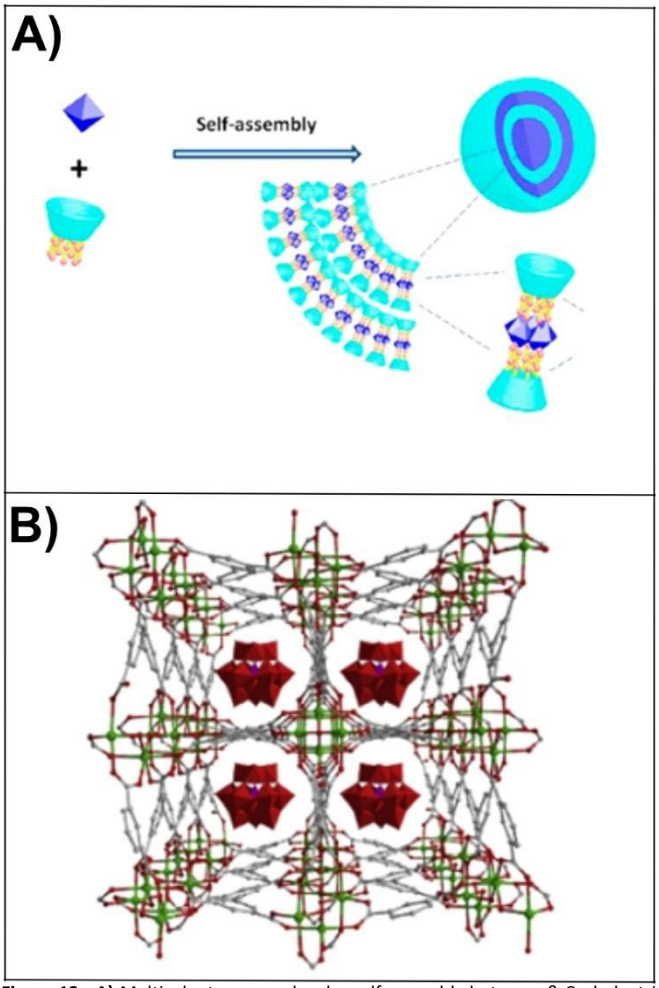

Figure 13. A) Multivalent supramolecular self-assembly between β-Cyclodextrin derivatives and polyoxometalate for photodegradation of dyes and antibiotics; Reproduced from Ref. 256 with permission from The American Chemical Society, Copyright 2019, **B)** Encapsulate polyoxometalate into metal-organic frameworks as efficient and recyclable photocatalyst for drugs degradation; Reproduced from Ref. 257 with permission from Elsevier, Copyright 2019.

View Article Online
DOI: 10.1039/D5EN00964B

Li *et al*. prepared a POM-based photocatalyst, PW_{12}@MFM-300(In) (**Figure 13.B**), by using an environmentally friendly solvent-free method for the encapsulation of the POM $[H_3PW^{VI}_{12}O_{40}]$ into the metal-organic framework MFM-300(In). The PW_{12}@MFM-300(In) composite displayed its activity for room temperature visible-light-driven catalytic degradation of the pharmaceutically active compound SMT with a 98 % removal efficiency within 2 h.[257]

3.2 Removal of pesticides, microbes and microplastic

POM-based catalysts have been used for decades in pesticide degradation. The decatungstate $[W^{VI}_{10}O_{32}]^{4-}$, mentioned in the context of the removal of pharmaceutical pollutants (Section 3.1), also showed photocatalytic activity in the degradation of two common pesticides, 2-(1-naphthyl)acetamide (NAD) and 2-mercaptobenzothiazole (MBT). In the study of da Silva *et al*., it was shown that $[W^{VI}_{10}O_{32}]^{4-}$ could promote UV-light-driven degradation of NAD with an efficiency of 89 % within 8 h.[258] Additionally, Allaoui *et al*. described the photodegradation of the pesticide MBT using $Na_4W^{VI}_{10}O_{32}$ as a catalyst with an efficiency of 90% within 8 h.[259] It has been proposed that the photodegradation of MBT occurs *via* e^- transfer and H-atom abstraction processes with $W^{VI}_{10}O_{32}{}^{4-*}$ excited species. The main products of such photodegradation when using decatungstate as a catalyst are monohydroxylated products, sulfoxide derivatives, and dimers of MBT. The whole process was shown to be O_2 dependent because photodegradation was restricted by $W^{VI}_{10}O_{32}{}^{5-}$ reoxidation.[259] The Keggin-type POM $[PW^{VI}_{12}O_{40}]^{3-}$ showed activity for the complete photocatalytic degradation of the pesticide lindane to CO_2, H_2O, and Cl^- in an aqueous solution.[260] Photocatalysis of lindane by $[PW^{VI}_{12}O_{40}]^{3-}$ follows the same principle as that of TiO_2 catalysis, *i.e.* processes involving both oxidation and reduction pathways such as chlorination, dechlorination, hydroxylation, hydrogenation, dehydrogenation, which lead to the C-C bond cleavage and complete mineralization to the final products.[260] Recently, a POM-IL[261] has also been used for the extraction of triazole pesticides (*e.g.,* penconazole, hexaconazole, diniconazole, tebuconazole, triticonazole, and difenconazole) from aqueous samples.[262] In that article, the prepared POM-IL nanomaterial ([3-(1-methylimidazolium-3-yl)propane-1-sulfonate]$_3PW^{VI}_{12}O_{40}$) was utilized as a coating for a new solid-phase microextraction (SPME) device that was then successfully applied for the extraction of the six triazole pesticides from real aqueous samples. The longevity experiments (at least 50 extractions) of POM-IL coated SPME devices compared with commercially available PDMS-coated SPME devices (PDMS = polydimethylsiloxane) showed that the newly prepared device offers higher extraction efficiency and better longevity.[262] Moreover, the type of POM-IL material (**Figure 6**), already described in Section 2.2, was shown to efficiently remove previously mentioned inorganic and organic contaminants from wastewater, as well as various microbial pollutants, *E. coli* and *B. subtilis*.[63] Recent developments in these organic/inorganic hybrid materials, POM-based ionic liquid crystals and POM-ILs, and their applications, mainly in pollutants degradation, including microplastics, have been reviewed.[263] Microplastics (MPs) are among the newly emergent health pollutants of worldwide concern, and their impact on human health and the environment is not yet completely understood.[264] The first reported example of magnetic polyoxometalate-based ionic liquid phases (magPOM-SILPs) for the removal of MPs was designed by anchoring a POM-IL composite (POM = $[\alpha\text{-}SiW^{VI}_{11}O_{39}]^{8-}$ (**Figure 2.F**); IL = (n-$C_7H_{15})_4N^+$) to an Si-enclosed Fe_2O_3 supermagnetic core, Fe_2O_3@SiO_2 (**Figure 14**). The magPOM-SILPs composite showed remarkable effectiveness (90%) for removing microplastic by binding MPs particles via the formation of hydrophobic interactions with the MPs surface and then removing MPs pollutants from water samples by magnetic recovery (**Figure 14**).[263]

Cobalt-based POMs, $Na_{10}[Co_4(H_2O)_2(V^VW^{VI}_9O_{34})_2]\cdot 34H_2O$ were also examined for dye degradation. MB and RhB dyes were chosen as the subject dyes for the degradation test because of their carcinogenic properties and wide use in the textile industry. A 10 mg/L dosage of this POM removed 87.8 % of MB in 30 min. The time required for the complete decomposition of RhB was almost twice as long as that of MB. In this study, in addition to the excellent dye catalytic activity, these CoV-POMs also showed anticancer activities.[265] However, POMs anticancer, antibacterial studies, and other biomedical studies are described elsewhere.[85,266,267,268] Another recent study, described the synthesis of two Keggin-type polyoxometalates ammonium phosphomolybdate $(NH_4)_3PMo^{VI}_{12}O_{40}$ (PMo) and ammonium phosphotungstate $(NH_4)_3PW^{VI}_{12}O_{40}$ (PW) that were used as adsorbents for the removal of various antibiotics and heavy metals from water systems. The adsorption efficiency of PMo for dyes and heavy metals was higher than that of PW for various antibiotics such as tetracycline. It was suggested that the more negative surface charges induced by Mo atoms with more electronegativity and higher specific surface area contributed to the superior adsorption efficiency of PMo for dyes and heavy metals.[269]

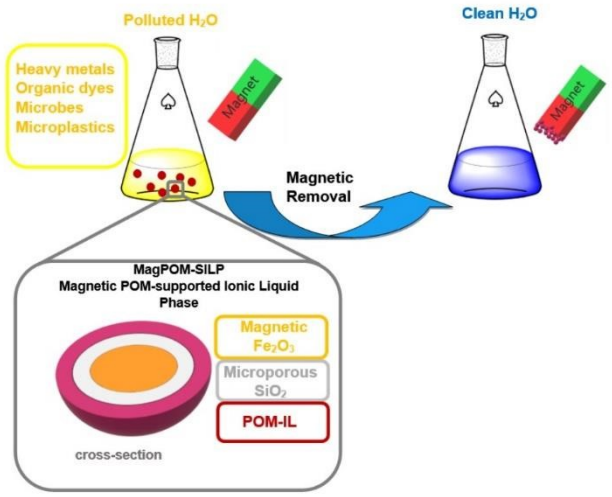

Figure 14. Magnetic polyoxometalate-supported ionic liquid (magPOM-SILPs) for heavy metals, organic dyes, microbes and microplastics water removal.[263]

View Article Online
DOI: 10.1039/D5EN00064B

Table 1 summarizes the recent examples of POMs applications in removal of EPs covered in Section 3.

3.3. Summary of POM-based technologies in removal of emerging health pollutants

Section 3 highlights emerging pollutants in the 21st century environment, such as drugs, pesticides, and microplastics, and emphasizes their dangers and consequences for human health. Several examples illustrate the use of pure POMs, nanoparticles, composites, or MOFs for removing organic and inorganic pollutants. The processes involving POMs in pollutant degradation are also discussed, many of which employ photocatalysis by UV and/or visible irradiation, in addition to adsorption or magnetic removal. In short, the different types of POMs mentioned in this section reveal their essential role in removing emerging pollutants from the environment, proving to be efficient and selective.

Table 1. Examples of recent polyoxometalates studies in pollutants degradation: antibiotics (A), dyes (D), plastics (P), industrial chemicals (IC) and pesticides (Pest).

Formula	POM Archetype	Pollutant	Conditions	Efficiency	Number of Cycles	Ref.
$Na_4W^{VI}_{10}O_{32}$	decatungstate	sulfasalazine	c(catalyst) = 40 µM; under UV irradiation	25 % removal within 120 min	1	252
		(A) sulfapyridine		75 % removal within 120 min		
g-C_3N_4-POMs POMs: $[PMo^{VI}_{12}O_{40}]^{3-}$, $[PW^{VI}_{12}O_{40}]^{3-}$, $[SiW^{VI}_{12}O_{40}]^{4-}$	Keggin	(A) ciprofloxacin	m(catalyst) = 0.01-0.1 g; under visible light	93 % removal within 5 min	1	250
g-C_3N_4/$H_3PW^{VI}_{12}O_{40}$/TiO_2	Keggin	(A) tetracycline	m(catalyst) = 20 mg	>70 % removal within 50 min (k = 0.03443 min^{-1})	1	251
		(P) bisphenol A	m(catalyst) = 20 mg	>38 % removal within 3 hours (k = 0.00712 min^{-1})	1	
		(IC) Cr(VI)	m(catalyst) = 20 mg	>65 % removal within 60 min (k = 0.025 min^{-1})	1	
POM-IL, [3-(1-methylimidazolium-3-yl) propane-1-sulfonate]$_3PW^{VI}_{12}O_{40}$	Keggin	(Pest) diniconazole	nsp	nsp	1	262
		(Pest) hexaconazole	nsp	nsp	1	
		(Pest) tebuconazole	nsp	nsp	1	
		(Pest) penconazole	nsp	nsp	1	
		(Pest) diniconazole	nsp	nsp	1	
		(Pest) triticonazole	nsp	nsp	1	
biochar-doped g-C_3N_4-$Co_2PMo_{11}VO_{40}$	Keggin	(A) sulfamethoxazole	m(catalyst) = 0.2 g/L; under visible light	98.5 % within 20 min (k = 0.215 min^{-1})	1	273
Ag-L-SiW_{12}@$BiVO_4$ (L = thiacalix [4]arene)	Keggin	(A) ciprofloxacin	pH = 4; v(catalyst) = 30 µL; under simulated solar light	95 % within 240 min (k = 0.0118 min^{-1})	1	274
$H_3PW_{12}O_{40}$-Fe_3O_4-biocar	Keggin	(A) metronidazole	pH = 1; c(catalyst) = 0.6 g/L	>94 % removal within 60 min	1	275
α-$K_8SiW_{11}O_{39}$-MIL-101(Cr)-$CoFe_2O_4$	Lacunary Keggin	(D) methylene blue (D) rhodamine B (D) methyl orange (A) ciprofloxacin	m(catalyst) = 30 mg	methylene blue = 100 % within 25 min rhodamine B = 84 % within 50 min methyl orange = 37 % within 20 min ciprofloxacin = 100 % within 15 min	1	276
EDA-CD-[$H_3PW^{VI}_{12}O_{40}$],	Keggin	(A) nitrofurazone	c(catalyst) = 0.055 mM; under UV irradiation or sunlight; H_2O_2	k = 0.163 min^{-1}	1	256

View Article Online
DOI: 10.1039/D5EN00964B

(EDA-CD = per-6-deoxy-6-ethylenediamine-β-cyclodextrine)		(A) tetracyclines	with H_2O_2	k = 0.152 min^{-1}	1	
		A) berberine	with H_2O_2	k = 0.115 min^{-1}	1	
		(D) rhodamine B	with H_2O_2	k = 0.868 min^{-1}	1	
		(D) xylenol Orange	with H_2O_2	k = 0.214 min^{-1}	1	
		(D) methyl Orange	with H_2O_2	k = 0.164 min^{-1}	1	
		(D) methylene blue	with H_2O_2	k = 0.119 min^{-1}	1	
		(D) crystal violet	with H_2O_2	k = 0.084 min^{-1}	1	
$[H_3PW^{VI}_{12}O_{40}]$,@MFM-300(In); MFM-300(In) = indium-based metal-organic framework	Keggin	(A) sulfamethazine (SMT)	nsp	98 % removal within 60 min	1	257
$LnTiO_2/P_2W^{VI}_{18}Sn_3$	Keggin	(D) methyl orange	nsp	100 % removal within 5 min	1	270
$Na_4W^{VI}_{10}O_{32}$	decatungstate	(Pest) 2-(1-naphthyl)acetamide (NAD)	c(catalyst) = 300 µM	89 % removal within 8 hours (k = 0.032 min^{-1})	1	258
$K_2[V^V_{10}O_{16}(OH)_6(CH_3CH_2CO_2)_6]$	decavanadate	(D) methylene blue	m(catalyst) = 5 mg	93 % removal within 45 min	1	271
$Cu(OH_2)_3(2–amp)]_2(trisH)_2[V^V_{10}O_{28}]$; 2-amp = 2-aminopyridine, tris = tris(hydroxymethyl)aminomethane	decavanadate	(D) methylene blue	m(catalyst) = 2-10 mg; with H_2O_2	93 % removal within 2 min	1	272
$Na_{10}[Co_4(H_2O)_2(V^VW^{VI}_9O_{34})_2]\cdot 34H_2O$	Keggin	(D) methylene blue (D) rhodamine B	c (catalyst) = 10 mg/L	88 % removal within 30 min 88 % removal within 60 min	1	265
$NH_4PW^{VI}_{12}O_{40}$ (PW) $NH_4PMo^{VI}_{12}O_{40}$ (PMo)	Keggin	(IC) Ni^{2+}	m (catalyst) = 30 mg	72 % removal within 1 min (PW) 90 % removal within 1 min (PMo)	1	269
		(D) tetracycline	m (catalyst) = 30 mg	71 % removal within 30 min (PW) 92 % removal within 30 min (PMo)		
α-$H_3PW^{VI}_{12}O_{40}\cdot 6H_2O$ α-$H_3PMo^{VI}_{12}O_{40}\cdot 14H_2O$	Keggin	(D) methylene blue (D) rhodamine B (D) crystal violet (D) methyl orange (D) sunset yellow	m (catalyst) = 5 mg	>90 % removal for all dyes within 30 min	1	277

View Article Online
DOI: 10.1039/D5EN00618B

4 Polyoxometalates in air pollution

Various POMs alone and in combination with other compounds[117,278], such as MOFs, CNTs and mesoporous silica supports, have shown promising results in the removal of air pollutants, such as refractory sulfur compounds[279] from fossil fuels (Section 4.1), toxic gases such as hydrogen sulfide[116] (Section 4.2.1), nitrogen oxides and sulfur dioxide[280] (Section 4.2.2) and carcinogenic volatile organic compounds (VOCs; Section 4.3) present in indoor and outdoor air.[281,282]

Among POM archetypes, Keggin-type structures dominate air purification applications due to their high catalytic activity, particularly in the oxidative desulfurization of refractory sulfur compounds from fossil fuels under mild conditions[61] (~85 % of the reported literature; **Table S1**). Anderson-Evans POMs also contribute effectively to the desulfurization of fossil fuels by showing promising desulfurization performance through alkyl peroxide formation mechanisms with extended catalyst lifetimes.[283,284] Wells-Dawson-type POMs, especially when doped with lanthanide ions, exhibit enhanced regeneration and stability, making them effective for toxic gas removal (Section 4.2; Table 2), such as H_2S, NO_x, and SO_2. Their tunable redox states and structural differences tailor their catalytic behavior, with rare-earth-doped Wells-Dawson POMs[116] showing superior H_2S oxidation and the photocatalytic activity of Keggin/g-C_3N_4 composites enabling efficient VOC removal under visible light.[285,286] These reported examples of using different POM structures highlight the unique functions and advantages that structural diversity in POM chemistry provides for air pollutant remediation.[116,282,283,248,285]

4.1 Removal of refractory sulfur compounds from fossil fuels

The governments worldwide have introduced stricter regulations and restrictions on the amount of sulfur in fuels to ultra-low levels (< 10 ppm).[53] Therefore, the main goal of industry and science is to find a way to make the fuel desulfurization method efficient, inexpensive, clean, and safe.[52,53] Currently, the established industrial standard for fossil fuel desulfurization is hydrodesulfurization (HDS). The HDS method has proven itself to be very effective in removing thiols, inorganic sulfides, and disulfides. However, due to new regulations requiring ultra-low sulfur fuels[53], HDS is insufficiently effective for removing the more difficult-to-remove refractory sulfur compounds. Moreover, HDS is a very expensive method and operates under harsh reaction conditions of 300–400 °C and 30–100 bar H_2 pressure. In contrast, POM-based oxidative desulfurization (ODS) operates under mild conditions (rt–100 °C, atmospheric pressure, H_2O_2/O_2 (**Table S1**)). POMs provide competitive advantages for the needed ultra-low sulfur fuels (< 10 ppm)[53] through their reversible multi-electron redox capability, oxygen-rich surfaces, and high catalytic stability. This eliminates high-pressure H_2 handling and reduces energy demands for heating and compression.[52,61] ODS-based systems achieve 84–98 % sulfur conversion from 3.5 wt % to < 0.5 wt % with 55.57 % energy efficiency, demonstrating superior energy utilization for refractory sulfur compounds like DBTs.[287] Electrochemical regeneration (H_2O_2/O_2) further enhances POM recyclability (in most reported literature: > 95 % recovery, and 10+ cycles, **Table S1**). These data show that the ODS system is more energy cost-efficient for deep desulfurization than HDS.[287,288]

He *et al*. reported a series of Keggin-type $K_x[PMo^{VI}_{12}O_{40}]$ (K_xPMo, x = 1, 2, 3, 4) polyoxometalate salts prepared by hydrothermal synthesis using commercial F127 templates (Pluronic F127). The prepared K_xPMo salts (**Figure 15.A**) were mesoporous with a high surface area (> 40 $m^2 g^{-1}$) and could be successfully utilized for complete ODS of model oil in 1 h. By comparing the catalytic activity of the prepared POM salts, K_4PMo showed the highest activity in the ODS process with a DBT removal rate of 99.5 % within 60 minutes (**Table S1** in Supporting Information, k = 0.076 min^{-1}). A reaction mechanism of DBT oxidation by the K_4PMo/H_2O_2 catalytic system has been proposed (**Figure 15.B**).[289] In addition, the K_4PMo catalyst also showed activity for the removal of other refractory sulfur compounds, DMDBT and BT, with removal efficiencies of 99.0 % and 60.3 %, respectively. The authors concluded that the ODS activity of K_xPMo catalysts has a linear correlation with their electrochemically active surface area (ECSA). The higher activity of the K_4Mo catalyst can therefore be attributed to its largest ECSA value, which shows that K_4PMo exposes the largest number of anions $[PMo^{VI}_{12}O_{40}]^{3-}$ among all prepared catalysts. XRD structural analysis confirmed the good structural stability and successful recovery of the K_4PMo catalyst that was used.[289]

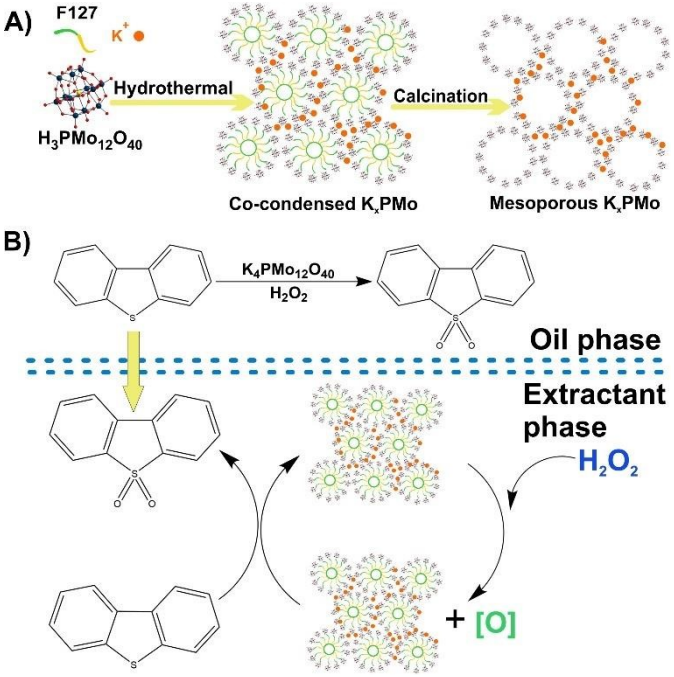

Figure 15. A) Illustration of one-pot hydrothermal synthesis of mesoporous K_xPMo material. The resulting K_xPMo material was highly crystalline with uniform and spherical morphology. It is denoted as K_xPMo, where x denotes the amount of HPMo added to the initial mixture. **B)** A schematic representation of the DBT oxidation mechanism in the presence of H_2O_2 catalysed by K_xPMo. DBT preferentially resides in the biphasic system's oil phase (n-octane), whereas the H_2O_2 oxidant and K_xPMo catalyst primarily reside in the extractant phase (methanol). Therefore, the first step is to extract into the extractant phase to react with H_2O_2 in the presence of K_xPMo.[289]

Besides commonly utilized Keggin-type POMs, other archetypes, especially Anderson-Evans and Wells-Dawson, have also been used in the ODS process. Eseva *et al*. prepared a series of Anderson-type polyoxometalates (**Figure 16**),

View Article Online
DOI: 10.1039/D5EN00964B

$(NR_4)_3[X^{III}Mo^{VI}_6O_{24}H_6]$ (X^{III} = Cr, Fe, Co; R = H or alkyl), and tested their catalytic properties in the ODS process of model fuel. The Co(III)-based Anderson type POM exhibited the highest catalytic activity in the desulfurization of model diesel with a 100 % conversion rate of DBT within 60 minutes with a molar ratio of n(S):n(cat.) = 50:1 (Table S1 in Supporting Information). By prolonging the reaction time to 120 min, 100 % conversion was also achieved for BT. However, for 3-methylbenzene, only 59 % conversion was achieved in 4 h.[283] A reaction mechanism for DBT oxidation by the Co(III)-POM has been proposed (**Figure 16**). The crucial oxidation step in the catalytic system is based on the oxidation of a solvent (decalin), with the formation of an alkyl peroxide as the active species. Alkyl peroxide formation occurs by the reaction with an O_2 molecule from the air in the presence of a Co(III)-POM to form alkyl peroxides and the subsequent formation of the polyoxometalate's metal-dioxo species, as the source of active oxygen in the further oxidation of DBT. The quaternary ammonium cation in the $(NR_4)_3[X^{III}Mo^{VI}_6O_{24}H_6]$ catalyst structure allows the catalyst to adsorb the substrate molecules (DBT) and coordinate with the sulfur atom, after which the coordinated DBT is oxidized to a sulfone, thus simultaneously reducing $(NR_4)_3[Co^{III}Mo^{VI}_6O_{24}H_6]$ POM. The reduced form of $(NR_4)_3[Co^{III}Mo^{VI}_6O_{24}H_6]$ POM is re-oxidized with a new peroxide molecule, and a new catalytic cycle is started.[283]

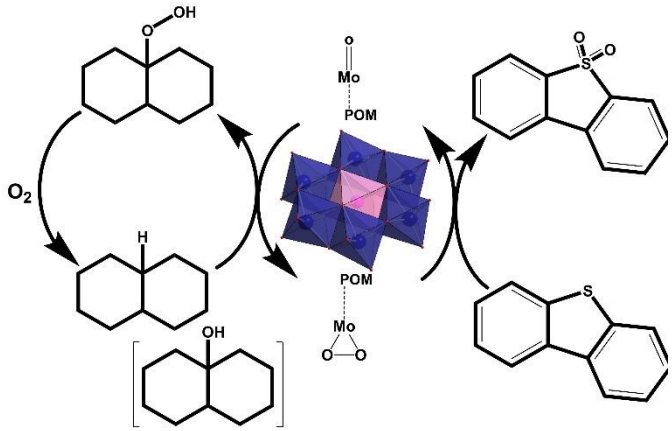

Figure 16. A schematic representation of DBT oxidation mechanism catalyzed by Anderson-type polyoxometalates ($(NR_4)_3[X^{III}Mo^{VI}_6O_{24}H_6]$ (X = Cr, Fe, Co; R = H or alkyl)) in the presence of O_2 from air.[283]

Hybrid POM-based materials have also been researched and have shown promising results as catalysts in ODS processes. Chi *et al*. reported the preparation of a new biomimetic catalytic system consisting of an Anderson-type POM ($[Na_3H_6Cr^{III}Mo^{VI}_6O_{24}]$) and deep eutectic solvents (DESs) and its successful application as a catalyst for the removal of sulfur compounds from both model and commercial diesel.[284] Six different DESs (PEG/PAS, PEG/SSA, PEG/SA, PEG/DHBA, PEG/PXA and PEG/DL-MA) were combined with $CrMo_6$ (**Figure 17**), and their activity was tested. Only the addition of PEG/SSA, DES, containing an -SO_3H group, resulted in 100% sulfur removal, while utilizing other DESs resulted in no higher than 30 % sulfur removal.[284] The desulfurization process followed the extraction-oxidation mechanism in which the POM and the DES acted as the electron transfer mediators and were both crucial for the process (**Figure 17**).[284]

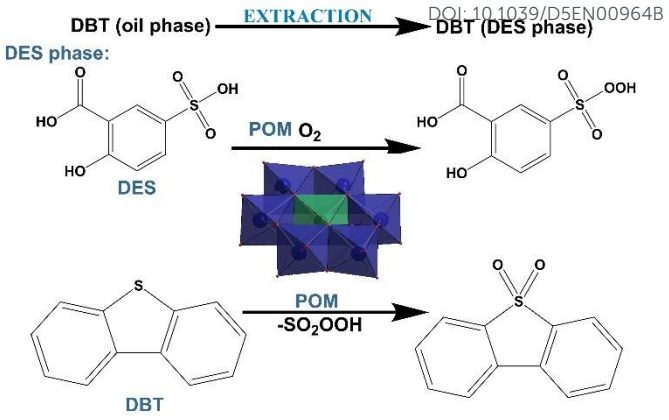

Figure 17. Schematic representation of the reaction mechanism for the oxidation desulfurization of DBT catalysed by coupling $CrMo_6$ polyoxometalate with DESs under mild conditions (T = 60 °C).[284]

Ye *et al*. designed a new porous POM-based hybrid material by encapsulating a Keggin-type polyoxometalate $[H_3PW^{VI}_{12}O_{40}]$ (PW) in the metal-organic framework UiO-66(Zr) and employed it as a catalyst in the ODS reaction of BT, DBT, and DMDBT at room temperature, with 98.2 % DBT removal efficiency.[290] A proposed reaction mechanism includes the extraction of DBT molecules from the model oil into the acetonitrile phase by the POM catalyst and H_2O_2. After extraction, DBT and H_2O_2 can be adsorbed into the catalyst pores, leading to the formation of •OH radicals via electron transfer from Zr-OH_2 active centers in UiO-66 (Zr). Another H_2O_2 molecule can react with a W(VI) metal ion in the $[H_3PW^{VI}_{12}O_{40}]$ POM to form the W(VI)-peroxo species that lead to the formation of $O_2^{\bullet-}$ radicals. Both $O_2^{\bullet-}$ and •OH radicals can oxidize DBT to $DBTO_2$. The existence of two types of active centers in the catalyst, W(VI) in $[H_3PW^{VI}_{12}O_{40}]$ and Zr-OH_2 in UiO-66 (Zr), which forms two different active species, is probably responsible for the high efficiency of the catalyst in the ODS process.[290]

For the desulfurization of fossil fuels, Gao *et al*. prepared a series of Wells-Dawson-type POMs $[H_{6+n}P_2Mo^{VI}_{18-n}V^{V}_{n}O_{62}{\cdot}mH_2O]$ (n = 1–5; $Mo_{17}V_1$, $Mo_{16}V_2$, $Mo_{15}V_3$, $Mo_{14}V_4$, and $Mo_{13}V_5$), immobilized them on CNT carriers, and thereby prepared two different types of catalysts, CNT@PDDA@POM and POM@CNT.[291] All prepared POM-based materials have shown to be catalytically active in the ODS process. CNT@PDDA@$Mo_{16}V_2$ showed the highest catalytic activity with 99.4 % desulfurization efficiency. The better efficiency of this type of catalyst was due to a different POM position in CNT@PDDA@POM (on the surface of CNT@PDDA) compared to POM@CNT (deep in the CNTs' channel). Moreover, it was observed that the number of Mo centers replaced with V centers affects the efficiency, with a 16:2 ratio being the optimal Mo:V ratio for obtaining a high desulfurization activity of both catalysts. By combining CNT carriers with high mechanical properties, high thermal stability, and a high specific surface area, Gao *et al.* overcame disadvantages such as a low specific surface area and the difficulty of reclamation for pure POMs.[291] More literature-known POM-based catalysts and their

View Article Online DOI: 10.1039/D5EN00964B

efficiency in the removal of refractory compounds from fossil fuels are summarized in **Table S1** in the Supporting Information.

4.2 Removal of toxic gases - H_2S, NO_x and SO_2

4.2.1 Hydrogen sulfide (H_2S) in air pollution. Hydrogen sulfide is naturally present in crude petroleum, natural gas, volcanic gases, and geothermal sources. It is also a common by-product of many human activities, such as wastewater treatment[292], fossil fuel combustion[54], sewage treatment facilities[55], paper factories[56], food processing factories, and agriculture.[57] Hydrogen sulfide is an odorous toxic gas with a corrosive nature and an adverse effect on human health and directly affects industrial production by reducing industrial catalysts' efficiency and causing equipment failure. It can also easily oxidize and form SO_2 gas (**Eq. 1**), one of the leading causes of acid rain:[58]

$$H_2S + 3/2\ O_2 \rightarrow SO_2 + H_2O \quad \textbf{(Eq. 1)}$$

Furthermore, hydrogen sulfide readily reacts with metals, such as copper, and forms the corresponding sulfides (Cu_2S) on the surface of electrical devices, causing electrical failures. H_2S can also cause corrosion on surfaces, which can cause damage to buildings, for example, sewage plant facilities.[293] In addition to SO_2 (Section 4.2.2), H_2S can react with different compounds present in the atmosphere and form many other toxic by-products, such as carbonyl sulfides (**Eq. 2**), carbon disulfides (**Eq. 3**), sulfurous acid (**Eq. 4**), and PMs, that have been linked to ozone layer depletion:[294]

$$H_2S + CO_2 \rightarrow COS + H_2O \quad \textbf{(Eq. 2)}$$
$$2H_2S + CH_4 \rightarrow CS_2 + 4H_2 \quad \textbf{(Eq. 3)}$$
$$2H_2S + 3O_2 \rightarrow 2H_2SO_3 \quad \textbf{(Eq. 4)}$$

Scientists and engineers have developed different methods for removing H_2S from the environment, such as metal oxide oxidation[295], adsorption using different adsorbents (activated carbon or wet scrubbing)[296], the Claus process[297], biofiltration, oxidative desulfurization, and the LRSR process[298]. The latter two methods are recently the most commonly used methods with a very high desulfurization capacity and efficient production of elemental sulfur using various redox mediators (e.g., Fe(III)/Fe(II)).[298] Such mediators have shown outstanding results, but they are still mostly chemically unstable and require low pH, which is unfavorable for H_2S removal processes.

POMs and different POM-based hybrid materials have shown high efficiency in H_2S removal due to their redox properties and structural stability. For the regeneration of these POM-based catalysts, a redox-mediated electrochemical regeneration method using oxidants such as H_2O_2 or O_2 has recently been shown to be effective.[280]

A purely inorganic POM was applied by Pei *et al*. who successfully synthesized a set of rare-earth Dawson-type polyoxometalates ($K_{17}[Pr^{III}(P_2Mo^{VI}_{17}O_{61})_2]$ (PrPMo), $K_{17}[Gd^{III}(P_2Mo^{VI}_{17}O_{61})_2]$ (GdPMo), $K_{17}[Sm^{III}(P_2Mo^{VI}_{17}O_{61})_2]$ (SmPMo) and $K_{17}[Eu^{III}(P_2Mo^{VI}_{17}O_{61})_2]$ (EuPMo)) and utilized them in the removal of H_2S. Due to the excellent redox properties of Ln(III)-doped POMs, the influence of different Ln(III) species on H_2S removal was investigated. From the experimental results, the prepared compounds were ranked according to their efficiency for the removal of H_2S in the following order: PrPMo (90 %) > EuPMo (88 %) > SmPMo (87 %) > GdPMo (85 %). The PrPMo polyoxometalate showed the best desulfurization and regeneration properties with 90 % efficiency at 25 °C within 400 min. The XPS spectral analysis showed that H_2S is first oxidized to S by a redox reaction with PrPMo, in which Mo(VI) is simultaneously reduced to Mo(IV). During the electrochemical regeneration of PrPMo, S is further oxidized to SO_4^{2-} as the main desulfurization product, and Pr(IV) is reduced to Pr(III) during the regeneration process. The results of repeated XPS measurements confirmed the successful regeneration of PrPMo.[116]

Ma *et al*. described a new approach for an H_2S oxidation and sulfur recovery system using the hybrid POM-based hybrid materials, $[C_4mim]_3PMo^{VI}_{12}O_{40}$-ILs ($[C_4mim]^+$ = 1-butyl-3-methylimidazolium cation), where they investigated the influence of several different $[C_4mim]^+$-based ionic liquids (ILs), $[C_4mim]Cl$, $[C_4mim]BF_4$, $[C_4mim]PF_6$ and $[C_4mim]NTf_2$. Of all the POM-IL systems tested, the $[C_4mim]_3PMo^{VI}_{12}O_{40}$-$[C_4mim]Cl$ system has shown to be the most effective for removing H_2S, with 100 % efficiency. The adsorption mechanism of H_2S desulfurization is explained by the theory of cavities and the strong interaction between H_2S and Cl^-. Additionally, they confirmed that the POM-IL material could be successfully recovered more than six times without losing its efficiency.[299]

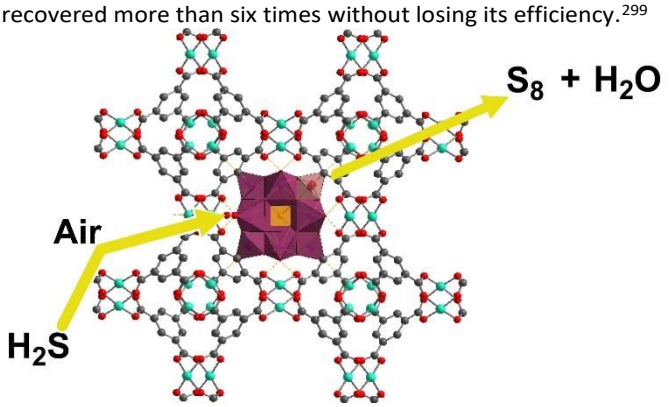

Figure 18. Crystal structure of POM-MOF ($[\{(CH_3)_4N\}_4CuPW_{11}O_{39}H]$) material. The $[CuPW_{11}O_{39}]^{5-}$ polyhedra are orientationally disordered into the pores. It was concluded that the catalytic decomposition of H_2S was taking place inside the pores.[300]

Song *et al*. prepared a POM-based metal-organic framework $[\{(CH_3)_4N\}_4CuPW^{VI}_{11}O_{39}H]$ (POM-MOF) hybrid material (**Figure 18**) by combining a Keggin-type polyoxometalate $[CuPW^{VI}_{11}O_{39}]^{5-}$ and MOF-199.[300] The POM-MOF/O_2 catalytic system effectively oxidizes H_2S to solid S_8 with up to 95 % H_2S removal efficiency. Additionally, it has been shown that the POM-MOF system can successfully oxidize mercaptans to disulfides. The POM-MOF catalyst can be successfully reused in the oxidation process after simple filtration, washing, and drying. The UV-VIS and FT-IR spectra showed that the $[CuPW^{VI}_{11}O_{39}]^{5-}$ structure was preserved in the POM-MOF catalyst at pH 11 for at least 12 h. The POM-MOF hybrid material showed better stability and pH resistance than the $[CuPW^{VI}_{11}O_{39}]^{5-}$ POM alone.[300]

View Article Online DOI: 10.1039/D5EN00964B

A summary of literature-reported POMs and POM-based hybrid materials and their efficiencies in H_2S removal are given in **Table 2** at the end of Section 4.

4.2.2 Nitrogen oxides (NO_x) and sulfur dioxide SO_2 in air pollution. Interest in NO_x emissions and their regulation began after 1952 with the confirmation of their role in the formation of photochemical smog.[301] Several different nitrogen oxides are present in the atmosphere, e.g., N_2O, NO, NO_2, N_2O_3, N_2O_4, NO_3, and N_2O_5. However, NO_x mainly refers to NO and NO_2 oxides because nitrogen oxides are primarily released into the environment in these forms, and NOx emissions contain 95 % NO and 5 % NO_2.[302] NO is considered less toxic than NO_2 and can cause eye irritation, but NO_2, even at low concentrations, can cause acute lung injury with pneumonitis[303] and fulminant pulmonary edema.[304] In urban areas where a higher concentration of NO_2 gas present, many respiratory and cardiovascular diseases and even increased mortality among the exposed population have been observed.[303,305]

Moreover, H_2S and NO_x gases are considered to be among the major air pollutants because they are thought to be responsible for various environmental issues, such as photochemical smog, acid rain[306], tropospheric ozone[307], ozone layer depletion, and even global warming, as a result of N_2O.[308,309] NO_x gases are also associated with the greenhouse effect, and in the higher layers of the atmosphere, they can react with various compounds present there (O_3, VOCs, etc.), leading to ozone depletion. Most air pollution occurs and remains within the lowest layer of the atmosphere, the troposphere. NO_x gases can lead to the formation of tropospheric ozone after photochemical degradation to NO (**Eq. 5**):

$NO_2 + h\nu\ (\lambda<440\ nm) \rightarrow NO + O$ (**Eq. 5**)

$O + O_2 \rightarrow O_3$ (troposphere) (**Eq. 6**)

With NO not absorbing radiation above 230 nm and thus not acting as an inhibitor in the lower atmosphere, the resulting atomic oxygen reacts with O_2 in the troposphere to form ozone (**Eq. 6**), leading to the tropospheric ozone formation.[301,307] Great efforts have been made to develop methods for removing NO_x from the atmosphere in the last few decades.[306,310,311] Adsorptive-desorption methods[307,309] and Fenton-like reactions[285], as examples of AOPs, have been extensively studied for the removal of NO_x and SO_2 gases. The Fenton-like oxidation process consists of oxidation and degradation of different pollutants in the presence of a catalyst and H_2O_2 as an oxidant activated by UV-light irradiation. [280,311]

In the oxidation process, the generated reactive $^{\bullet}OH$ radicals (**Eq. 7**) oxidize a wide range of different substrates. Such radical-assisted oxidation processes have been shown to be particularly effective in removing organic dyes, phenols, antibiotics, and insecticides from wastewater and are a popular research topic for pollution removal applications.[212]

$H_2O_2 + hv(cat.) \rightarrow 2\ ^{\bullet}OH$ (**Eq. 7**)

Zhao *et al*.[312] reported the synthesis of an iron-substituted Keggin-type polyoxometalate-based catalyst Fe^{III}AspPW from ferric chloride ($FeCl_3$), aspartic acid (Asp), and phosphotungstic acid ($[H_3PW^{VI}_{12}O_{40}]$). The Fe^{III}AspPW was used to activate H_2O_2 to form active $^{\bullet}OH$ species, which are crucial for the removal of NO from flue gas. The proposed catalytic mechanism consists of two redox cycles that occur on the surface of the Fe^{III}AspPW catalyst: the redox cycles of $Fe^{III} \leftrightarrow Fe^{II}$ and $POM \leftrightarrow POM^{-}$. In the Fenton-like process, first, in the redox cycle of $Fe^{III} \leftrightarrow Fe^{II}$, Fe^{3+} reacts with H_2O_2 to first form $HOO^{\bullet}$ (**Eq. 8**) and then $^{\bullet}OH$ (**Eq. 9**) active species:

$Fe^{3+} + H_2O_2 \rightarrow Fe^{2+} + H^+ + HOO^{\bullet}$ (**Eq. 8**)

$Fe^{2+} + H_2O_2 \rightarrow Fe^{3+} + OH^- + {}^{\bullet}OH$ (**Eq. 9**)

$Fe^{3+} + HOO^{\bullet} \rightarrow Fe^{2+} + H^+ + O_2$ (**Eq. 10**)

$Fe^{2+} + HOO^{\bullet} + H^+ \rightarrow Fe^{3+} + H_2O_2$ (closing the cycle) (**Eq. 11**)

In the $POM \leftrightarrow POM^{-}$ redox cycle, the POM component is firstly reduced to the POM^{-} form in a reversible reaction, and then the reduced POM^{-} form further reacts with H_2O_2 to form active $^{\bullet}OH$ species (**Eq. 13**). In addition, to close the redox cycle, POM^{-} is oxidized by O_2 or $O_2^{\bullet}$:

$Fe^{2+} + POM \rightleftarrows POM^{-} + Fe^{3+}$ (**Eq. 12**)

$POM^{-} + H_2O_2 + H^+ \rightarrow POM + H_2O + {}^{\bullet}OH$ (**Eq. 13**)

$POM^{-} + O_2 \rightarrow POM + O2^{\bullet-}$ (**Eq. 14**)

$POM^{-} + O_2^{\bullet-} + 2H^+ \rightarrow POM + H_2O_2$ (**Eq. 15**)

This catalytic system showed great activity for removing NO with 94.6 % efficiency.[312] Moreover, Liu *et al*. showed that the Fe^{III}AspPW/H_2O_2 catalytic system could also be used to simultaneously remove SO_2 and NO from flue gas in a UV-Fenton-like process with efficiencies of the Fe^{III}AspPW catalyst of 100 % for SO_2 removal and 84.27 % for NO removal.[312] Wang *et al*. presented a series of Ge(IV)-based Keggin-type polyoxometalates (($[H_4GeW^{VI}_{12}O_{40}]$ (HGeW), $[H_5GeW^{VI}_{11}V^{V}O_{40}]$ (HGeWV), $[H_5GeMo^{VI}_{11}V^{V}O_{40}]$ (HGeMoV), $[H_5GeW^{VI}_{9}Mo^{VI}_{2}V^{V}O_{40}]$ (HGeWMoV)) and utilized them in the removal of NO_x pollutants.[313] The adsorption-desorption experiments showed the following adsorption efficiencies for the removal of NO_x gases: HGeW 81.5 %) > HGeWV (74 %) > HGeWMoV (67 %) > HGeMoV (52 %). The Keggin-type polyoxometalate HGeW (**Figure 2.E**) showed the highest NO_x removal activity with 81.5 % removal and 68.3 % N_2 selectivity, of which 65% was from fractionated NO and 35 % NO_2 gas. Additionally, the H_2S removal efficiency of HGeW was compared with that of the parent Keggin $[H_3PW^{VI}_{12}O_{40}]$ (HPW) polyoxometalate (54.1 % efficiency). The FT-IR studies revealed that NO_x is adsorbed on HGeW mainly in the form of NOH^+ and $NO^{\bullet}$ species, but on the HPW, only NOH^+ is observed as the main form during adsorption. Moreover, TPD-MS experiments were carried out to investigate the further decomposition mechanism of NO_x over HGeW and HPW. The TPD-MS analysis showed that while the decomposition products (NO, N_2O, N_2, and O_2) appear in the same order for both HPW and HGeW, they appear at different temperatures, lower in the case of HPW. The NO species appeared at the lowest temperature for both NO_x decomposition experiments. It is believed that a significant part of the NO_x is physically adsorbed onto HPW and HGeW in the

View Article Online
DOI: 10.1039/D5EN00964B

form of NO at a lower temperature. Meanwhile, the later appearing N_2O could be a product of the disproportionation reaction of NO in which N_2 is formed because of the bonding effect of N-atom, which comes from N-O bond breakage. The difference in NO_x removal efficiency and N_2 selectivity between HPW and HGeW could be due to the HGeW's ability to intensively loosen the N-O bond, resulting in easier NO_x decomposition, and by better NO_x adsorption for HGeW in the form of both NO• and NOH$^+$. It is believed that the presence of the Ge(IV) atom instead of P as the central atom plays a significant role in the processes described above.[313]

4.3 Volatile organic compounds in air pollution (VOCs)

4.3.1 Removal of volatile organic compounds - refractory BETX compounds (benzene, ethylbenzene, toluene, and xylenes). VOCs are a group of liquid organic compounds that can easily evaporate at room temperature. In addition to their volatility, this group of compounds has variable lipophilicity, small molecular size, and are uncharged, resulting in inhalation as the primary route of human exposure.[314] VOCs are classified according to molecular structure and functional groups and include aliphatic hydrocarbons, aromatic hydrocarbons, alcohols, ethers, esters, aldehydes, etc. Due to their properties and wide application in different areas of everyday life, they are common indoor and outdoor air pollutants.[314,285] As outdoor pollutants, they result from the development of industry and urbanization, which involves the increased use of fossil fuels in transport, industrial production, and wastewater treatment plants. As indoor air pollutants, VOCs are found in tobacco smoke, various air fresheners and perfumes, paints and coatings, cleaning products, etc., and can be harmful to human health at excessive concentrations.[285,286,314] Especially, the group of so-called refractory BETX compounds, which stands for benzene, ethylbenzene, toluene, and xylenes, is problematic due to their high toxicity and confirmed carcinogenic nature.[285,314] Besides being confirmed carcinogens, depending on the concentration and length of exposure, various consequences of VOCs exposure have been reported: eye and respiratory tract irritation, headache, dizziness, allergic skin reaction, fatigue, memory impairment, loss of consciousness, and even death.[286,315,316]

Various methods[314] have been studied in search of an efficient and affordable method for removing volatile organic compounds (VOCs) from the air, such as condensation, adsorption[317,318], and (photo)catalytic oxidation.[314] Photocatalytic oxidation (PCO) is a promising method for removing VOCs from the air, and so far, TiO_2-based photocatalytic oxidation[318] has mainly been investigated. Due to the tendency to develop a sunlight/visible-light-driven method, TiO_2 has been shown to be a non-ideal photocatalyst due to its poor solar energy utilization.[320] Therefore, there is a need to design new materials that could be successfully applied as photocatalysts for VOCs' photocatalytic oxidation.[315,321]

Meng *et al*. have shown that photoactive PW_{12}/g-C_3N_4 optical films (**Figure 19.B**) can be obtained by combining the Keggin-type POM, $[H_3PW^{VI}_{12}O_{40}]$, with polymeric graphitic carbon nitride (g-C_3N_4) and then successfully utilized them as photocatalysts for the efficient removal of benzene, toluene, and m-xylene. The PW_{12}/g-C_3N_4 optical films showed excellent removal efficiencies for benzene (90.3 %), toluene (100 %) and *m*-xylene (97.5 %). They also demonstrated excellent stability and reusability for up to 30 cycles without signs of activity loss. The results of DMPO spin-trapping ESR measurements indicated that the PW_{12}/g-C_3N_4 films follow a simulated sunlight-driven direct Z-scheme-dictated charge carrier transformation mechanism that accelerates interfacial charge carrier separation and the formation of $O_2^{-\bullet}$ and HO• radicals that are involved in VOCs oxidation. In the suggested mechanism (**Figure 19.A**), charge separation and formation of e_{CB}^--h_{VB}^+ pair occur (photocurrent), resulting in the formation of $O_2^{-\bullet}$ and HO• active species that directly participate in the complete mineralization of VOCs to CO_2 and H_2O (**Figure 19.A**).[286] Also, Gamelas *et al*. presented a series of new cellulose/silica hybrid composites functionalized with different Keggin-type POMs ($[PV^V_2Mo^{VI}_{10}O_{40}]^{5-}$, $[PV^VMo^{VI}_{11}O_{40}]^{4-}$, $[PMo^{VI}_{12}O_{40}]^{3-}$ and $[PW^{VI}_{12}O_{40}]^{3-}$) and investigated their potential application in the catalytic oxidation of VOCs present in urban air.[281] The new cellulose/silica hybrid materials were composed of approximately 56 wt % of polysaccharides, ca. 37 wt % of propylamine-modified silica, 2 wt % of POM, and 5 wt % of hydration water. Catalytic activity experiments were performed by pumping polluted air through Teflon tubes filled with the catalysts and then analyzing the treated air by GC-chromatography.

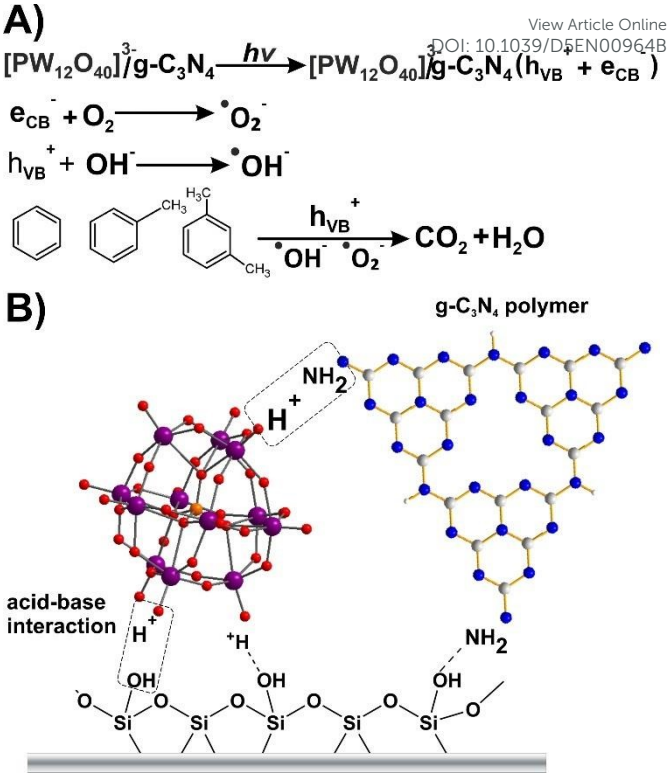

Figure 19. A) Reaction mechanism of photocatalytic oxidation of VOCs catalysed by PW_{12}/g-C_3N_4 films. **B)** Schematic representation of the preparation of PW_{12}/g-C_3N_4 catalyst and its framework structure.[286]

View Article Online
DOI: 10.1039/D5EN00964F

The catalytic activity of the new POM-based hybrid material for VOCs oxidation was visible as a change in the color of the material from yellow to green, indicating the occurrence of V(V)→V(IV) reduction in the POM. The GC-chromatography of a real air sample treated with the new hybrid material indicated complete oxidation of most C_5-C_{11} volatile organic compounds. The successful recovery of the used catalyst was achieved by passing purified air through the Teflon tubes filled with used catalyst, which was noticeable by the color change of the material from green to yellow.[281]

POMs have also proven as suitable adsorbents for adsorption techniques to remove VOCs from the air. Ma *et al*. reported a newly synthesized POM/MOF hybrid material, $K_2[Cu_{12}(BTC)_8{\cdot}12H_2O][HPW^{VI}{}_{12}O_{40}]{\cdot}28H_2O$ or NENU-28 and its possible application as an adsorbent for the adsorption of VOCs, including short-chain alcohols (MeOH and EtOH), cyclohexane, benzene, and toluene.[322] The adsorption capacity of NENU-28 for methanol, ethanol, 1-propanol, 2-propanol, cyclohexane, benzene and toluene was tested in VOCs adsorption experiments. The adsorption amount of MeOH for NENU-28 is 6.70 mmol g^{-1} which corresponds to the adsorption of 37.52 molecules of MeOH per catalyst formula unit. Comparison with the initial MOF ($Cu_3(BTC)_2$), which can adsorb 5.14 mmol g^{-1} methanol (14.36 MeOH molecules per formula unit), shows that POM-functionalized MOFs bring a significant improvement in the adsorption capacity for MeOH. The NENU-28 hybrid material also showed an increase in the amount of adsorbed EtOH (4.78 mmolg^{-1} or 26.77 molecules of EtOH per formula unit) compared to $Cu_3(BTC)_2$ (3.54 mmol g^{-1} or 9.89 molecules of EtOH per formula unit). Although the mechanistic details are not fully understood yet, the results indicate that the presence of the Keggin-type POM [$HPW_{12}O_{40}$] in the NENU-28 has a favorable effect on the adsorption properties of the POM-MOF material.[322]

4.3.2 Removal of aldehydes. Aldehydes, especially formaldehyde and acetaldehyde, are the most common VOCs present in the air as indoor air pollutants.[323] The primary sources of these air pollutants come from building materials, varnishes, and paints, flooring, and furniture materials. Formaldehyde and acetaldehyde are classified as Group 1 carcinogens and are therefore proven harmful to human health.[323,324] Several approaches have been developed to reduce their concentration. They can be divided into passive (e.g., better ventilation, using formaldehyde-free materials) and active (e.g., removal techniques − adsorption and catalytic oxidation) approaches.[323,324] In this section, the focus will be on the development of different active approaches for the removal of aldehydes.

[$H_4SiW^{VI}{}_{12}O_{40}$] and [$K_8SiW^{VI}{}_{11}O_{39}$] (0 % efficiency). Kholdeeva *et al*. developed a new Ce-containing polyoxometalate $NaH_3[SiW^{VI}{}_{11}Ce^{IV}O_{39}]$ (Ce-POM; **Figure 20**)[278] and its dimer in the solid-state, and tested their promising efficiency in the removal of formaldehyde (CH_2O) under mild conditions (20–40 °C). Although the reaction mechanism itself is complex and involves CH_2O autooxidation, the Haber-Weiss radical-chain process,[325] and product formation inhibition, the reaction stoichiometry itself satisfies the equation in **Figure 20**. The efficiency of an unoptimized oxidation process of CH_2O in the presence of Ce-POM/O_2 (efficiency 25 %) was compared to the oxidation of CH_2O in the presence of $Ce(SO_4)_2$ (efficiency 9 %) and in the presence of two POMs without Ce(IV) metal atom. The results of these efficiency comparisons suggested that the activity of the Ce-POM catalyst could be attributed to the synergistic action of the POM and Ce(IV). By optimizing the reaction conditions (adding a small amount of H_2O_2), the conversion efficiency of CH_2O increased from 25 % to 85 % with a yield of 66 % HCOOH in the presence of $NaH_3[SiW^{VI}{}_{11}Ce^{IV}O_{39}]$.[278]

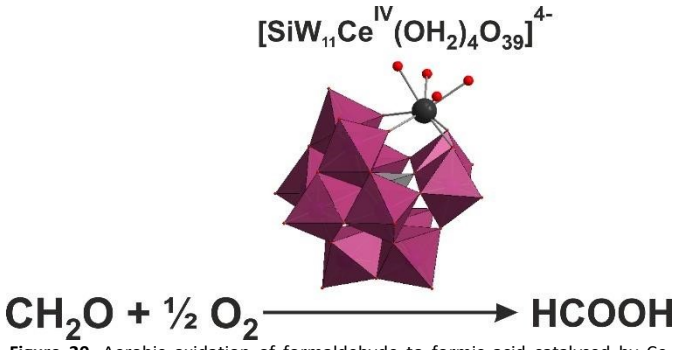

Figure 20. Aerobic oxidation of formaldehyde to formic acid catalysed by Ce-containing Keggin-type POM ($NaH_3[SiW_{11}Ce^{IV}O_{39}]$) under mild conditions (air, T = 25 °C).[278]

Gamelas *et al*. successfully immobilized the α-isomer of the polyoxometalate $[SiW^{VI}{}_9O_{37}Ru^{III}{}_3(H_2O)_3Cl_3]^{7-}$ (Ru-POM) onto a CSH support, obtaining a heterogeneous catalyst Ru-POM-CSH that was active in formaldehyde oxidation.[326] Oxidation of CH_2O was performed at room temperature by flushing an air/formaldehyde gas mixture through a Teflon tube filled with Ru-POM-CSH catalyst or only the CSH carrier without POM. Initially, the CH_2O degradation results for the first two cycles did not differ significantly between CSH and Ru-POM-CSH. This lack of degradation increase could be explained by chemisorption and the reaction between the amino groups of the CSH carrier and CH_2O:

$$Si(O)_3{-}(CH_2)_3{-}NH_2 + CH_2O \rightarrow Si(O)_3{-}(CH_2)_3{-}N{=}CH_2 + H_2O \quad \textbf{(Eq. 6)}$$

After the second cycle, the efficiency of CSH in the removal of CH_2O dropped sharply. By the 4th cycle, it was 0 %, which indicates the simple saturation of the CSH carrier. When Ru-POM-CSH was used as a catalyst, efficiency decreased more slowly, with about an 8 % decrease between cycles after the 5th cycle. No catalyst saturation was observed, which can be attributed to the oxidation of CH_2O catalyzed by Ru-POM. After passing purified air through a Teflon tube containing Ru-POM-CSH material, unlike CSH alone, the material was successfully regenerated. Product analysis revealed that CO_2 and H_2O were the main reaction products formed by catalytic oxidation of CH_2O in the presence of Ru-POM-CSH. These results indicate that the reaction undergoes a predominantly non-radical mechanism because the final product would be formic acid and carbon monoxide in the case of a radical mechanism.[326]

The following mechanism of a CH_2O oxidation reaction in the presence of Ru-POM-CSH was proposed:

View Article Online DOI: 10.1039/D5EN00964B

$POM\text{-}Ru_3^{III}(H_2O) + CH_2O \rightleftarrows POM\text{-}Ru_3^{III}(CH_2O) + H_2O$ **(Eq. 7)**

$POM\text{-}Ru^{III}(CH_2O) \rightarrow HPOM\text{-}Ru_2^{III}Ru^{II} + {}^{\bullet}CHO$ **(Eq. 8)**

The initial step probably involves oxidation of the substrate (CH_2O) by a catalyst through ligand replacement, binding of O_2 to the partially reduced catalyst (**Eq. 9**), and its activation and further reaction with $^{\bullet}CHO$:

$HPOM\text{-}Ru_2^{III}Ru^{II} + O_2 \leftrightarrow HPOM\text{-}Ru_2^{III}Ru^{II}\text{-}O_2 \leftrightarrow HPOM\text{–}Ru_2^{III}Ru^{III}\text{-}O_2{}^{\bullet}$ **(Eq.9)**

$HPOM\text{–}Ru_2^{III}Ru^{III}\text{-}O_2{}^{\bullet} + {}^{\bullet}CHO \rightarrow POM\text{-}Ru_3^{III} + CO_2 + H_2O$ **(Eq. 10)**

The oxidation reaction of CH_2O with Ru-POM-CSH can be summarized as follows:[325]

$CH_2O + O_2 \rightarrow CO_2 + H_2O$ **(Eq. 11)**

Kholdeeva *et al*. also synthesized tetra-n-butylammonium (TBA) salts of Co-substituted Keggin-type polyoxometalates $[TBA_4HPW^{VI}{}_{11}CoO_{39}]$ (**I**) and $[TBA_5PW^{VI}{}_{11}CoO_{39}]$ (**II**) (Co-POM) and immobilized them onto both NH_2^- and NH_3^+ modified mesoporous silica surfaces.[282]

The catalytic activity of the solid Co-POM materials (**I**) and (**II**) was tested for the oxidation of isobutyraldehyde (IBA) and compared with the activity of the homogeneous Co-POM salts (**I**) and (**II**). The results showed that the IBA conversion rate in MeCN under mild conditions (1 atm of air, T = 20–40 °C) without a catalyst was 28 %. In the presence of only the NH_2-modified mesoporous silica support, the IBA conversion rate was only 6 %, indicating that the NH_2^- silica support is an inhibitor of the IBA oxidation. When one of the solid Co-POM catalysts, $[TBA_4HPW^{VI}{}_{11}CoO_{39}]$ (**I**) or the non-protonated $[TBA_5PW^{VI}{}_{11}CoO_{39}]$ (**II**), (immobilized on NH_2^- or NH_3^+-silica support) was added to the reaction mixture, the IBA oxidation to IBAc continued at room temperature. The protonated salt $[TBA_4HPW^{VI}{}_{11}CoO_{39}]$ (**I**) had a higher redox potential and better catalytic activity for IBA oxidation than the non-protonated salt (**II**). The catalytic activity of the immobilized Co-POM (**I**) and the homogeneous salt (**I**) exhibited similar catalytic performance (92 % IBA conversion) for the first two cycles. However, after the third cycle, the immobilized Co-POM (**I**) catalyst lost up to 15 % of its activity due to Co-POM leaching, showing that the homogeneous Co-POM (I) salt had better long-term stability.[282] All literature-known polyoxometalates and their applications in removing aldehydes are summarized in **Table 2**.

4.4 Summary of POM-based technologies in air purification

Various POMs alone and combined with MOFs, CNTs, and mesoporous silica supports show promising results for removing air pollutants including refractory sulfur compounds from fossil fuels (**Section 4.1**), toxic gases like H_2S (**Section 4.2.1**), NO_x/SO_2 (**Section 4.2.2**), and carcinogenic VOCs (**Section 4.3**) in indoor/outdoor air. Keggin-type POM structures dominate oxidative desulfurization of fossil fuels under mild conditions (~85 % of literature; **Table S1**), outperforming traditional HDS processes and avoiding high pressures/temperatures while meeting ultra-low sulfur regulations. Anderson-Evans POMs enable efficient desulfurization through alkyl peroxide mechanisms with extended lifetimes, while lanthanide-doped Wells-Dawson POMs exhibit superior H_2S oxidation and stability for NO_x/SO_2 removal (**Table 2**).

POM-based hybrid materials further enhance performance, such as K_4PMo mesoporous salts for rapid DBT removal (**Table S1**), $PW_{12}/g\text{-}C_3N_4$ films mineralizing BETX VOCs under visible light via Z-scheme mechanism, and POM-MOFs like NENU-28 boosting VOC adsorption (**Section 4.3**). Ce- and Ru-containing Keggin POMs catalyze aldehyde oxidation to CO_2/H_2O at room temperature, with Ru-POM-CSH showing sustained activity over cycles without saturation (**Table 2**). Structural diversity tailors redox properties and active oxygen species (●OH, $O_2{}^{\bullet-}$), addressing key air pollutants effectively.

Table 2. List of polyoxometalates and POM-based materials utilized in air purification. All POMs are ordered chronologically from the most recent to the oldest published paper.

REMOVAL OF H_2S					
Formula	**POM Archetype**	**Conditions**	**Efficiency**	**Number of cycles**	**Ref.**
PMo_{12}@RH-MCM-14; $PMo_{12} = [H_3PMo^{VI}{}_{12}O_{40}]$	Keggin (Figure 2F)	T = rt; t = 120 min; m(catalyst) = 0.3 g; $c_0(H_2S)$ = 1000 mg/m^3; flow rate = 100 mL/min (N_2/H_2S gas mixture)	61.3 % yield of H_2S transformation to S	more than 8	328
$(Himi)_2[S^{VI}Mo^{VI}{}_{12}O_{40}]\cdot(imi)_2\cdot H_2O$; imi = imidazole	Keggin (Figure 2F)	T = 0-50 °C; pH = 4-9; c(POM) = 1 mmol/L; $c(H_2S)$ = 2 g/m^3; flow rate = 100 mL/min (N_2/H_2S gas mixture)	H_2S capacity in water: 627 mg/g; after electro treatment up to 2174 mg/g	4 cycles	329
$(n\text{-}Bu_4N)_3[VMo^{VI}{}_{12}O_{40}]$/[Bmim]Oac; [Bmim] = 1-butyl-3-methylimidazolium	Keggin (Figure 2F)	T = 150 °C; c(POM) = 0.005 mol/L; flow rate = 100 mL/min (N_2/H_2S gas mixture); t = 10 h	98.6 % within 10 h	at least 4 cycles	330
$(NH_4)_{11}[Ln^{III}(PMo^{VI}{}_{11}O_{39})_2]$; Ln = Sm, Ce, Dy and Gd	lacunary Keggin (Figure 2G)	T = rt; pH = 5; t = 360 min; c(catalyst) = 0.002 M; $c_0(H_2S)$ = 2900 mg/m^3	94.8 % within 360 min	at least 4	331

View Article Online DOI: 10.1039/D5EN00964B

$K_{17}[Pr^{III}(P_2Mo^{VI}_{17}O_{61})_2]$, $K_{17}[Gd^{III}(P_2Mo^{VI}_{17}O_{61})_2]$, $K_{17}[Sm^{III}(P_2Mo^{VI}_{17}O_{61})_2]$, $K_{17}[Eu^{III}(P_2Mo^{VI}_{17}O_{61})_2]$	Wells-Dawson (Figure 2H)	T = 25 °C; pH = 6.8; t = 400 min; c(catalyst) = 0.015 M; $c_0(H_2S)$ = 2200 mg/m³	90 % within 400 min	nsp	116
$[C_4mim]_3[PMo^{VI}_{12}O_{40}]$-[C4mim]Cl; [C4mim] = 1-butyl-3-methylimidazolium	Keggin (Figure 2F)	T = 80-180 °C; t = 60 min; H_2S flow rate 100 mL/min; c(catalyst) = 0.001 M	100 % within 60 min	more than 6	299
TM-salts of $[H_4PMo^{VI}_{11}V^{V}O_{40}]$, (TM = Cu^{II}, Fe^{III}, Zn^{II}, Mn^{IV} and Cr^{VI})	Keggin (Figure 2F)	T = 25 °C; t = 300 min; H_2S gas flow = 200 mL/min; $c_0(H_2S)$ = 1241 mg/m³; c(catalyst) = 0.01 M, H_2O_2 – oxidant	98 % within 300 min	nsp	54
PyBs-PW, PhPyBs-PW and QBs-PW; $PW = H_3PW^{VI}_{12}O_{40}$	Keggin (Figure 2F)	T = 70 °C; t = 10 min; $n(H_2S)_0$ = 1 mmol, 30 % H_2O_2 (n = 1 mmol); solvent mixture H_2O/EtOH (v:v = 7:3); m(catalyst) = 80 mg	98 % within 10 min	at least 5	332
$[\{(CH_3)_4N\}_4Cu^{II}PW^{VI}_{11}O_{39}H]$	lacunary Keggin (Figure 2G)	T = rt.; t = 20 h; m(cat.) = 10 mg; $c(H_2S)_0$ = 0.1M	95.0 % within 20 h	at least 2	300
$[Na_2HPMo^{VI}_{12}O_{40}]$	Keggin (Figure 2F)	T = 20 °C; c(catalyst) = 1.25 x 10^{-2} M; $c_0(H_2S)$ = 240.72 mg/m³; H_2S gas flow = 0.5 L/min	sulfur loading capacity of 1.14 mol of H_2S per mol of POM	nsp	333
$[Na_3PMo^{VI}_{12}O_{40}]$, ($[Na_3PMo^{VI}_{12}O_{40}]$:$NaVO_3$:$Na_2CO_3$:NaCl = 1:1:0.377:5.472)	Keggin (Figure 2F)	T = rt; t = 47 min; c(adsorbent) = 5 x 10^{-3} M; $c_0(H_2S)$ = 500.863 mg/m³; H_2S gas flow = 3.931 L/min	up to 99.67 % within 35-50 min	nsp	334
PCDES@3C_{14}-2Im; PCDES = long-chain ionic liquid hybrid POM deep eutectic solvent, POM present as $[C_{14}mim]_3PMo^{VI}_{12}O_{40}$; [$C_{14}$mim] = 1-tetradecyl-3-methylimidazolium	Keggin (Figure 2F)	T= 25-200 °C; c(adsorbent) = 0.01 mol/L; t = 150 min, H_2O_2; 12.93 mg H_2S / g adsorbent	Up to 100 % within 150 min	at least 5	334
PPILs@IBuPN-9; PPILs = phosphazene POM ionic liquid, 1-bityl-3-methylimidazolium chloride with phosphazenes and $H_3PMo^{VI}_{12}O_{40}$	Keggin (Figure 2F)	T = 100 – 200 °C; t = 2 h; c(PPILs@IBuPN-9) = 0.015 mol/L; 21.88 mg H_2S / g PPILs@IBuPN-9	Up to 100 % fpr 120 min	at least 4 cycles	336
PMo_{12}@UiO-66@H_2S-MIP-β-CDs; CD = β-cyclodextrin, MIP = molecular imrinted polymers; UiO-66 = metal-organic framework	Keggin (Figure 2F)	T = room temperature; 31.67 mg H_2S/ g; m(adsorbent) = 0.3 g, H_2S 1000 mg/m³	Up to 31.67 mg/g H_2S within 150 min	5 cycles	337
PMo12-BmimCl@SiO2-0.05 %	Keggin (Figure 2F)	m(PMo12-BmimCl@SiO2-0.05 %) = 5 g; H_2S 1000 mg/m³, flow rate = 100 mL/min; T = 100 – 200 °C; BmimCl = 1-butyl-3-methylimidazolium chloride	97 % desulfurization for 480 min	3 cycles	338
Formula	**POM Archetype**	**Conditions**	**Efficiency**	**Number of cycles**	**Ref.**
REMOVAL OF NO_x AND SO_2					
PW_{12}@Bi_2O_{3-x}/Bi; $PW_{12} = H_3PW^{VI}_{12}O_{40}$, x = nsp	Keggin (Figure 2F)	LED lamp (λ > 420 nm); m(catalyst) = 0.3 mg; c(NO) = 600 ppb (in air mixture), flow rate(NO) = 500 mL/min	83.3 % within 30 min (in gas phase)	nsp	339
$[H_4GeW^{VI}_{12}O_{40}]$(HGeW), $[H_5GeW^{VI}_{11}V^{V}O_{40}]$ (HGeWV), $[H_5GeMo^{VI}_{11}V^{V}O_{40}]$ (HGeMoV), $[H_5GeW^{VI}_{9}Mo^{VI}_{2}V^{V}O_{40}]$ (HGeWMoV)	Keggin (Figure 2F)	T = 100-350 °C; rate = 4 °C/min; t = 90 min; $c(NO_x)$ = 1696 mg/m³; $c(O_2)$ = 8 vol %; $c(H_2O$ vapor) = 5 vol %	81.5 % NO_x removal with N_2 selectivity of 68.3 % within 90 min	at least 3	314
$H_6P_2W^{VI}_{18}O_{62}$·28H_2O	Wells-Dawson (Figure 2H)	T = 50-200 °C; t = 60 min; $c_0(NO_x)$ = 1696 mg/m³; $c(O_2)$ = 8 vol %; c(vapor) = 4.5 vol %	up to 90 % of NO_x adsorption within 60 min	at least 2	340
$[Fe^{III}(C_4H_5NO_4)]_3PW^{VI}_{12}O_{40}]$·14$H_2O$ (Fe^{III}AspPW)	Keggin (Figure 2F)	T = 50 °C; t = 15 min; $c(H_2O_2)$ = 4mol/L; pH = 5.5; $c_0(NO)$ = 603 mg/m³	94.6 % within 15 min	3	312
$Ce^{IV}O_2$/$H_3PW^{VI}_{12}O_{40}$	Keggin (Figure 2F)	T = 160-220 °C; t = 30 min; $c_0(NO)$ = 600 mg/m³; $c(NH_3)$ = 600 mg/m³	90 % NO removal within 30 min	nsp	341

View Article Online DOI: 10.1039/D5EN00964B

$H_4[(Cu_4Cl)_3(BTC)_8]_2[SiW^{VI}_{12}O_{40}]\cdot(C_4H_{12}N)_6\cdot 3H_2O$ (NENU-15)	Keggin (Figure 2F)	T = 20-300 °C; c(NO) = 1.74 mmol/g; m(cat.) = 0.2 g; gas mixture NO (5 %) and He (95 %), gas flow rate = 30 mL/min	NO adsorption efficiency of 1.74 mmol/g of NO at rt, and 64 % efficiency at 300 °C	nsp	342
$[Fe^{III}(C_4H_5NO_4)]_3PW^{VI}_{12}O_{40}] \cdot 14H_2O$, ($Fe^{III}$AspPW)	Keggin (Figure 2F)	T = 65-80 °C; t = 15 min; $c(NO)_{inlet}$ = 614 mg/m³; $c(SO_2)_{inlet}$ = 2094 mg/m³; c(catalyst) = 0.5 g/L	84.27 % (NO) and 100 % (SO_2) within 15 min	3	280
HPW^{VI}-M/$Ce^{IV}_xZr^{IV}_{4-x}O_8$ and HPW^{VI}-M/$Ti^{IV}_xZr^{IV}_{1-x}O_4$ (M = Pt^{IV}, Pd^{II} or Rh^{III} (1 wt %); Zr^{IV}/Ce^{IV} = 0.5; Zr^{IV}/Ti^{IV} = 0.5)	Keggin (Figure 2F)	T = 170-250 °C; t = 31-32 min; m(catalyst) = 300 mg, gas mixture: NO = NO_2 = 500 ppm, O_2 = 10 %, CO_2 = 5 %, H_2O = 5 %	48 % NO_x reduction efficiency and 84 % NO_x storage efficiency within 31-32 min	12	343
$H_3PW^{VI}_{12}O_{40}\cdot 6H_2O$ (HPW)	Keggin (Figure 2F)	T = 80-170 °C; m(HPW) = 330 mg; gas mixture: NO = NO_2 = 500 ppm, O_2 = 10 %, CO_2 = 5 %, H_2O = 5 %	NO_X adsorption amount is equal to 38 mg/g of HPW	6	344
$[(NH_4)_3PW^{VI}_{12}O_{40}]$	Keggin (Figure 2F)	T = 150 °C; t = 60 min; He gas flow = 15 mL/min; $n(NO_2)$ = 17.0 µmol	68 % NO_2 removal within 60 min	3	345
$MnCeO_x$-SiW, where SiW = $H_4[SiW^{VI}_{12}O_{40}]$	Keggin (Figure 2F)	gas mixture: 100 ppm chlorobenzene, 500 ppm NO and 500 ppm NH_3, 11 vol % O_2; T = 120-180 °C; t = 30 min; m(catalyst) = 200 mg	100 % NO and chlorobenzene conversion at 180 °C	nsp	346
10HPW-CS-$Ce_{0.3}$-TiO_2, HPW = $H_3PW^{VI}_{12}O_{40}$, CS = chitosan	Keggin (Figure 2F)	gas mixture: 50 ppm chlorobenzene, 500 ppm NO, 500 ppm NH_3, 5 vol % O_2, and N_2 as balance gas; m(catalyst) = 100 mg; T = 167-291 °C	100 % conversion of NO at 167 – 288 °C, 90 % conversion of chlorobenzene at 291 °C	nsp	347
Formula	**POM Archetype**	**Conditions**	**Efficiency**	**Number of cycles**	**Ref.**
REMOVAL OF ALDEHYDES					
$[SiW^{VI}_9O_{37}Ru^{III}_3(H_2O)_3Cl_3]^{7-}$/CSH; CSH = cellulose propylamine-modified silica	Keggin (Figure 2F)	T = rt; $c(CH_2O)$ = 833 ppm ± 10 %; CH_2O gas flow rate = 0.25 dm³/min; m(catalyst) = 110 mg	44 % for 1st cycle	5	327
$[n\text{-}Bu_4N]_4H_5PW^{VI}_6V^V_6O_{40}\cdot 20H_2O$ (PW_6V_6); $[n\text{-}Bu_4N]_6[PW^{VI}_9V^V_3O_{40}]$ (PW_9V_3); $[n\text{-}Bu_4N]_5H_2PW^{VI}_8V^V_4O_{40}$ (PW_8V_4)	Keggin (Figure 2F)	T = rt; t = 144 h; $c(CH_2O)$ = 0.52 mol/L; P(air) = 1 atm; c(catalyst) = 3.8 mmol/L; solvent – DMA:H_2O (v/v = 20/1); v(solvent) = 2 mL	up to 42 % of CH_2O conversion within 144 h	at least 3	348
$H_5PMo^{VI}_{10}V^V_2O_{40}$/APTS/SBA-15; $H_6PMo^{VI}_9V^V_3O_{40}$/APTS/SBA-15; $H_4PMo^{VI}_{11}V^VO_{40}$/APTS/SBA-15; APTS = γ-aminopropyltriethoxysilane; SBA-15 = aminosilylated silica	Keggin (Figure 2F)	T = 20 °C; t = 24 h; m(catalyst) = 0.1 g; $v(O_2)$ = 500 mL; O_2 – oxidant	up to 73 % acetaldehyde conversion after 24 h	5	349
$NaH_3[SiW^{VI}_{11}Ce^{IV}O_{39}]$	Keggin (Figure 2F)	T = 20-60 °C; t = 5 h; P = 1 atm; $c(CH_2O)$ = 4 mM; c(catalyst) = 5.2 mM; solvent H_2O	85 % CH_2O conversion within 5 h	30	278
$TBA_4HPW^{VI}_{11}Co^{III}O_{39}$	Keggin (Figure 2F)	T = 20-40 °C; t = 6 h; P = 1 atm; m(catalyst) = 100 mg; solvents: MeCN or H_2O	92 % conversion of isobutyraldehyde	at least 3	282

*nsp- not specified by authors

View Article Online
DOI: 10.1039/D5EN00964B

5 Polyoxometalates in sensor applications

Immobilization of POMs on the different supporting surfaces facilitates their electrochemical properties for sensor applications.[350] Numerous methods, such as chemical adsorption[351,352], electrodeposition[353,354], encapsulation[355], the Langmuir-Blodgett process[356,357], and layer-by-layer deposition[358,359], have been used to deposit POMs on electrodes to form monolayer or multilayer structures.[352] As can be seen in **Figure 21**, POM-based sensors are used as the analytical unit, in which the POM is immobilized onto a solid substrate utilized as a transducer. If the POM has been successfully immobilized onto the transducer while preserving its structural integrity, the POM part of the sensor should be able to recognize and catalyze the analyte *via* an induced chemical reaction followed by the transformation of the chemical reaction energy into an electrical signal. The electrical signal is later amplified and converted by signal processing equipment into a display.[349] The POM-based sensors, like other sensors, show all main characteristics such as sensitivity, selectivity, linear range, response time, detection limit, and stability.[360] The most critical properties of most POM-based sensors are selectivity and response rate, and often, they are not addressed by authors. For sensors to have high selectivity, the sensor should have a heightened response to a substrate but an inadequate response to interferences. Recently, it has been shown that these issues could be solved by combining the POMs with organic moieties or CNTs with the addition of noble metal NPs. Generally, the POM-based sensors showed good selectivity and low response time while being stable and active at neutral pH.[360,361]

POM-based sensors operate through a synergistic mechanism that involves redox-driven signal transduction, coordination-induced structural alterations, and catalytic amplification processes. This enables the highly sensitive detection of various chemical and biological analytes. The multi-electron redox functionality of POM clusters allows them to undergo reversible changes in oxidation state upon interaction with target species, resulting in measurable outputs that can be electrochemical, optical, or conductometric. In the realm of electrochemical sensing, POMs facilitate rapid electron transfer at the electrode–analyte interface, a process that can be enhanced through their incorporation into conductive matrices or nanostructured supports, thereby optimizing charge-transfer kinetics and reducing detection limits.[362] Optical sensors utilize intervalence charge-transfer transitions or ligand-to-metal charge-transfer phenomena that occur when analytes interact with or reduce the POM framework, resulting in observable shifts in absorbance or luminescence.[363] Furthermore, the catalytic sensing mechanisms exploit the inherent oxidative or reductive catalytic properties of POMs, where reactions initiated by the analyte generate amplified signals under controlled conditions such as specific pH levels, ionic strength adjustments, or the presence of co-substrates.[364] The overall performance of these sensors is heavily influenced by various experimental factors, including the speciation of POMs, electrode modification strategies, solvent polarity, and the stability range of the POM in the working environment. Consequently, methodological optimization becomes vital for achieving selectivity, reproducibility, and reliability in practical applications.[365]

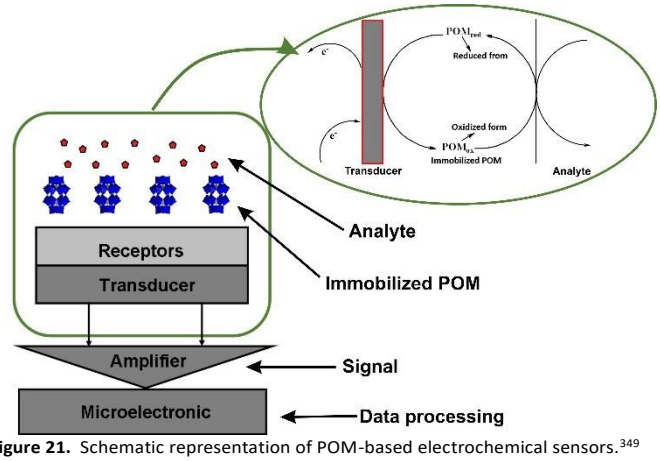

Figure 21. Schematic representation of POM-based electrochemical sensors.[349]

5.1 POM-based sensors in the detection of water pollution

The POM-based sensors have already explored various analyte classes dispersed in either the gas or liquid phase. The electrocatalytic reduction of nitrate, iodate, bromate, nitrite, and hydrogen peroxide by POMs immobilized on a substrate was carried out for sensing applications. Starting with stable Keggin and Dawson type POMs ($[H_3PMo^{VI}_{12}O_{40}]$, $[H_6P_2Mo^{VI}_{18}O_{62}\cdot nH_2O]$, $[H_3PW^{VI}_{12}O_{40}]$, $[P_2W^{VI}_{18}O_{62}]^{6-}$, and α-$[H_4SiMo^{VI}_{12}O_{40}]$) are extensively explored as electrochemical sensors.[361,366–369] Though the sensors showed prominent sensitivity and wide linear range, they operated at a low pH (pH < 2) to stabilize the POM architecture.[370] In 2012, Ma *et al.*[371] synthesized a layer-by-layer composite film using palladium nanoparticles and a Dawson-type POM ($[K_7P_2W^{VI}_{17}O_{61}(FeOH_2)\cdot 8H_2O]$, ($P_2W^{VI}_{17}Fe$)) to determine the electrolytic behavior towards the oxidation of hydrazine sulfate ($N_2H_4SO_4$) and reduction of hydrogen peroxide. The H_2O_2 exhibits sensitivity, detection limit, and linear concentration in the range of 66.7 μA mM^{-1}, 1 μM (S/N = 3), 1.5 μM to 3.9 mM, respectively. Likewise, $N_2H_4SO_4$ displays the same parameter in the range of 0.2 μA mM^{-1}, 1.5 μM (S/N = 3), 2 μM to 3.4 mM, respectively, with sensing response time around 4s.[371] Furthermore, Zhu *et al.*[372] synthesized four Preyssler-type POM-based organic-inorganic crystals to effectively detect non-enzymatic H_2O_2. The compounds exhibit the lowest detection limit of 0.13 mM with a high sensitivity of 4.35 μA mM^{-1} and a response time of 1 s.[372] Ag-doped MoO_3 immobilized on the graphene-like carbon nitride (C_3N_4) was first prepared and employed as an electrochemical sensor by Zhao *et al.*[373] to detect H_2O_2. Herein, $[Ag_6Mo^{VI}_7O_{24}]$/Ag–MOF precursor was used to synthesize the nanoporous structure resulting in a linear detection range of 0.25 μM–0.43 mM towards H_2O_2 owing to its efficient electrocatalytic property.[373] Additionally, isopolymolybdate-based compounds are explored as photoelectric sensors for detecting inorganic ions (e.g., Cr(VI), Hg^{2+}, NO_2^-).[374] Additionally, complex POM structures (*e.g.*, pyrazole derivative Keggin ions,[375] 3D coordination polymers doped with Keggin POM[376] or hourglass-type POM

crystals[377] have been explored as the active electrode for the acute and faster sensing of bromate, nitrate, and heavy, metal ions.

5.2 POM-based sensors in the detection of air pollution

Krutovertsev *et al*. first addressed POM-based gas sensors by employing various Wells-Dawson type POMs doped with polyaniline to detect ammonia gas.[378] POM-doped conducting polymer film is ideal for gas sensing as POMs react with the gas, and conducting polymer substrate converts that into an electrical signal. The recognition of other hazardous gases, such as NO_x, CO, and the vapors of organic solvents, can also be determined because the proton-conducting POMs enhance the material's selectivity and sensitivity.[379,380] Ammam *et al*.[381] recently reported a sensitive and selective NO_x gas sensor using the $[K_6P_2Mo^{VI}_{18}O_{62}{\cdot}H_2O]$ POM and polypyrrole (PPy), exhibiting extended linearities (up to 5500 ppm NO_x). Although all so far mentioned POM-modified electrodes shows catalytic properties and can recognize the analyte, not all can be employed as sensors. In order to achieve a high-performance sensor, the modified electrode should fulfill the conditions of molecular recognition between POMs and specific analytes.[381]
A high-performance gas sensor was developed by Wang *et al.*[382] by using heteropolytungstate (HPT) doped SnO_2 nanorods [HPT abbreviation as $(C_4H_{10}ON)_{23}[HN(CH_2CH_2OH)_3]_{10}H_2[Fe^{III}(CN)_6(\alpha_2\text{-}P_2W^{VI}_{17}O_{61}Co^{II})_4]{\cdot}27H_2O]{\cdot}SnO_2$/HPT composite film, which demonstrated higher photoconductivity than pristine SnO_2 and revealed improved gas sensing for the methylbenzene and formaldehyde at room temperature (25 °C). Electron-hole recombination in the composite was retarded due to the photo-induced transfer of an electron from SnO_2 to HPT. An n-type semiconductor material $BiVO_4$ loaded with different POMs, was exploited as a photo-anode for photoelectrochemical gas sensing capability for NO_2.[382] Among different Keggin type POMs ($[Na_7PW^{VI}_{11}O_{39}]$, $[H_3PW^{VI}_{12}O_{40}]$, $[H_3PMo^{VI}_{12}O_{40}]$, $[Na_{10}SiW^{VI}_{9}O_{34}]$), $[H_3PW^{VI}_{12}O_{40}]$ displayed the highest photocurrent response intensity. In addition, $BiVO_4/[H_3PMo^{VI}_{12}O_{40}]$ demonstrates an enhanced response of 32.8 % toward 50 ppm of NO_2.[383] In similarity with the previous discussion, herein, the electron-hole recombination was slowed down as the POM facilitates charge separation and photogenerated electron transfer to the semiconductor. Shi *et al.*[384] made an interface modification on the grain boundary by integrating TiO_2, and Ti^{IV} substituted POMs ($K_5[PW^{VI}_{11}Ti^{IV}O_{40}]$ and $K_5[PW^{VI}_{10}Ti^{IV}_{2}O_{40}]$). The resultant nanocomposite exhibited improved photoconductivity and elevated gas sensing properties towards acetone gas.[384] Tian *et al*.[385] investigated the effect of $[H_3PW^{VI}_{12}O_{40}]$ doped In_2O_3 compound for gas sensing at room temperature toward formaldehyde. The doping of the POM successfully suppressed the recombination of photo-induced carriers in the system resulting in a 35 % enhancement in photoconductivity alongside a 26 % gas sensing response compared with pristine In_2O_3.[385] Similarly, Wang *et al.*[386] also incorporated $[PW^{VI}_{12}O_{40}]^{3-}$ with Cu_2ZnSnS_4 for high-performance NO_2 gas sensors. The composite exhibited 88.83 % enhanced gas sensing properties compared with pristine Cu_2ZnSnS_4 due to the restriction of electron-hole recombination and effective charge transfer through the POM. Furthermore, Sun *et al.*[387] developed dye-sensitized TiO_2-PW_{12} using a simple, economical sol-gel method followed by a screen-printing technique for faster NO_2 gas sensing at room temperature under visible light irradiation. The heterostructure enabled faster separation and transportation of the photogenerated carriers as the POM acted as the electron acceptors. The effective increase in sensitivity (233.1−1 ppm) over a wide range of NO_2 concentration (50 ppb−5 ppm) for POM decorated dye/TiO_2 film occurred due to the expansion of the narrow bandgap of the POM doped dye under visible light without loss in thermal energy.[387] An inorganic-organic hybrid film was fabricated by Kida *et al.* for selective H_2 (50−500 ppm) and NH_3 (10−100 ppm) sensing using yttrium-stabilized zirconia with $Mo^{VI}_{7}O_{24}^{6-}$/hexylamine hybrid film. Calcination of the POM alkylamine hybrid film resulted in porous MoO_3 particles, making them an effective precursor for synthesizing nanosized metal oxide.[388] POM-based supramolecular chemosensors were developed for the acute gas sensing of toxic gases. Wei *et al.* demonstrated a CO_2 sensor using $Na_9DyW^{VI}_{10}O_{36}$ and block copolymer poly (ethylene oxide-*b*-*N*, N-dimethyl aminoethyl methacrylate).[389] Likewise, Guo *et al.* developed POM-based supramolecular chemosensors for H_2S detection (detection limit 1.25 μM) with dual signals (*via* absorption spectra and fluorescence).[390] In the field, rapid detection of acutely corrosive and toxic gases like H_2S at room temperature is important. Bezdek *et al.* developed enhanced chemiresistive gas sensors to detect H_2S using highly oxidized Pt-doped POM with single-walled CNT. They have also demonstrated ppb level detection with high stability and a wide range of selectivity.[391] Furthermore, Liu *et al.*[392] immobilized POMs on a polyelectrolyte matrix and then used them for the sensitive detection of NO. The ability to electrocatalyze the reduction of NO resulted in a wide range of selectivity (1 nM to 10 μM).[392] Triethylamine gas sensors developed by *Cai et al.*[393] exhibited ultra-sensitive selectivity and stability over repeated use. One-dimensional heterostructure nanofibers of ZnO and $ZnWO_4$ were synthesized *via* POM (varying the molar ratio of $H_3PW^{VI}_{12}O_{40}$) assisted electrospinning methods. The highly porous structure of the nanofibers and the synergistic effect between the ZnO and $ZnWO_4$ resulted in an enhanced relative response of 108.5 for 50 ppm triethylamine. The barrier-control electron transfer at the interface was attributed to remarkable selectivity with a low detection level of 150 ppb.[393] The recent advances led Tian *et al.*[394] to fabricate POM-semiconductor heterojunctions via a one-step coaxial electrospinning technique for the effective sensing of ethanol gas. One-dimensional tandem heterojunctions SnO_2/POM/WO_3 significantly increased the sensing characteristics compared with the SnO_2/WO_3 nanofibers. The sensitivity was optimized to 100 ppm of ethanol. The construction of the interface allowed the POM to act as the electron acceptor, promoting faster carrier separation and exhibiting enhanced sensing behavior.[394] Next, a bottom-up POM-assisted *in-situ* growth of 1D nanofilament architecture was achieved by electrospinning, followed by the thermal oxidation method for the detection of

View Article Online DOI: 10.1039/D5EN00645

acetone. A broad range of concentration, *i.e.*, 50 ppb–50 ppm, was detected with enhanced selectivity and sensitivity owing to the charge transfer to the interface of the ZnO-$ZnMoO_4$ nanofilament.[395] A unique nanostructure was developed by Ren *et al.*[396] using Pt-draped Si-doped WO_3 nanowires interwoven into a three-dimensional mesoporous superstructure for low-temperature ethanol gas sensing (with a detection limit of 0.5 ppm).[396] Selective and ultrasensitive dual detection (Raman and photochromic) of ethylenediamine gas was demonstrated by Zhang *et al.* using POM/viologen hybrid crystal. It exhibits a very low detection limit of 0.1 ppb via Raman signal output.[397]

5.3 POM-based sensors in the detection of emerging health pollutants

Very recently, Wang *et al*.[398] synthesized isostructural Anderson-type POM-based compounds and fabricated photoelectric sensors to detect inorganic ions. Three different transition metal ions (M^{II} = Co^{II}, Cd^{II}, Zn^{II}) were incorporated for the preparation of the $[M_2^{II}(H_3bdpm)_2TeMo^{VI}_6O_{24}.6H_2O]$ (H_3bdpm = 1-1'-bis(3,5-dimethyl-1H-pyrazolatemethane) compounds which contain a 2D supramolecular layer and 1D chain structures. All prepared $[M_2^{II}(H_3bdpm)_2TeMo^{VI}_6O_{24}\cdot6H_2O]$ compounds have been successfully utilized as fluorescence sensors toward $Cr_2O_7^{2-}$ at different concentrations. Furthermore, the compounds with Co^{II} and Cd^{II} also exhibited electrochemical sensing behavior for detecting NO_2^- (Cd-containing compound possesses a response time of 2.16 s at a detection limit of 5.11×10^{-5} M alongside a sensitivity of 43.10 μA mM^{-1}).[398]

POM and Zn-based complexes derived from pyrazole were reported by Tian *et al.* for photocatalysis and electrochemical sensors to detect hydrogen peroxide, bromate, and nitrite by tuning pH.[399] Likewise, Zhang *et al.* tuned the N and O coordination donors in morpholine and piperazine derivatives to derive various POM-based compounds for photocatalysis, electrochemical, and fluorescent sensor applications (towards Hg^{2+}).[400] Furthermore, researchers explored POM-modified MOFs for various sensing applications, e.g., photocatalytic, electrochemical (towards the detection of inorganic ions, H_2O_2, Cr(VI), bromate, *etc*.).[401–405]

All literature known polyoxometalates and their applications in sensing are summarized in **Table 3**.

5.4. Summary of POM-based sensors

POM-based sensors for water pollution, air pollution, and emerging health pollutants are discussed thoroughly. In aqueous sensing, Keggin, Dawson, Preyssler, and isopolymolybdate POMs exhibit strong electrocatalytic activity toward species such as hydrogen peroxide, nitrate, bromate, nitrite, and heavy metal ions, often achieving low detection limits and quick response times. For gas sensing, POM–polymer, POM–metal oxide, and POM–semiconductor heterostructures enable the sensitive and selective detection of gases, including NO_2, NH_3, H_2S, formaldehyde, acetone, ethanol, and volatile amines, mainly by promoting charge separation and reducing electron–hole recombination. Lastly, emerging health-related pollutants are addressed through advanced POM-based supramolecular systems, MOFs, and hybrid complexes that offer electrochemical, photoelectrochemical, and fluorescent sensing modes. Overall, the manuscript highlights the versatility of POMs as functional building blocks for high-performance, multifunctional sensors that operate under mild and environmentally friendly conditions.

Table 3. Summarization of the reported POM-based sensors.

POM-based Composite	POM Archetype	Type of Sensor	Significant Results	Ref.
$(P_2W^{VI}_{17}Fe)$ and palladium NPs; NPs = nanoparticles	Wells-Dawson (Figure 2H)	electrochemical sensor towards H_2O_2 and $N_2H_4SO_4$	The H_2O_2 and $N_2H_4SO_4$ exhibit sensitivity, detection limit, and linear concentration in the range of 66.7 μA mM^{-1}, 1 μM (S/N = 3), 1.5 μM to 3.9 mM, and 0.2 μA mM^{-1}, 1.5 μM (S/N = 3), 2 μM to 3.4 mM, respectively.	36
$[M^{n+}(H_2O)P_5W_{30}O_{110}]^{(15-n)-}$	Preyssler-type	electrochemical sensor towards H_2O_2	exhibit the lowest detection limit of 0.13 mM with a high sensitivity of 4.35 μA mM^{-1} and response time of 1 s	369
$K_6P_2Mo^{VI}_{18}O_{62}.H_2O$ with polypyrrole	Wells-Dawson (Figure 2H)	NO_x gas sensor	exhibits extended linearities up to 5500 ppm NO_x	374
SnO_2/HPT composite film	Keggin (Figure 2F)	gas sensor for the formaldehyde and methylbenzene	higher photoconductivity compared with pristine SnO_2	375
$BiVO_4/H_3PW^{VI}_{12}O_{40}$	Keggin (Figure 2F)	NO_2 gas sensor	enhanced response of 32.8 % towards the 50 ppm of NO_2	376
$[M_2^{II}(H_3bdpm)_2TeMo^{VI}_6O_{24}.6H_2O]$; H_3bdpm = 1-1'-bis(3,5-dimethyl-1H-pyrazolatemethane	Anderson-Evans (Figure 2I)	photoelectric sensors for the detection of inorganic ions	Cd-based compound possesses a response time of 2.16 s at a detection limit of 5.11×10^{-5} M with a sensitivity of 43.10 μA mM^{-1}	377
$BiVO_4/(H_3PW^{VI}_{12}O_{40}$ or $H_3PMo^{VI}_{12}O_{40}$ or	Keggin (Figure 2F)	NO_2 gas sensor	$BiVO_4/PW_{12}$ exhibits highest response of 32.8 % towards 50 ppm of NO_2	379

View Article Online
DOI: 10.1039/D5EN00964B

$Na_7PW^{VI}_{11}O_{39}$ or $Na_{10}SiW^{VI}_{9}O_{34}$)				
$TiO_2/[PW^{VI}_{11}TiO_{40}]^{5-}$ and $TiO_2/[PW^{VI}_{10}Ti_2O_{40}]^{7-}$	Keggin (Figure 2F)	acetone gas sensor	low detection concentration level of acetone is 50 and 80 ppm for$TiO_2/[PW^{VI}_{11}TiO_{40}]^{5-}$ and $TiO_2/[PW^{VI}_{10}Ti_2O_{40}]^{7-}$, respectively	380
$H_3PW^{VI}_{12}O_{40}$ doped In_2O_3 compound	Keggin (Figure 2F)	gas sensor for the formaldehyde at room temperature.	35 % enhancement in photoconductivity alongside a 26 % of gas sensing response compared with pristine In_2O_3	381
$H_3PW^{VI}_{12}O_{40}$ with Cu_2ZnSnS_4	Keggin (Figure 2F)	NO_2 gas sensor	exhibits 88.83 % enhanced gas sensing property compared with pristine Cu_2ZnSnS_4	382

6 Polyoxometalate based battery and supercapacitors

POMs emerge as an exceptional electrode component for supercapacitors (SCs) or batteries due to their high proton mobility and extraordinary redox chemistry.[406–408] POM's variable redox activities and outstanding electron/proton transport capacities apply POM-based composite materials in electrochemical fields. As a powerful electron reservoir in the multi-electron reduction process, POM enables high proton conductivity even in the composite. This interesting behavior has led to various applications of POM-based composites such as green catalysis, sensors, and electrochemical energy storage devices (batteries and SCs). However, POMs are pH-sensitive; therefore, a well-known strategy of coordination chemistry has been used to enhance the mechanical and electrochemical properties of the electrode material for better performance.[407–411]

6.1 POM-based battery electrodes

6.1.1 POM as the electrode for lithium-ion batteries (LiBs).

Transition metal oxides are used as the cathode/anode material for LiBs as they are oxidized to their highest oxidation state when the Li has been released.[412] The first reported POMs for LiB are focused on polyoxomolybdates.[413] Further improvements of the electrode material have been made by modifying the structural and electronic states of POMs, altering the reversible faradaic reaction associated with them. Vanadium-based POMs are being explored as cathode materials for rechargeable batteries to achieve high energy and power density by multi-electron redox processes via fast transfer of Li ions. Chen *et al*.[414] reported $Li_7[V^V_{15}O_{36}(CO_3)]$ as a cathode material with a specific capacity of 250 mA h g^{-1} alongside energy and power densities of 1.5 kW h L^{-1} and 55 kW L^{-1}, respectively. Additionally, $Li_7[V^V_{15}O_{36}(CO_3)]$ exhibits a very high potential window (1.9 to 4.0 V) for reversible redox reactions. The theoretical calculation for the specific capacity for the oxometalate mentioned above at the same potential window (by considering n is 14, which is the next nearest integer no. of electrons) shows the specific capacity of 259 mA h g^{-1}, which is in corroboration with the experimental data.[414] Further, the vanadium-based $K_7[NiV^V_{13}O_{38}]$ structure is explored by Ni *et al*.[415] The maximum discharge capacity of 218.2 mA h g^{-1} was recorded at a discharge current density of 17 mA g^{-1} with 93.2 % coulombic efficiency.[415] Thus, the nano-sized polyoxovanadates can be utilized as cathode materials for LiBs for moderate capacity and rate capability.

Furthermore, POMs are combined with carbonaceous nanostructures for better cycle and rate performance. Ma *et al*.[416] synthesized covalent functional pyrene (Py) with $[H_4SiW^{VI}_{12}O_{40}]$ (SiW_{12}) and attached it to the surface of SWCNTs *via* spontaneous adsorption. SWCNT/Py-SiW_{11} exhibited an initial discharge capacity of 1569.8 mA h g^{-1} at a current density of 0.5 mA cm^{-2}. However, the capacity decreased to 580 mA h g^{-1} after 100 cycles at the same current density.[416] Graphene sheets are represented by single-layer two-dimensional sp^2-bonded carbon atoms, having a high affinity towards POMs. Wang *et al*.[417] synthesized environmentally friendly nanomaterials by incorporating reduced graphene oxide (rGO) with Keggin type $[H_4SiW^{VI}_{12}O_{40}]$ (SiW_{12}) clusters. rGO/SiW_{12} exhibits a discharge capacity of 275 mA h g^{-1} with an increased potential of 4 V at a current density of 50 mA g^{-1}. The nanocomposite can hold a capacity of 120 mA h g^{-1} at 1.5 V operating potential even at a high current density of 2000 mA g^{-1}.[417] Besides carbonaceous nanostructures, POMs are often synthesized with silver nanoparticles due to their chemical structure, elevated surface area, and high electrical conductivity.[418,419]

In recent years, the POM-based composite structure has been further modified by including MXenes, e.g., i) POM@PANI/$Mo_2TiC_2T_x$MXene/CNTs delivers lithium storage capacity of 621 mA h g^{-1} at 0.1 A g^{-1} and promising cyclic stability (445 mA h g^{-1} after 1000 periods at 1.0 A g^{-1})[390]; and ii) PMo_{12}@PPy/$Ti_3C_2T_x$ delivers high capacity of 764 mA h g^{-1} at 0.1 Ag^{-1} with long cycling stability of 2000 cycles at 3 A g^{-1}.[420] Additionally, the hybridization of various POMs with different supports such as porphyrins[420], CoS_2/MoS_2/functionalized rGO[421], and various MOFs[422–425] results in enhanced lithium capacity and overall stability as an anode.

6.1.2 POM as the electrode for sodium-ion batteries. Besides LiBs, POM-based composites are applied as cathode/anode material for Na-ion batteries. Liu *et al*.[426] prepared a robust composite by coating $Na_2H_8[MnV^V_{13}O_{38}]$ (POM) clusters on the graphene nanoflakes. The discharge process of the composite demonstrates a two-phase reaction due to the presence of V(V)/V(IV) redox couple related to Na-ion insertion, and a high capacity of 202 mA h g^{-1} is recorded at 1.5 V (at the end of the

View Article Online
DOI: 10.1039/D5EN00964B

discharge). Furthermore, the composite can retain 81 % of its initial capacity over 100 cycles at 0.2 C with 95 % coulombic efficiency.[426] Hartung *et al*.[427] reported that the sodium salt of decavanadate, $Na_6[V^V_{10}O_{28}]$, acts as a high-performance cathode material for rechargeable Na-ion batteries. The potential discharge range observed from the CV graph is within the range of 0.01−3.0 V. The capacitive process associated with the $Na_6[V^V_{10}O_{28}]$ ion is completed by the insertion of the Na ion in the voids of $[V^V_{10}O_{28}]^{6-}$ cluster.[427]

Additionally, MOFs are proven to be effective supporting materials for POMs. Using a simple impregnation strategy, Cao *et al*.[428] demonstrated that PMo_{12}/MIL-88B/GO composite delivers an excellent specific capacity of 214.2 mA h g^{-1} for 600 cycles at 2 A g^{-1}. Another example is a layer-by-layer arrangement of vanadium-based POM immobilized on Co-based MOF resulted in a capacity of 413 mA h g^{-1} due to accommodating the larger Na^+ ions efficiently.[428]

6.2 POM-based supercapacitor electrodes

Electrochemical capacitors or SCs, on the other hand, are promising energy storage devices that meet a significant performance gap between batteries and electrostatic capacitors. They supply high-power electric pulses over a short time scale, exhibiting a high dynamic of charge propagation with elevated charge and discharge rates.[429] In the maximum reported SC, high capacitance and energy are achieved by incorporating a pseudocapacitive or faradaic type of active material with a double-layer capacitive component. Mostly, metal oxides and sulfides show promising results for SC electrodes as they generate a large number of charges at the electrode interface via multi-step reversible redox reactions.

6.2.1 Composite-type hybrid electrode. Early in 2005, Gómez-Romero et al.[407] established the POM-based composite hybrid electrode for SC as they dispersed three different POMs, namely, $[H_3PW^{VI}_{12}O_{40}]$, $[H_4SiW^{VI}_{12}O_{40}]$, and $[H_3PMo^{VI}_{12}O_{40}]$, in the conducting polymer PANI. The highest specific capacitance of 120 F g^{-1} with cycle stability over 1000 cycles was observed for PANI/$[H_3PMo^{VI}_{12}O_{40}]$, which is higher than the other two POM ($[H_3PW^{VI}_{12}O_{40}]$, $[H_4SiW^{VI}_{12}O_{40}]$) composite, due to the higher proton conductivity of the $[H_3PMo^{VI}_{12}O_{40}]$ in 1 M $HClO_4$ electrolyte.[407] In the later years, the same group deposited $[H_3PMo^{VI}_{12}O_{40}]$ on different conducting polymers (e.g., poly(3,4-ethylenedioxythiophene) (PEDOT)) with an external oxidizing agent (H_2O_2) for further electrochemical improvement (**Figure 22**).[408] Later, the Freund's[430] group used the same Keggin POM, $[H_3PMo^{VI}_{12}O_{40}]$, incorporated into the porous PPy, exhibiting a specific capacitance of 210 F g^{-1} in 0.5 M H_2SO_4 electrolyte in three-electrode configuration.[430] Recently, Vannathan *et al*.[431] reported high-performance pseudocapacitors of vanadium substituted Keggin POMs and combined with a conducting polymer for enhancement of electrochemical activity.[431]

Carbonaceous nanostructures (*e.g.*, CNT, GO/rGO, AC) come into play as the supporting elements to the POMs as they provide better mechanical and electrochemical stability.[429] To replace the conducting polymer as a supporting element for POM, inventors need a high electrical conducting substrate like the former. CNTs exhibit higher electrical conductivity due to their hierarchical architecture among all the carbonaceous

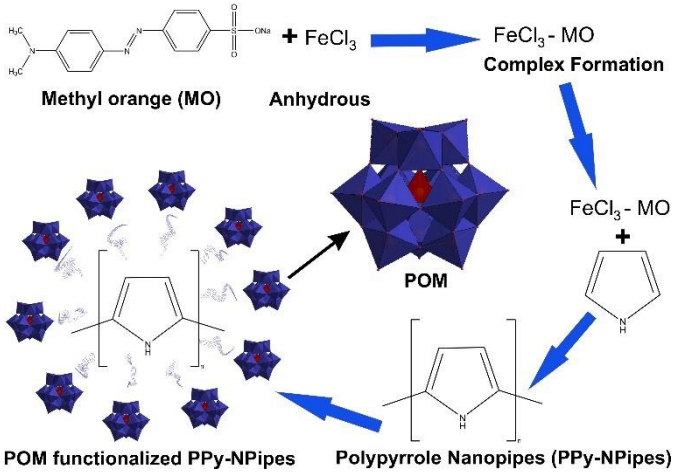

Figure 22. Schematic illustration of steps involved in synthesizing polypyrrole nanopipes and polyoxometalates (POMs, PMo_{12}, or PW_{12}) hybrid material with the simple chemical method.[408]

nanostructures. At first, Cuentas-Gallegos *et al*.[432] prepared a single-wall CNT and POM composite using Cs substituted phosphomolybdate (Cs-$[PMo^{VI}_{12}O_{40}]^{3-}$). The composite material presented a specific capacitance of 285 F g^{-1} and an energy density of 57 W h kg^{-1}.[432] Later Shunik *et al*.[433] further developed this concept using multi-walled CNT instead of a single wall. Phosphomolybdic acid-modified multi-walled CNT revealed a specific capacitance of 40 F g^{-1} at a discharged current of 7 mA.[433] Furthermore, to achieve a higher surface area substrate without compromising electrical conductivity, the researchers employed AC as a supporting material because it possesses a larger surface area (up to 3000 m^2 g^{-1}) with different pore distribution (micro, meso, or macropores). Ruiz *et al*.[434] prepared a hybrid electrode by integrating activated carbon with Keggin-type phosphomolybdate $[H_3PMo^{VI}_{12}O_{40}]$ (PMo_{12}). The highest specific capacitance was generated due to the faradaic component, around 183 F g^{-1} at 2 A g^{-1} current density.[434] In 2014, the same group used molybdenum-based POMs instead of phosphotungstate $[H_3PW^{VI}_{12}O_{40}]$ for an electrochemical study and observed an enhancement of the capacitance to 254 F g^{-1} in an operating potential of 1.6 V. Moreover, the composite can possess 98 % capacitance over 30000 cycles.[435] Besides Keggin-type POMs, Mu *et al*.[436] for the first time embedded a Dawson-type POM, $(NH_4)_6[P_2Mo^{VI}_{18}O_{62}]$ on AC and achieved the highest capacitance of 308 F g^{-1} at 2 A g^{-1} current density due to the high proton conductivity and unique redox behavior of the faradaic component.[436] Besides commercially available activated carbon, Lian *et al*. used biomass-derived pinecone activated carbon, in which POMs ($PMo^{VI}_{12}O_{40}^{3-}$) contributed to a high specific capacitance of 361 F g^{-1}, showing the trend of proton-coupled electron transfer (**Figure 23**).[437] Recently, Maity *et al*.[438] developed vanadium-substituted Keggin structures ($PMo^{VI}_{11}VO_{40}$ and $PMo^{VI}_{10}V^V_2O_{40}$) impregnated into the surface of AC. The vanadium

concentration in the polyanion plays a vital role as it decides the morphology and microstructure of the nanocomposite.[438]

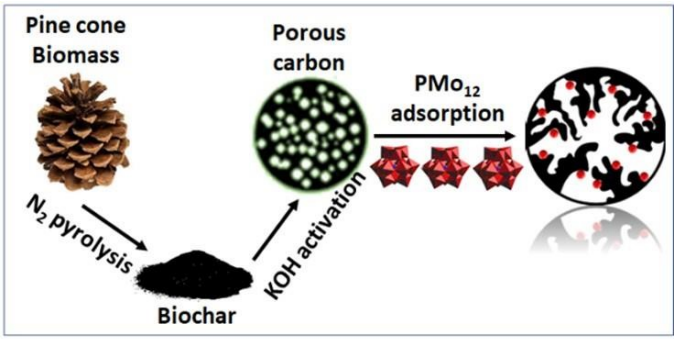

Figure 23. Synthesis schematic for porous pinecone biomass carbon and fabrication of pinecone – polyoxometalate hybrid material.[437]

Graphene or its oxide derivatives (GO and rGO) are used mainly as substrate components other than CNTs and AC because of their high surface area with sizeable electrical conductivity. Additionally, the presence of oxygen-containing functional groups in GO and rGO enables many active sites for the physisorption of a faradaic component. Gomez-Romero and his team did permutation and combined possible routes to achieve high-performance SC using POM and graphene offshoots.[439,440] In this course, they have found a new route to synthesize the hybrid PMo_{12}-rGO nanoelectrode with a hydroquinone-doped hybrid gel hybrid electrolyte. The double hybridization enhances cell potential (1.6 V) and electrochemical properties by increasing the volumetric capacitance to 3.18 F cm^{-3}. Similarly, for the phosphotungstate composite (rGO-PW_{12}), the areal capacitance is calculated as 2.95 F cm^{-3}.[439,440]

Instead of a single supporting medium for POMs, Qin *et al.*[441] (**Figure 24**) prepared a new type of composite by anchoring PMo_{12} to PPy/rGO by layer-by-layer deposition for high-performance micro-SC in solid gel electrolyte medium (PVA/H_2SO_4; PVA = polyvinyl alcohol). The resultant composite exhibited high energy and power densities of 4.8 mW h cc^{-1} and 645.1 mW cc^{-1}, respectively. Also, due to the presence of a solid electrolyte, it presents excellent mechanical flexibility (96 % capacitance retention at a highly bending angle of 180°).[441] Furthermore, surface modifications of graphene derivatives were made using various POM structures, demonstrating enhanced electrochemical performances.[442–445] To achieve seamless ion transportation to the electrode/electrolyte interface Maity *et al.*[446] designed and tailored a facile bottom-up approach in which vanadium-substituted Keggin POMs ($PMo_{11}VO_{40}$) were used to oxidize pyrrole monomer followed by the deposition on the GO surface. The resultant nanohybrid not only exhibits unique architecture but displays high-performance supercapacitive behavior.[446] The designing and construction of polyoxometalates-based metal-organic frameworks composites further expands the search for promising high-performance electrode materials for SCs. A Dawson type[447] the basket-shaped heteropoly blue[448], Keggin type[449], and Anderson type[450,451] POMs hybridized in metal or covalent organic frameworks overcome the limitations of POMs, e.g., high solubility in common electrolytes and results in better stability over longer cycles with improved capacitance.

View Article Online
DOI: 10.1039/D5EN00964B

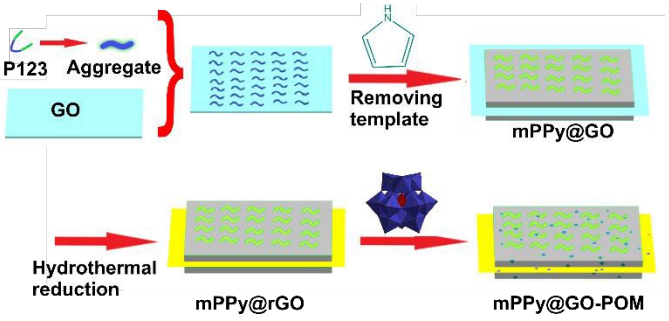

Figure 24. Scheme illustration of fabrication procedure of mPPy@rGO-POM nanosheets.[441]

6.2.2 Asymmetric type hybrid electrode. Asymmetric type hybrid enhances electrochemical performances in two ways; for instance, incorporating two types of material in a single device enables different charge storage mechanisms simultaneously. Secondly, the cell voltage is tuneable (mainly can be enhanced) due to the presence of various active materials in electrodes. Chen *et al.*[452] studied the electrochemical properties of vanadium-based iso-polyanion, sodium decavanadate ($[Na_6V^V_{10}O_{28}]$) in 1 M $LiClO_4$ organic solution, exhibiting an excellent electrochemical behavior in a 3-electrode configuration. Furthermore, an asymmetric SC configuration was developed using activated carbon as the positive and $[Na_6V^V_{10}O_{28}]$ as the negative electrode, exhibiting a maximum specific capacitance of 269 F g^{-1}, with energy and power densities of 73 W h kg^{-1} and 312 W kg^{-1}, respectively, in a 2.8 V operating potential.[452] Hu *et al.*[453] studied a composite type of electrode using regular PMo_{12} anchored on AC in a protic ionic liquid electrolyte. Later, the nanocomposite was assembled as an asymmetric SC device with commercially available AC. The asymmetric cell operates in an elevated potential window of 0-0.85 V, even at a high current density (10 A g^{-1}).[453]

Dubal *et al.*[454] developed a high-performance symmetric SC based on PMo^{VI}_{12} and PMo^{VI}_{12}-rGO. They assembled an asymmetrical SC device using rGO-PMo^{VI}_{12} and rGO-PW^{VI}_{12} electrodes for higher energy density. The SC cell also operates at 1.6 V potential and elevated energy density of 39 Whkg^{-1} at a power density of 658W kg^{-1}.[454] Maity *et al.*[455] optimized the effective loading of POM $(NiV^V_{14}O_{40})^{7-}$ on the AC surface for the first time and employed the nanocomposite as the cathode in an asymmetric configuration with AC as the anode. The resultant device exhibited an enhanced specific energy of 90 W h kg^{-1} and specific power of 2400 W kg^{-1}. Moreover, the nanocomposite-based asymmetric configuration with pristine POM as the positive electrode showed supercapattery behavior.[455]

All literature-known POM-based batteries and supercapacitors are summarized in **Table 4**.

6.3. Summary of POM-based batteries and supercapacitors

The use of polyoxometalates (POMs) as advanced electrode materials for electrochemical energy storage highlights their

View Article Online
DOI: 10.1039/D5EN00964D

remarkable redox activity, high proton mobility, and fast electron/proton transport. These inherent qualities make POMs appealing for use in batteries and supercapacitors, although their sensitivity to pH and solubility issues necessitate structural modifications and hybridization via coordination chemistry to develop mechanically durable and electrochemically stable electrodes. In batteries, especially those based on vanadium- and molybdenum-based clusters, POMs serve as active materials in lithium- and sodium-ion batteries. Their multi-electron redox processes allow for moderate to high specific capacities and a wide range of operating potentials. Hybridizing POMs with conductive supports, such as carbon nanotubes, graphene, MXenes, metal nanoparticles, MOFs, and polymer matrices, significantly improves capacity retention, rate performance, and long-term cycling stability. These approaches effectively overcome the limitations of pure POMs and facilitate efficient ion accommodation. In supercapacitors, POM-based composite and asymmetric electrodes bridge the performance gap with batteries by combining faradaic pseudocapacitance and electric double-layer storage. Key supports such as conducting polymers, carbon materials, graphene derivatives, and porous carbons enhance electrical conductivity, surface area, and mechanical strength. Advanced hybrid structures—including layer-by-layer assemblies, POM–graphene gels, MOF-supported POMs, and asymmetric devices—offer high specific capacitance, broader voltage ranges, excellent energy and power densities, and long cycle life. Overall, this manuscript presents POM-based composites as versatile, high-performance electrode platforms for future energy storage solutions.

Table 4. Summarization of the reported POM-based battery and supercapacitors.

POM-based Composite	POM Archetype	Type of Energy Storage	Significant Results	Ref.
$Li_7[V^{V}_{15}O_{36}(CO_3)]$	spherical isopolyvanadate	Li-ion Battery	specific capacity of 250 mA h g^{-1} alongside energy and power density of 1.5 kW h L^{-1} and 55 kW L^{-1}, respectively	392
SWCNT/Py-SiW^{VI}_{11}; SWCNT = single-walled carbon nanotubes	lacunary Keggin	Li-ion Battery	exhibits an initial discharge capacity of 1569.8 mA h g^{-1} at a current density of 0.5 $mAcm^{-2}$	394
$Na_2H_8[MnV^{V}_{13}O_{38}]$ cluster on the graphene nanoflakes	trimeric polyoxovanadate	Na ion Battery	high capacity of 202 mA h g^{-1} is recorded at 1.5 V with 81 % of its initial capacity retention over 100 cycles	396
PANI/$H_3PMo^{VI}_{12}O_{40}$; PANI = polyaniline	Keggin	composite type SC	highest specific capacitance of 120F/g with cycle stability over 1000 cycles	385
($[PV^{V}Mo^{VI}_{11}O_{40}]^{4-}$, $[PV^{V}_{2}Mo^{VI}_{10}O_{40}]^{5-}$) with AC	Keggin	composite type SC	AC-VMo_{11} composite displayed an enhanced capacitance of 450 F g^{-1} with an improved energy density of 59.7 W h kg^{-1} alongside 99.99 % capacitance retention of over 5000 cycles	407
PMo^{VI}_{12} to PPy/rGO by layer-by-layer deposition; PPy = polypyrrole; rGO = reduced graphene oxide	Keggin	composite type SC	composite possesses high energy and power densities of 4.8 mW h/cc and 645.1 mW/cc, respectively	410
$[MnV^{V}_{14}O_{40}]^{6-}$ on the AC and GO; AC = activated carbon; GO = graphene oxide	Lindqvist	composite type SC	AC/MnV_{14} nanohybrid exhibits a specific capacitance of 547 F g^{-1} with specific energy and power of 76 W h kg^{-1} and 1600 W kg^{-1}, respectively, at 0.8 Ag^{-1} current density. GO/MnV_{14} shows a specific capacitance of 330 F g^{-1} with specific energy and power of 30 W h kg^{-1} and 1276 W kg^{-1}, respectively, at the same current density	414
PMo^{VI}_{12} anchored on AC in a protic ionic liquid; AC = activated carbon	Keggin	asymmetric SC	asymmetric cell operates in a potential window of 0-0.85 V at 10 A g^{-1} of current density	417
rGO-PMo^{VI}_{12} and rGO-PW^{VI}_{12}; rGO = reduced graphene oxide	Keggin	asymmetric SC	the cell operates at 1.6 V potential and elevated energy density to 39 W h/kg with a power density of 658 W/kg	426
AC//AC-$K_2H_5[NiV^{V}_{14}O_{40}]$; AC = activated carbon	Lindqvist	asymmetric SC	increased the potential window up to 1.5 V and enhanced the specific energy and power values (90.1 W h kg^{-1} and 2400 W kg^{-1}, respectively), with 98 % coulombic efficiency	427

DOI: 10.1039/D5EN00964B

7 Conclusions and Outlook

It is almost impossible to overemphasize the applications of POMs in environmental remediation. By looking at the number of environmental studies mentioning POMs in the removal of various pollutants from water, soil or air, it seems that POMs are involved everywhere. This increasing number of environmental degradation studies (**Figure 3**) involving POMs could be mostly explained by the versatility of the structural chemistry of POMs (**Figure 2**) and the catalytic features specific to transition metals.

POMs in water column filters and/or in porous organic-inorganic composites proved to be effective in the removal of toxic heavy metals, aromatic organic pollutants, and bacteria (**Figures 4, 5** and **7**). POMs in porous nanosheets are capable of the photocatalytic degradation of emergent pollutants, particularly antibiotics (**Figure 8**, **Tables 1** and **S2**), with enhanced photocatalytic performance under visible light (**Figure 9**), but also dyes, plastics, industrial chemicals, and pesticides (**Tables 1** and **S2**). Moreover, a magnetic core enclosed by polyoxometalate-based ionic liquid phases (**Figure 12**) was used to remove dyes, heavy metals, microbes, and microplastics (MPs). MPs are not only one of the new emergent health pollutants but also a major one of worldwide concern, in addition to being associated with joint contamination with heavy metals.

POMs, alone and/or in combination with other compounds, such as metal-organic frameworks (MOFs), carbon nanotubes (CNTs) and mesoporous silica supports, have shown promising results in the removal of air pollutants from fossil fuels due to their selective catalytic properties for the oxidation of sulfur compounds (**Figures 13**, **14**, and **15**, **Table S1**). In addition, toxic gases such as hydrogen sulfide, nitrogen oxides and sulfur dioxide are efficiently removed by POMs (**Figure 16**, **Table 2**), whereas the volatile organic compounds' reaction mechanism involves a photocatalytic oxidation catalyzed by the PW_{12}/g-C_3N_4 hybrid material (**Figure 17**).

The immobilization of POMs on different supporting surfaces facilitates their electrochemical properties for sensor application (**Figure 19**, **Table 3**). Conversely, their variable redox activities and outstanding electron/proton transport capacities make POM-based composite materials suitable for use in electrochemical fields as an exceptional electrode component for supercapacitors and batteries (**Table 4**). A high-performance pseudocapacitor was obtained by replacing multiple Mo centers in $[H_3PMo^{VI}_{12}O_{40}]$ with vanadium and incorporating modified a phosphomolybdate with a conducting polymer for improved electrochemical activity (**Figure 20**), whereas a biomass-derived pinecone activated carbon, that includes POMs contributed to a high specific capacitance (**Figure 21**). Carbon nanostructures, graphene oxide/reduced graphene oxide, and activated carbon composites come into play as supporting elements for the POMs as they provide better mechanical and electrochemical stability for broader electrochemical applications (**Figures 22** and **23**). Although this review does not reveal everything, it may help to get closer to viable solutions for the effective use of the POM-based materials for the removal of the environmental pollutants. The future is bright for POM applications in environmental treatments!

Data availability

Data sharing does not apply to this article as no datasets were generated or analyzed during the current study.

Conflicts of interest

There are no conflicts to declare.

Acknowledgements

M.M. is grateful to Ferdowsi University of Mashhad and RADA Think Tank (Research for Academic Development & Advancement) for financial support. This study received Portuguese national funds from FCT - Foundation for Science and Technology through contracts UID/04326/2025, UID/PRR/04326/2025 and LA/P/0101/2020 (DOI:10.54499/LA/P/0101/2020) (M.A.)

This research was also funded in whole or in part by the Austrian Science Fund (FWF) (Grant DOI: 10.55776/PAT4299925 (A.R.)). For open access purposes, the author has applied a CC BY public copyright license to any author accepted manuscript version arising from this submission.

The authors would like to acknowledge Dr João Mateus for providing the professional illustration of **Figure 1** and also for the **Graphical abstract** illustration.

Notes and references

Abbrevations. Ac, acetic acid; AC, activated carbon; AOP, advanced oxidation process; APTMS, 3-aminopropyltrimethoxysilane; APTS, γ-aminopropyltriethoxysilane; Asp, aspartic acid; Bbi, 1,1'-(1,4-butanediyl)bis(imidazole); BE, berberine; bimb, 1,4-bis(1-imidazolyl)benzene; bipy, bipyridine; BMIM or bmim, 1-butyl-3-methylimidazolium; BPA, bisphenol A; BPA-Br, bromobisphenol-A; BPy, 1-butylpyridinium or N-butylpyridinium; BR46, basic red 46; BT, benzothiophene; BTC, 1,3,5-benzenetricarboxylate; CCNF, carbonized cellulose nanofiber; CNTs, carbon nanotubes; CP, chlorphenole; 4-CP, 4-chlorphenole; CPF, ciprofloxacin; CPBPY, *N*-(3-carboxyphenyl)-4,4'-bipyridinium); cpt, 4-(4'-carboxyphenyl)-1,2,4-triazolate; CSH, cellulose propylamine-modified silica; CTS, chitosan; CV, crystal violet; DBP, di-n-butyl phthalate; DBT, dibenzothiophene; DESs, deep eutectic solvents; DMDBT, 4,6-dimethyldibenzotiophene; DODA·Br, dimethyldioctadecylammonium bromide; DODMAC, dimethyldioctadecylammonium chloride; ECSA, electrochemically active surface area; EDA-CD, per-(6-deoxy-6-iodo)-β-cyclodextrin; ELSA, electrochemically active surface area; en, ethylenediamine; EPs, emergent pollutants; EtOH, ethanol; etpy, 4-ethylpyridine; EY, eosin Y; g-BN, graphene-like hexagonal boron nitride; GA, graphene aerogel; GO, graphene oxide; Gr, graphene; HOMO, highest occupied molecular orbital; HPW or PW_{12}, $[H_3PW^{VI}_{12}O_{40}\cdot 6H_2O]$; H_2pyttz-I, 3-(pyrid-2-yl)-5-(1H-1,2,4-triazol-3-yl)-1,2,4-triazolyl; H_2pyttz-II, 3-(pyrid-4-yl)-5-(1H-1,2,4-triazol-3-yl)-1,2,4-triazolyl; H_3bdpm, 1,1'-bis(3,5-dimethyl-1H-pyrazolatemethane; IBA, isobutyraldehyde; IBAc, isobutyric acid; IBP, ibuprofen; IL, ionic liquid; imi, imidazole; iPAF-1, porous aromatic framework; LiBs, lithium-ion batteries; LDH, layered double hydroxide; LMCT, ligand to metal charge transfer; LPMS, large-pore mesoporous silica; LRSR, liquid-redox sulfur recovery; LUMO, lowest unoccupied molecular

DOI: 10.1039/D5EN00964B

orbital; MB, methylene blue; MBT, 2-mercaptobenzothiazole; MCM-41, conventional molecular sieve MCM-41; MeCN, acetonitrile; MeOH, methanol; mepy, 4-methylpyridine; MO, methyl orange; MOFs, metal-organic frameworks; MOG, metal-organic gel; MPs, microplastics; MR, methyl red; M-TCS, methyl triclosan; NAD, 2-(1-naphthyl)acetamide; NBZ, nitrobenzene; NFZ, nitrofurazone; NPs, (metal) nanoparticles; ODS, oxidative desulfurization; PANI, polyaniline; PBV, patent blue V; pca, pyridine-2-carboxylic acid; PDDA, poly(diallyldimethylammonium chloride); PEI, polyetherimide; phen, 1,10-phenanthroline; PIL, protic ionic liquid; PMIn, polyionene; PMOE, (ethylene-bridged) periodic mesoporous organosilica; PMs, particulate matters; POM, polyoxometalate; POMCP, POM-based coordination polymer; POM-IL, polyoxometalate-based ionic liquid; POMos, polyoxomolybdates; POM-SILP, polyoxometalate-supported ionic liquid phase; POT, polyoxotungstate; PPI, proton pump inhibitor; PPy, polypyrrole; PS, ponceau S; PTMS, 3-aminopropyl trimethoxysilane; PVA, polyvinyl alcohol; PVDF, polyvinylidene fluoride; py, pyrene; PyPS, 3-(pyridine-1-ium-1-yl)propane-1-sulfonate; PZC, point-of-zero charge; RB, rose bengal; RB5, reactive black 5; RhB, rhodamine B; RH, rice husk; rGO, reduced graphene oxide; SAB, sodium-activated bentonite; SBA-15, aminosilylated silica; SC, supercapacitor; SCR, selective catalytic reduction; SDV, sodium decavanadate; SMT, sulfamethazine; SPD, sulfapyridine; SPME, solid-phase microextraction; SSA, 5-sulfosalicylic acid; SSZ, sulfasalazine; SWCNTs, single-walled carbon nanotubes; TB, toluidine blue; TBA, tetra-n-butylammonium ion; TBBA, tetrabromobisphenol-A; TC, tetracycline; TCS, triclosan; TCY, tetracycline; TMA, *N*-trimethoxysilypropyl-*N*, *N*, *N*-trimethylammonium; TMR4A, resorcin[4]arene-based ligand; TOA, tetraoctylammonium; TPD-MS, temperature-programmed desorption-mass spectroscopy; VOCs, volatile organic compounds; 4,6-DMDBT, 4,6-dimethyl dibenzothiophene; $[mim(CH_2)_3COO]$, 1-carboxypropyl-3-methyl imidazole; $[C_4mim]^+$, 1-butyl-3-methylimidazolium ion; β-EDA-CD, per-6-deoxy-6-ethylenediamine-β-cyclodextrin.

1 Rizzo L, Malato S, Antakyali D, Beretsou VG, Đolić MB, Gernjak W, et al. Consolidated vs new advanced treatment methods for the removal of contaminants of emerging concern from urban wastewater. *Sci Total Environ*. 2019;655:986–1008. doi:10.1016/j.scitotenv.2018.11.265

2 Mustapha MA, Manan ZA, Wan Alwi SR. A New Quantitative Overall Environmental Performance Indicator for a Wastewater Treatment Plant. *J Clean Prod.* 2017;167:815–823. doi: 10.1016/j.jclepro.2017.08.169

3 Leung DYC, Drakaki E. Outdoor-Indoor Air Pollution in Urban Environment: Challenges and Opportunity. *Front Environ Sci.* 2015;2(69):1–7. doi: 10.3389/fenvs.2014.00069

4 Nathanson JA. Pollution. In: Encyclopedia Britannica [Internet]. Chicago: Encyclopædia Britannica, Inc.; [updated 2025 Sep 12; cited 2025 Sep 17]. Available from: **https://www.britannica.com/science/pollution-environment**

5 Directorate-General for Energy, European Commission. In focus: renewable energy in Europe [Internet]. Brussels: European Commission; 2020 Mar [cited 2025 Sep 17]. Available from: **https://ec.europa.eu/info/news/focus-renewable-energy-europe-2020-mar-18_en**

6 Klepac P, Locatelli I, Korošec S, Künzli N, Kukec A. Ambient air pollution and pregnancy outcomes: a comprehensive review and identification of environmental public health challenges. *Environ Res*. 2018;167:144–59. doi:10.1016/j.envres.2018.07.008

7 Briggs D. Environmental Pollution and the Global Burden of Disease. *Br Med Bull.* 2003;68(1):1–24. doi: 10.1093/bmb/ldg019

8 Parker L. What You Need to Know About the World's Water Wars. National Geographic. Mar 2020. https://www.nationalgeographic.com/science/article/world-aquifers-water-wars. Accessed Sep 17, 2025.

9 Gleick PH. Water In Crisis: Paths To Sustainable Water Use. *Ecol Appl.* 1998;8(3):571–579. doi: 10.1890/1051-0761(1998)008[0571:WICPTS]2.0.CO;2

10 Geissen V, Mol H, Klumpp E, Umlauf G, Nadal M, van der Ploeg M, et al. Emerging pollutants in the environment: a challenge for water resource management. *Int Soil Water Conserv Res*. 2015;3(1):57–65. doi:10.1016/j.iswcr.2015.03.002

11 United Nations Environment Programme and World Meteorological Organization. International Conference on Water and the Environment: Development Issues for the 21st Century [Internet]. Nairobi: UNEP; 1992 [cited 2025 Sep 1]. Available from: **https://wedocs.unep.org/20.500.11822/30961**

12 Zhuo R, Fan F. A Comprehensive Insight into the Application of White Rot Fungi and Their Lignocellulolytic Enzymes in the Removal of Organic Pollutants. *Sci Total Environ.* 2021;778:146132. doi: 10.1016/j.scitotenv.2021.146132

13 Alipoori S, Rouhi H, Linn E, Stumpfl H, Mokarizadeh H, Esfahani MR, et al. Polymer-based devices and remediation strategies for emerging contaminants in water. *ACS Appl Polym Mater*. 2021;3(2):549–77. doi:10.1021/acsapm.0c0117

14 Witkowski KM, Johnson NE. Organic-solvent water pollution and low birth weight in Michigan. *Social Biology*. 1992;39(1–2):45–54. doi: 10.1080/19485565.1992.9988803

15 United Nations World Water Assessment Programme. UN World Water Development Report: Water for people, water for life (WWDR1) [Internet]. Paris: UN-Water; 2003 Mar [cited 2025 Sep 1]. Available from: **https://www.unwater.org/publications/un-world-water-development-report-2003**

16 Richardson SD, Ternes TA. Water Analysis: Emerging Contaminants and Current Issues. *Anal Chem.* 2011;83(12):4614–4648. doi: 10.1021/ac200915r

17 von der Ohe PC, Dulio V, Slobodnik J, De Deckere E, Kühne R, Ebert R-U, et al. A new risk assessment approach for the prioritization of 500 classical and emerging organic microcontaminants as potential river basin specific pollutants under the European Water Framework Directive. *Sci Total Environ*. 2011;409(11):2064–77. doi:10.1016/j.scitotenv.2011.01.054

18 de Andrade JR, Oliveira MF, da Silva MGC, Vieira MGA. Adsorption of Pharmaceuticals from Water and Wastewater Using Nonconventional Low-Cost Materials: A Review. *Ind Eng Chem Res*. 2018;57(9):3103–3127. doi: 10.1021/acs.iecr.7b05137

19 Marican A, Durán-Lara EF. A Review on Pesticide Removal through Different Processes. *Environ Sci Pollut Res*. 2018;25(3):2051–2064. doi: 10.1007/s11356-017-0796-2

20 Juliano C, Magrini GA. Cosmetic Ingredients as Emerging Pollutants of Environmental and Health Concern. A Mini-Review. *Cosmetics*. 2017;4:11–29. doi: 10.3390/cosmetics4020011

21 Bilal M, Mehmood S, Iqbal HMN. The Beast of Beauty: Environmental and Health Concerns of Toxic Components in Cosmetics. *Cosmetics*. 2020;7(1):13–31. doi: 10.3390/cosmetics7010013

22 Brausch JM, Rand GM. A Review of Personal Care Products in the Aquatic Environment: Environmental Concentrations and Toxicity. *Chemosphere*. 2011;82(11):1518–1532. doi: 10.1016/j.chemosphere.2010.11.018

23 Oliveira M, Slezakova K, Delerue-Matos C, Pereira MC, Morais S. Children Environmental Exposure to Particulate Matter and Polycyclic Aromatic Hydrocarbons and Biomonitoring in School Environments: A Review on Indoor and Outdoor Exposure Levels, Major Sources and Health Impacts. *Environ Int.* 2019;124:180–204. doi: 10.1016/j.envint.2018.12.052

24 Sanseverino I, Loos R, Navarro Cuenca A, Marinov D, Lettieri T. State of the art on the contribution of water to antimicrobial resistance. EUR 29592 EN. Luxembourg:

Publications Office of the European Union; 2018. doi:10.2760/771124
25 Rodriguez-Mozaz S, Vaz-Moreira I, Varela Della Giustina S, Llorca M, Barceló D, Schubert S, et al. Antibiotic residues in final effluents of European wastewater treatment plants and their impact on the aquatic environment. *Environ Int*. 2020;140:105733. doi:10.1016/j.envint.2020.105733
26 Wołejko E, Jabłońska-Trypuć A, Wydro U, Butarewicz A, Łozowicka B. Soil Biological Activity as an Indicator of Soil Pollution with Pesticides – A Review. *Appl Soil Ecol*. 2020;147:103356. doi: 10.1016/j.apsoil.2019.09.006
27 Hussain S, Siddique T, Saleem M, Arshad M, Khalid A. Impact of pesticides on soil microbial diversity, enzymes, and biochemical reactions. In: Advances in agronomy. Vol. 102. San Diego: Academic Press; 2009. p. 159-200. doi:10.1016/S0065-2113(09)01005-0
28 Köhler H-R, Triebskorn R. Wildlife Ecotoxicology of Pesticides: Can We Track Effects to the Population Level and Beyond? *Science*. 2013;341(6147):759–765. doi: 10.1126/science.1237591
29 Rattner BA. History of wildlife toxicology. *Ecotoxicology*. 2009;18:773–83. doi:10.1007/s10646-009-0354-x
30 Berny P. Pesticides and the intoxication of wild animals. *J Vet Pharmacol Ther.* 2007;30:93–100. doi: 10.1111/j.1365-2885.2007.00836.x
31 Carvalho FP. Pesticides, environment, and food safety. *Food Energy Secur*. 2017;6(2):48–60. doi:10.1002/fes3.108
32 George J, Shukla Y. Pesticides and cancer: Insights into toxicoproteomic-based findings. *J Proteomics*. 2011;74(12):2713–2722. doi: 10.1016/j.jprot.2011.09.024
33 Bassil KL, Vakil C, Sanborn M, Cole DC, Kaur JS, Kerr JK. Cancer health effects of pesticides. *Can Fam Physician*. 2007;53(10):1704–11. Available from: **https://www.cfp.ca/content/53/10/1704**
34 Kumar M, Sarma DK, Shubham S, Kumawat M, Verma V, Prakash A, Tiwari R. Environmental Endocrine-Disrupting Chemical Exposure: Role in Non-Communicable Diseases. *Public Health Front.* 2020;8:553850. doi: 10.3389/fpubh.2020.553850
35 Jiang F, Peng Y, Sun Q. Pesticides exposure induced obesity and its associated diseases: recent progress and challenges. *J Future Foods*. 2022;2(2):119−124. doi: 10.1016/j.jfutfo.2022.03.005
36 Kim YA, Park JB, Woo MS, Lee SY, Kim HY, Yoo YH. Persistent Organic Pollutant-Mediated Insulin Resistance. *Int J Environ Res Public Health*. 2019;16:448−462. doi: 10.3390/ijerph16030448
37 de Araujo JSA, Delgado IF, Paumgartten FJR. Glyphosate and Adverse Pregnancy Outcomes, a Systematic Review of Observational Studies. *BMC Public Health*. 2016;16:472−485. doi: 10.1186/s12889-016-3153-3
38 Carrasco Cabrera L, Medina Pastor P. The 2019 European Union Report on Pesticide Residues in Food. *EFSA Journal.* 2021;19(4):6491. doi: 10.2903/j.efsa.2021.6491
39 Arutyunov VS, Lisichkin GV. Energy Resources of the 21st Century: Problems and Forecasts. Can Renewable Energy Sources Replace Fossil Fuels? *Russ Chem Rev.* 2017;86(8):777−804. doi: 10.1070/rcr4723
40 Barbir F, Veziroğlu TN, Plass HJ. Environmental damage due to fossil fuels use. *Int J Hydrog Energy*. 1990;15(10):739−749. doi: 10.1016/0360-3199(90)90005-J
41 Mukhopadhyay K, Forssell O. An empirical investigation of air pollution from fossil fuel combustion and its impact on health in India during 1973-1974 to 1996-1997. *Ecol Econ.* 2005;55(2):235−250. doi:10.1016/j.ecolecon.2004.09.022
42 Loppi S, Nascimbene J. Monitoring H_2S air pollution caused by the industrial exploitation of geothermal energy: The pitfall of using lichens as bioindicators. *Environ Pollut.* 2010;158(8):2635−2639. doi: 10.1016/j.envpol.2010.05.002
43 McK. Ellison J, Waller RE. A review of sulphur oxides and particulate matter as air pollutants with particular reference to effects on health in the United Kingdom. *Environ Res*. 1978;16(1−3):302−325. doi: 10.1016/0013-9351(78)90164-0
44 Wong T-Y. Smog induces oxidative stress and microbiota disruption. *J Food Drug Anal*. 2017;25(2):235−244. doi: 10.1016/j.jfda.2017.02.003
45 Singh A, Agrawal M. Acid rain and its ecological consequences. *J Environ Biol.* 2008;29(1):15−24. https://pubmed.ncbi.nlm.nih.gov/18831326/. doi: 10.4103/0254-8704.44191
46 Galán I, Tobías A, Banegas JR, Aránguez E. Short-term effects of air pollution on daily asthma emergency room admissions. *Eur Respir J.* 2003;22:802−808. doi: 10.1183/09031936.03.00013003
47 Linaker CH, Coggon D, Holgate ST, Clough J, Josephs L, Chauhan AJ, et al. Personal exposure to nitrogen dioxide and risk of airflow obstruction in asthmatic children with upper respiratory infection. *Thorax*. 2000;55(11):930–3. doi:10.1136/thorax.55.11.930
48 Kar Kurt O, Zhang J, Pinkerton KE. Pulmonary Health Effects of Air Pollution. *Curr Opin Pulm Med*. 2016;22(2):138−143. doi: 10.1097/MCP.0000000000000248
49 Miller KA, Siscovick DS, Sheppard L, Shepherd K, Sullivan JH, Anderson GL, Kaufman JD. Long-Term Exposure to Air Pollution and Incidence of Cardiovascular Events in Women. *N Engl J Med.* 2007;356:447−458. doi: 10.1056/NEJMoa054409
50 Schwela D. Air Pollution and Health in Urban Areas. *Rev Environ Health.* 2000;15(1−2):13−42. doi: 10.1515/REVEH.2000.15.1-2.13
51 Aribike DS, Usman MA, Oloruntoba MM. Adsorptive desulfurization of diesel using activated sewage sludge: kinetics, equilibrium and thermodynamics studies. *Appl Petrochem Res.* 2020;10:1−12. doi: 10.1007/s13203-019-00239-2
52 Song C. An overview of new approaches to deep desulfurization for ultra-clean gasoline, diesel fuel and jet fuel. *Catal Today*. 2003;86(1−4):211−263. doi: 10.1016/S0920-5861(03)00412-7
53 ang H, Jiang B, Sun Y, Zhang L, Huang Z, Sun Z, et al. Heterogeneous oxidative desulfurization of diesel fuel catalyzed by mesoporous polyoxometallate-based polymeric hybrid. *J Hazard Mater*. 2017;333:63–72. doi:10.1016/j.jhazmat.2017.03.017
54 Ma Y-Q, Liu X-P, Li J-P, Wang R, Yu M-Q. Transition Metal Salts of H4PMo11VO40 for Efficient H_2S Removal in the Liquid Redox Process. *Chem Pap.* 2017;71:647−652. doi: 10.1007/s11696-016-0064-9
55 Zhang J, Zuo W, Tian Y, Yin L, Gong Z, Zhang J. Release of Hydrogen Sulfide during Microwave Pyrolysis of Sewage Sludge: Effect of Operating Parameters and Mechanism. *J Hazard Mater.* 2017;331:117−122. doi: 10.1016/j.jhazmat.2017.02.040
56 Jaakkola JJ, Vilkka V, Marttila O, Jäppinen P, Haahtela T. The South Karelia Air Pollution Study: The effects of malodorous sulfur compounds from pulp mills on respiratory and other symptoms. *Am Rev Respir Dis*. 1990;142(6 Pt 1):1344−1350. doi:10.1164/ajrccm/142.6_Pt_1.1344.
57 Chaudhari NS, Bhirud AP, Sonawane RS, Nikam LK, Warule SS, Rane VH, et al. Ecofriendly hydrogen production from abundant hydrogen sulfide using solar light-driven hierarchical nanostructured $ZnIn_2S_4$ photocatalyst. *Green Chem*. 2011;13(9):2500–2506. doi:10.1039/C1GC15515F.
58 Lim E, Mbowe O, Lee ASW, Davis J. Effect of Environmental Exposure to Hydrogen Sulfide on Central Nervous System and Respiratory Function: A Systematic Review of Human Studies. *Int J Occup Environ Health*. 2016;22(1):80−90. doi: 10.1080/10773525.2016.1145881
59 European Environment Agency. State of Europe's environment not good: threats to nature and impacts of climate change top challenges. Copenhagen: EEA; 2025. doi:10.2800/3817344

View Article Online
DOI: 10.1039/D5EN00964B

60 Cheng X, Bi XT. A review of recent advances in selective catalytic NO_x reduction reactor technologies. *Particuology*. 2014;16:1–18. doi:10.1016/j.partic.2014.01.006
61 Song C. An Overview of New Approaches to Deep Desulfurization for Ultra-Clean Gasoline, Diesel Fuel and Jet Fuel. *Catal Today*. 2003;86(1–4):211–263. doi: 10.1016/S0920-5861(03)00412-7
62 Ng SJC, Choi AES, Dugos NP, Wan M-W. Driving sustainable solutions: exploring supported-polyoxometalate catalysts for enhanced oxidative desulfurization. *Chem Eng Trans.* 2024;113:79–84. doi:10.3303/CET24113014
63 Herrmann S, de Matteis L, de la Fuente JM, Mitchell SG, Streb C. Removal of Multiple Contaminants from Water by Polyoxometalate Supported Ionic Liquid Phases (POM-SILPs). *Angew Chem Int Ed.* 2017;56(6):1667–1670. doi: 10.1002/anie.201611072
64 Mamun MAA, Yuce MR. Recent Progress in Nanomaterial Enabled Chemical Sensors for Wearable Environmental Monitoring Applications. *Adv Funct Mater*. 2020;30:2005703. doi: 10.1002/adfm.202005703
65 Hanrahan G, Patila DG, Wang J. Electrochemical sensors for environmental monitoring: design, development and applications. *J Environ Monit.* 2004;6:657–664. doi: 10.1039/B403975K
66 Justino CILL, Duarte AC, Rocha-Santos TAP. Recent Progress in Biosensors for Environmental Monitoring: A Review. *Sensors.* 2017;17(12):2918–2943. doi: 10.3390/s17122918
67 Tajik S, Beitollahi H, Nejad FG, Sheikhshoaie I, Nugraha AS, Jang HW, et al. Performance of metal-organic frameworks in the electrochemical sensing of environmental pollutants. *J Mater Chem A*. 2021;9:8195–8220. doi:10.1039/D0TA08344E
68 Rassaei L, Marken F, Sillanpää M, Amiri M, Cirtiu CM, Sillanpää M. Nanoparticles in Electrochemical Sensors for Environmental Monitoring. *Trends Analyt Chem*. 2011;30(11):1704–1715. doi: 10.1016/j.trac.2011.05.009
69 Priyadarshini E, Pradhan N. Gold nanoparticles as efficient sensors in colorimetric detection of toxic metal ions: A review. *Sens Actuators B Chem.* 2017;238:888–902. doi: 10.1016/j.snb.2016.06.081
70 Horn MR, Singh A, Alomari S, Goberna-Ferrón S, Benages-Vilau R, Chodankar N, et al. Polyoxometalates (POMs): from electroactive clusters to energy materials. *Energy Environ Sci*. 2021;14(4):1652–1700. doi:10.1039/D0EE03407J
71 Whittingham MS. Lithium Batteries: 50 Years of Advances to Address the Next 20 Years of Climate Issues. *Nano Lett.* 2020;20(12):8435–8437. doi: 10.1021/acs.nanolett.0c04347
72 Delmas C. Sodium and Sodium-Ion Batteries: 50 Years of Research. Adv Energy Mater. 2018;8(17):1703137. doi: 10.1002/aenm.201703137
73 Weber AZ, Mench MM, Meyers JP, Ross PN, Gostick JT, Liu Q. Redox Flow Batteries: A Review. *J Appl Electrochem*. 2011;41(10):1137–1164. doi: 10.1007/s10800-011-0348-2
74 Arico AS, Bruce P, Scrosati B, Tarascon JM, van Schalkwijk W. Nanostructured materials for advanced energy conversion and storage devices. In: Materials for sustainable energy. London: Nature Publishing Group; 2010:148–159. doi:10.1142/9789814317665_0022
75 Vannathan AA, Kella T, Shee D, Mal SS. One-Pot Synthesis of Polyoxometalate Decorated Polyindole for Energy Storage Supercapacitors. ACS Omega. 2021;6(17):11199-11208. doi: 10.1021/acsomega.0c05967
76 Herrmann S, Aydemir N, Nägele F, Fantauzzi D, Jacob T, Travas-Sejdic J, et al. Enhanced capacitive energy storage in polyoxometalate-doped polypyrrole. *Adv Funct Mater*. 2017;27(25):1700881. doi:10.1002/adfm.201700881
77 Pope MT, Müller A. Polyoxometalate Chemistry From Topology via Self-Assembly to Applications. Dordrecht: Springer; 2001. doi: 10.1007/0-306-47625-8
78 Streb C. New Trends in Polyoxometalate Photoredox Chemistry: From Photosensitisation to Water Oxidation Catalysis. *Dalton Trans.* 2012;41:1651–1659. doi: 10.1039/C1DT11220A
79 Coronado E, Giménez-Saiz C, Gómez-García CJ. Recent Advances in Polyoxometalate-Containing Molecular Conductors. *Coord Chem Rev.* 2005;249(17):1776–1796. doi: 10.1016/j.ccr.2005.02.017
80 López X, Fernández JA, Poblet JM. Redox Properties of Polyoxometalates: New Insights on the Anion Charge Effect. *Dalton Trans.* 2006;9:1162–1167. doi: 10.1039/B507599H
81 Wang S-S, Yang G-Y. Recent Advances in Polyoxometalate-Catalyzed Reactions. *Chem Rev*. 2015;115(11):4893–4962. doi: 10.1021/cr500390v
82 Lotfian M, Heravi MM, Mirzaei M, Heidari B. Applications of inorganic-organic hybrid architectures based on polyoxometalates in catalyzed and photocatalyzed chemical transformations. *Appl Organomet Chem*. 2019;33(4):e4808. doi:10.1002/aoc.4808
83 Clemente-Juan JM, Coronado E, Gaita-Ariño A. Magnetic Polyoxometalates: From Molecular Magnetism to Molecular Spintronics and Quantum Computing. *Chem Soc Rev.* 2012;41(22):7464–7478. doi: 10.1039/C2CS35205B
84 Wang S, Sun W, Hu Q, Yan H, Zeng Y. Synthesis and Evaluation of Pyridinium Polyoxometalates as Anti-HIV-1 Agents. *Bioorg Med Chem Lett.* 2017;27(11):2357–2359. doi: 10.1016/j.bmcl.2017.04.025
85 Bijelic A, Aureliano M, Rompel A. Polyoxometalates as Potential Next-Generation Metallodrugs in the Combat Against Cancer. *Angew Chem Int Ed Engl*. 2019;58(10):2980–2999. doi: 10.1002/anie.201803868
86 van Rompuy LS, Parac-Vogt TN. Interactions between Polyoxometalates and Biological Systems: From Drug Design to Artificial Enzymes. *Curr Opin Biotechnol.* 2019;58:92–99. doi: 10.1016/j.copbio.2018.11.013
87 Bijelic A, Rompel A. The Use of Polyoxometalates in Protein Crystallography – An Attempt to Widen a Well-Known Bottleneck. *Coord Chem Rev.* 2015;299:22–38. doi: 10.1016/j.ccr.2015.03.018
88 Bijelic A, Rompel A. Polyoxometalates: More than a Phasing Tool in Protein Crystallography. *ChemTexts*. 2018;4(10):1–28. doi: 10.1007/s40828-018-0064-1
89 Blazevic A, Al-Sayed E, Roller A, Giester G, Rompel A. Tris-Functionalized Hybrid Anderson Polyoxometalates: Synthesis, Characterization, Hydrolytic Stability and Inversion of Protein Surface Charge. *Chem Eur J*. 2015;21(12):4762–4771. doi: 10.1002/chem.201405644
90 Ji Y, Huang L, Hu J, Streb C, Song Y-F. Polyoxometalate-Functionalized Nanocarbon Materials for Energy Conversion, Energy Storage and Sensor Systems. *Energy Environ Sci*. 2015;8:776–789. doi: 10.1039/C4EE03749A
91 Long D-L, Tsunashima R, Cronin L. Polyoxometalates: Building Blocks for Functional Nanoscale Systems. *Angew Chem Int Ed.* 2010;49(10):1736–1758. doi: 10.1002/anie.200902483
92 Pope MT, Kortz U. Polyoxometalates. In: Encyclopedia of Inorganic and Bioinorganic Chemistry. Hoboken (NJ): John Wiley & Sons Ltd; 2012. doi: 10.1002/9781119951438.eibc0185.pub2
93 Al-Sayed E, Rompel A. Lanthanides Singing the Blues: Their Fascinating Role in the Assembly of Gigantic Molybdenum Blue Wheels. *ACS Nanosci Au*. 2022;2(3):179–197. doi: 10.1021/acsnanoscienceau.1c00036
94 Cherevan AS, Nandan SP, Roger I, Liu R, Streb C. Polyoxometalates on Functional Substrates: Concepts, Synergies, and Future Perspectives. *Adv Sci.* 2020;7:1903511. doi: 10.1002/advs.201903511
95 Zeng L, Xiao L, Long Y, Shi X. Trichloroacetic acid-modulated synthesis of polyoxometalate@UiO-66 for selective adsorption of cationic dyes. *J Colloid Interface Sci.* 2018;516:274–283. doi: 10.1016/j.jcis.2018.01.070
96 Zhu T-T, Zhang Z-M, Chen W-L, Liu Z-J, Wang E-B. Encapsulation of tungstophosphoric acid into harmless MIL-101(Fe) for effectively removing cationic dye from aqueous

solution. *RSC Adv.* 2016;6:81622–81630. doi: 10.1039/C6RA16716K

97 Chai D-F, Wang M, Zhang C, Ning F, Xu W, Pang H, et al. A novel 3D POMOF based on dinuclear copper (II)-oxalate complexes and Keggin polyoxoanions with excellent photocatalytic activity. *Inorg Chem Commun*. 2017;83:16–19. doi:10.1016/j.inoche.2017.05.028

98 ong B-W, Su Z-H, Zhao Z-F, Zhao W-Q, Ma X-J, Xu Q, et al. A new 3D POMOF with two channels consisting of Wells–Dawson arsenotungstate and $\{Cl_4Cu_{10}(pz)_{11}\}$ complexes: synthesis, crystal structure, and properties. *New J Chem*. 2018;42:4596–4602. doi:10.1039/C7NJ04854H

99 Huo M, Yang W, Zhang H, Zhang L, Liao J, Lin L, et al. A new POM–MOF hybrid microporous material with ultrahigh thermal stability and selective adsorption of organic dyes. *RSC Adv*. 2016;6:111549–111555. doi:10.1039/C6RA10422C

100 Mialane P, Mellot-Draznieks C, Gairola P, Duguet M, Benseghir Y, Oms O, et al. Heterogenisation of polyoxometalates and other metal-based complexes in metal–organic frameworks: from synthesis to characterisation and applications in catalysis. *Chem Soc Rev*. 2021;50:6152–6220. doi:10.1039/D0CS00323A

101 Samaniyan M, Mirzaei M, Khajavian R, Eshtiagh-Hosseini H, Streb C. Heterogeneous Catalysis by Polyoxometalates in Metal–Organic Frameworks. *ACS Catal.* 2019;9:10174–10191. doi: 10.1021/acscatal.9b03439

102 Hoseini A-A, Farhadi S, Zabardasti A. Yolk–shell microspheres assembled from Preyssler-type $NaP_5W_{30}O_{110}^{14-}$ polyoxometalate and MIL-101(Cr) metal–organic framework: A new inorganic–organic nanohybrid for fast and selective removal of cationic organic dyes from aqueous media. *Appl Organometal Chem.* 2019;33:e4656. doi: 10.1002/aoc.4656

103 Jarrah A, Farhadi S. Preparation and characterization of novel polyoxometalate/$CoFe_2O_4$/metal-organic framework magnetic core-shell nanocomposites for the rapid removal of organic dyes from water. *RSC Adv.* 2020;10:39881–39893. doi: 10.1039/D0RA04603E

104 Liu X, Luo J, Zhu Y, Yang Y, Yang S. Removal of methylene blue from aqueous solutions by an adsorbent based on metal-organic framework and polyoxometalate. *J Alloys Compd.* 2015;648:986–993. doi: 10.1016/j.jallcom.2015.07.065

105 Sun J-W, Yan P-F, An G-H, Sha J-Q, Li G-M, Yang G-Y. Immobilization of Polyoxometalate in the Metal-Organic Framework rht-MOF-1: Towards a Highly Effective Heterogeneous Catalyst and Dye Scavenger. *Sci Rep.* 2016;6:25595. doi: 10.1038/srep25595

106 Li D, Guo Y, Hu C, Mao L, Wang E. Photocatalytic degradation of aqueous formic acid over the silica composite films based on lacunary Keggin-type polyoxometalates. *Appl Catal A Gen.* 2002;235:11–20. doi: 10.1016/S0926-860X(02)00238-7

107 Maldotti A, Molinari A, Varani G, Lenarda M, Storaro L, Bigi F, et al. Immobilization of $(n\text{-}Bu_4N)_4W_{10}O_{32}$ on Mesoporous MCM-41 and Amorphous Silicas for Photocatalytic Oxidation of Cycloalkanes with Molecular Oxygen. *J Catal*. 2002;209:210–216. doi: 10.1006/jcat.2002.3618

108 Zhang H, Wang X, Li N, Xia J, Meng Q, Ding J, et al. Synthesis and characterization of TiO_2/graphene oxide nanocomposites for photoreduction of heavy metal ions in reverse osmosis concentrate. *RSC Adv*. 2018;8(60):34241–34251. doi:10.1039/C8RA06681G

109 Zhang X, Li L, Shao D. Uptake of uranium from wastewater by polyoxometalate modified graphene oxide. *Sep Purif Technol.* 2022;302:122154. doi: 10.1016/j.seppur.2022.122154

110 He J, Sun H, Indrawirawan S, Duan X, Tade MO, Wang S. Novel polyoxometalate@g-C_3N_4 hybrid photocatalysts for degradation of dyes and phenolics. *J Colloid Interface Sci*. 2015;456:15–21. doi: 10.1016/j.jcis.2015.06.003

111 Ghali M, Brahmi C, Benltifa M, Dumur F, Duval S, Simonnet-Jégat C, et al. New hybrid polyoxometalate/polymer composites for photodegradation of eosin dye. *J Polym Sci Part A Polym Chem*. 2019;57:1538–1549. doi:10.1002/pola.29416

112 Heravi MM, Mirzei M. Polyoxometalate-Based Hybrids and their Applications. 1st ed. Elsevier; 2023. Paperback ISBN: 9780323917315, eBook ISBN: 9780323983464

113 Uchida S. Frontiers and progress in cation-uptake and exchange chemistry of polyoxometalate-based compounds. *Chem Sci.* 2019;10:7670−7679. doi: 10.1039/C9SC02823D

114 Kandasamy B, Sudmeier T, Ayass WW, Lin Z, Feng Q, Bassil BS, et al. Selective Rb^+ vs. K^+ Guest Incorporation in Wheel-Shaped 27-Tungsto-3-Arsenate(III) Host, $[M\subset(\beta\text{-}As^{III}W_8O_{30})(WO(H_2O))_3]^{14-}$ (M= K, Rb). *Eur J Inorg Chem.* 2019;(3−4):502−505. doi: 10.1002/ejic.201800788

115 Kawahara R, Uchida S, Mizuno N. Redox-Induced Reversible Uptake-Release of Cations in Porous Ionic Crystals Based on Polyoxometalate: Cooperative Migration of Electrons with Alkali Metal Ions. *Chem Mater*. 2015;27(6):2092−2099. doi: 10.1021/cm504526z

116 Pei X, Wang R. Desulfurization Performance of Rare Earth Mono-Substituted Heteropoly Compounds. *Aerosol Air Qual Res.* 2019;19(12):2888−2898. doi: 10.4209/aaqr.2019.10.0540

117 Dehghani R, Aber S, Mahdizadeh F. Polyoxometalates and Their Composites as Photocatalysts for Organic Pollutants Degradation in Aqueous Media-A Review. *CLEAN Soil Air Water*. 2018;46(12):1800413. doi: 10.1002/clen.201800413

118 Lindqvist I. On the Structure of the Paratungstate Ion. *Acta Crystallogr.* 1952;5:667−670. doi: 10.1107/S0365110X52001817

119 Saddington K, Cahn RW. The Formula of Sodium Paratungstate. *J Chem Soc.* 1950:3526−3529. doi: 10.1039/JR9500003526

120 Shimao E. Structure of the $Mo_7O_{24}^{6-}$ Ion in a Crystal of Ammonium Heptamolybdate Tetrahydrate. *Nature*. 1967;214:170−171. doi: 10.1038/214170a0

121 Sturdivant JH. The Formula of Ammonium Paramolybdate. *J Am Chem Soc*. 1937;59(4):630−631. doi: 10.1021/ja01283a010

122 Fuchs J, Hartl H. Anion Structure of Tetrabutylammonium Octamolybdate $[N(C_4H_9)_4]_4Mo_8O_{26}$. *Angew Chem Int Ed Engl.* 1976;15:375−376. doi: 10.1002/anie.197603751

123 Bridgeman AJ. The Electronic Structure and Stability of the Isomers of Octamolybdate. *J Phys Chem A*. 2002;106(50):12151−12160. doi: 10.1021/jp027037l

124 Fuchs J, Hartl H, Schiller W, Gerlach U. Die Kristallstruktur des Tributylammoniumdekawolframats $[(C_4H_9)_2NH]_4W_{10}O_{23}$. *Acta Cryst B.* 1976;32:740−749. doi: 10.1107/S0567740876003907

125 Chemseddine A, Sanchez C, Livage J, Launay JP, Fournier M. Electrochemical and photochemical reduction of decatungstate: a reinvestigation. *Inorg Chem.* 1984;23(17):2609−2613. doi: 10.1021/ic00185a014

126 Evans HT Jr. The Molecular Structure of the Isopoly Complex Ion, Decavanadate ($V_{10}O_{28}^{6-}$). *Inorg Chem*. 1966;5(6):967−977. doi: 10.1021/ic50040a004

127 Rossotti FJC, Rossotti H. Equilibrium Studies of Polyanions. *Acta Chem Scand.* 1956;10(6):957−984. http://actachemscand.org/pdf/acta_vol_10_p0957-0984.pdf

128 Keggin JF. Structure of the Molecule of 12-Phosphotungstic Acid. *Nature*. 1933;131:908−909. doi: 10.1038/131908b0

129 Linz A. Preparation of Phosphomolybdic Acid from Phosphoric Acid and Pure Molybdic Acid. *Ind Eng Chem Anal Ed.* 1943;15(7):459. doi: 10.1021/i560119a015

View Article Online
DOI: 10.1039/D5EN00964B

130 Khajavian R, Jodaian V, Taghipour F, Mague JT, Mirzaei M. Roles of Organic Fragments in Redirecting Crystal/Molecular Structures of Inorganic-Organic Hybrids Based on Lacunary Keggin-Type Polyoxometalates. *Molecules*. 2021;26:5994–6020. doi: 10.3390/molecules26195994

131 Dawson B. The Structure of the 9(18)-Heteropoly Anion in Potassium 9(18)-Tungstophosphate, $K_6(P_2W_{18}O_{62})x14H_2O$. *Acta Crystallogr.* 1953;6:113–126. doi: 10.1107/S0365110X53000466

132 Khermann F. Zur Kenntnis der komplexen anorganischen Säuren. III. Abhandlung. *Z Anorg Allg Chem.* 1892;1:423–441. doi: 10.1002/zaac.18920010139

133 Evans HT. The Crystal Structures Of Ammonium And Potassium Molybdotellurates. *J Am Chem Soc*. 1948;70(3):1291–1292. doi: 10.1021/ja01183a521

134 Meloche VW, Woodstock W. The Preparation And Study Of Two Ammonium Molybdotellurates. J *Am Chem Soc.* 1929;51(1):171–174. doi: 10.1021/ja01376a020

135 Alizadeh MH, Harmalker SP, Jeannin Y, Martin-Frere J, Pope MT. A heteropolyanion with fivefold molecular symmetry that contains a nonlabile encapsulated sodium ion. The structure and chemistry of $[NaP_5W_{30}O_{110}]^{14-}$. *J Am Chem Soc*. 1985;107:2662–2669. doi: 10.1021/ja00295a019

136 Hedman B, Strandberg R. Multicomponent polyanions. 19. The molecular and crystal structure of $Na_5HMo_5P_2O_{23}(H_2O)_{11}$, a superstructure with sodium-coordinated monohydrogenpentamolybdodiphosphate anions. *Acta Cryst B.* 1979;35:278–284. doi: 10.1107/S0567740879003356

137 Pettersson L. Multicomponent Polyanions. I. On Yellow and Colorless Molybdophosphates in 3 M $Na(ClO_4)$. A Determination of Formation Constants for Three Colourless Pentamolybdodiphosphates in the pH-range 3-9. *Acta Chem Scand.* 1971;25:1959–1974. doi: 10.3891/acta.chem.scand.25-1959

138 Weakley TJR, Evans HT, Showell JS, Tourné GF, Tourné CM. 18-Tungstotetracobalto(II)Diphosphate and Related Anions: A Novel Structural Class of Heteropolyanions. *J Chem Soc Chem Commun*. 1973;(4):139–140. doi: 10.1039/C39730000139

139 Evans HT, Tourn CM, Tourn GF, Weakley TJR. X-Ray crystallographic and tungsten-183 nuclear magnetic resonance structural studies of the $[M_4(H_2O)_2(XW_9O_{34})_2]^{10-}$ heteropolyanions (M = CoII or Zn, X = P or As). *J Chem Soc Dalton Trans*. 1986;(12):2699–2705. doi: 10.1039/DT9860002699

140 Müller A, Roy S. En route from the mystery of molybdenum blue via related manipulatable building blocks to aspects of materials science. *Coord Chem Rev*. 2003;245(1–2):153–166. doi: 10.1016/S0010-8545(03)00110-3

141 Müller A, Peters F, Pope MT, Gatteschi D. Polyoxometalates: Very Large Clusters-Nanoscale Magnets. *Chem Rev*. 1998;98(1):239–272. doi: 10.1021/cr9603946

142 Jeannin YP. The Nomenclature of Polyoxometalates: How To Connect a Name and a Structure. *Chem Rev*. 1998;98(1):51–76. doi: 10.1021/cr960397i

143 Gumerova NI, Romel A. Speciation atlas of polyoxometalates in aqueous solutions. *Sci Adv*. 2023;9(25):eadi0814. doi:10.1126/sciadv.adi0814

144 Zdrnja M, Gumerova NI, Rompel A. Exploring polyoxometalate speciation: the interplay of concentration, ionic strength, and buffer composition. *Front Chem Biol*. 2024;3:1444359. doi:10.3389/fchbi.2024.1444359

145 Gregorovic I, Gumerova NI, Rompel A. Speciation atlas of polyoxometalates in aqueous solution (Part II): molybdenum browns. *Sci Adv*. 2025;11(44):eaea1910. doi:10.1126/sciadv.aea1910

146 Guo Y, Hu C, Jiang S, Guo C, Yang Y, Wang E. Heterogeneous photodegradation of aqueous hydroxy butanedioic acid by microporous polyoxometalates. *Appl Catal B Environ.* 2002;36:9–17. doi: 10.1016/S0926-3373(01)00260-0

147 Chen X, Souvanhthong B, Wang H, Zheng H, Wang X, Huo M. Polyoxometalate-based Ionic liquid as thermoregulated and environmentally friendly catalyst for starch oxidation. *Appl Catal B Environ.* 2013;138:161–166. doi: 10.1016/j.apcatb.2013.02.028

148 Rezvani MA, Aghmasheh M. Synthesis of t-B.PWFe/NiO nanocomposite as an efficient and heterogeneous green nanocatalyst for catalytic oxidative-extractive desulfurization of gasoline. *Environ Prog Sustain Energy*. 2021;40:e13616. doi: 10.1002/ep.13616

149 Xun S, Ti Q, Wu L, He M, Wang C, Chen L, et al. Few layer g-C_3N_4 dispersed quaternary phosphonium ionic liquid for highly efficient catalytic oxidative desulfurization of fuel. *Energy Fuels*. 2020;34(10):12379–12387. doi:10.1021/acs.energyfuels.0c02357

150 Wang P, Jiang L, Zou X, Tan H, Zhang P, Li J, et al. Confining polyoxometalate clusters into porous aromatic framework materials for catalytic desulfurization of dibenzothiophene. *ACS Appl Mater Interfaces*. 2020;12(23):25910–25919. doi:10.1021/acsami.0c05392

151 Li J, Yang Z, Hu G, Zhao J. Heteropolyacid supported MOF fibers for oxidative desulfurization of fuel. *Chem Eng J.* 2020;388:124325. doi: 10.1016/j.cej.2020.124325

152 Zhao XY, Wang X, Zhao Y, Sun H, Tan H, Qiu T, et al. Polyoxometalates-doped TiO_2/Ag hybrid heterojunction: removal of multiple pollutants and mechanism investigation. *Environ Sci Nano.* 2021;8:3855–3864. doi:10.1039/D1EN00827G

153 Chen K, She S, Zhang J, Bayaguud A, Wei Y. Label-free colorimetric detection of mercury via Hg^{2+} ions-accelerated structural transformation of nanoscale metal-oxo clusters. *Scientific Reports.* 2015;5:16316. doi:10.1038/srep16316.

154 Sun J-W, Yan P-F, An G-H, Sha J-Q, Li G-M, Yang G-Y. Immobilization of polyoxometalate in the metal-organic framework rht-MOF-1: towards a highly effective heterogeneous catalyst and dye scavenger. *Scientific Reports.* 2016;6:25595. doi:10.1038/srep25595

155 Song H, Guo M-S, Wang J-F, Liu Y-Q, Bi H-X, Du J, et al. Reduced phosphomolybdate as photoassisted electrochemical crystalline sensor for trace Cr(VI) detection. *Polyoxometalates*. 2024;3(4):9140065. doi:10.26599/POM.2024.9140065

156 Li S, Zheng Y, Liu G-C, Li X-H, Zhang Z, Wang X-L. New two-fold interpenetrating 3D polyoxovanadate-based metal–organic framework as bifunctional catalyst for the removal of 2-chloroethyl ethyl sulfide and phenolic compounds. *Polyoxometalates.* 2024;3(3):9140061. doi:10.26599/POM.2024.9140061

157 Dai Y-C, Zhang S-Y, Xiao X-X, Li M-J, Liu J-C, Chen L-J, et al. A double-tartrate-bridged deca-nuclearity europium–tungsten cluster embedded selenotungstate and its selective optical sensing of o-nitrophenol. *Polyoxometalates*. 2023;2(4):9140041. doi:10.26599/POM.2023.9140041

158 Xia Z, Wang L, Zhang Q, Li F, Xu L. Fast degradation of phenol over porphyrin–polyoxometalate composite photocatalysts under visible light. *Polyoxometalates*. 2022;1(1):9140001. doi:10.26599/POM.2022.9140001

159 Liang R, Huang R, Ying S, Wang X, Yan G, Wu L. Facile in situ growth of highly dispersed palladium on phosphotungstic-acid-encapsulated MIL-100(Fe) for the degradation of pharmaceuticals and personal care products under visible light. *Nano Res*. 2018;11:1109–1123. doi:10.1007/s12274-017-1730-0.

160 Chen K, Bayaguud A, Li H, Chu Y, Zhang H, Jia H, et al. Improved peroxidase-mimic property: sustainable, high-efficiency interfacial catalysis with H_2O_2 on the surface of vesicles of hexavanadate–organic hybrid surfactants. *Nano Res*. 2018;11:1313–1321. doi:10.1007/s12274-017-1746-5

161 Mohamed AM, Abbas WA, Khedr GE, Abass W, Allam NK. Computational and experimental elucidation of the boosted

stability and antibacterial activity of ZIF-67 upon optimized encapsulation with polyoxometalates. *Scientific Reports.* 2022;12:15989. doi:10.1038/s41598-022-20392-4.

162 Ma X-Y, Bi H-X, Zhang X-J, Du J, Ma Y-Y, Han Z-G. Effect of bridging units on the detection performance of $Cd\{P_4Mo_6\}_2$-based electrochemical sensors for trace chromium(VI) and tetracycline. *Polyoxometalates*. 2025;4(2):9140090. doi:10.26599/POM.2025.9140090

163 Hao Y, Ji T, Zhang J, Chen W. Triboelectric nanogenerator based on changing the nanomorphology of polyoxometalates for gait monitoring of teenagers. *Nano Res.* 2025;18(2):94907192. doi:10.26599/NR.2025.94907192

164 Srivastav AL, Ranjan M. Chapter 1 - Inorganic Water Pollutants. In: Inorganic Pollutants in Water. 1st ed. Elsevier; 2020:1–15. doi: 10.1016/B978-0-12-818965-8.00001-9

165 Wasewar KL, Singh S, Kansal SK. Chapter 13 - Process Intensification of Treatment of Inorganic Water Pollutants. In: Inorganic Pollutants in Water. 1st ed. Elsevier; 2020:245–271. doi: 10.1016/B978-0-12-818965-8.00013-5

166 D'Cruz B, Amin MO, Al-Hetlani E. Polyoxometalate-Based Materials for the Removal of Contaminants from Wastewater: A Review. *Ind Eng Chem Res*. 2021;60(30):10960–10977. doi: 10.1021/acs.iecr.1c02007

167 Xu F-L, Jorgensen SE, Shimizu Y, Silow E. Editorial Persistent Organic Pollutants in Fresh Water Ecosystems. *Sci World J.* 2013;2013:303815. doi: 10.1155/2013/303815

168 Bolisetty S, Peydayesh M, Mezzenga R. Sustainable technologies for water purification from heavy metals: review and analysis. *Chem Soc Rev*. 2019;48:463–487. doi: 10.1039/C8CS00493E

169 Hu M, Xu Y. Visible light induced degradation of chlorophenols in the presence of H_2O_2 and iron substituted polyoxotungstate. *Chem Eng J.* 2014;246:299–305. doi: 10.1016/j.cej.2014.02.072

170 Taghdiri M, Saadatjou N, Zamani N, Farrokhi R. Heterogeneous degradation of precipitated hexamine from wastewater by catalytic function of silicotungstic acid in the presence of H_2O_2 and H_2O_2/Fe^{2+}. *J Hazard Mater.* 2013;246:206–212. doi: 10.1016/j.jhazmat.2012.12.029

171 Lan J, Wang Y, Huang B, Xiao Z, Wu P. Application of polyoxometalates in photocatalytic degradation of organic pollutants. *Nanoscale Adv.* 2021;3:4646–4658. doi: 10.1039/D1NA00408E

172 Wang Y, Fang G, Ordomsky VV, Khodakov AY. Polyoxometalate photocatalysts: solar-driven activation of small molecules for energy conversion and greenhouse gas valorization. *Chem Commun*. 2025;61:10630–10642. doi: 10.1039/D5CC01494H

173 Lu N, Wang Y, Ning S, Zhao W, Qian M, Ma Y, et al. Design of plasmonic Ag-TiO_2/$H_3PW_{12}O_{40}$ composite film with enhanced sunlight photocatalytic activity towards o-chlorophenol degradation. *Sci Rep*. 2017;7:17298. doi:10.1038/s41598-017-17221-4

174 Tahmasebi M, Mirzei M, Frontera A. Noble metals in polyoxometalates. *Inorg Chim Acta*. 2021;523:120410. doi: 10.1016/j.ica.2021.120410

175 Fashapoyeh MA, Mirzaei M, Eshtiagh-Hosseini H, Rajagopal A, Lechner M, Liu R, et al. Photochemical and electrochemical hydrogen evolution reactivity of lanthanide-functionalized polyoxotungstates. *Chem Commun.* 2018;54:10427–10430. doi: 10.1039/C8CC06334F

176 Li K, Guo Y, Ma F, Li H, Chen L, Guo Y. Design of ordered mesoporous $H_3PW_{12}O_{40}$-titania materials and their photocatalytic activity to dye methyl orange degradation. *Catal Commun*. 2010;11:839–843. doi: 10.1016/j.catcom.2010.03.004

177 Liu Y, Tang C, Cheng M, Chen M, Chen S, Lei L, et al. Polyoxometalate@Metal-Organic Framework Composites as Effective Photocatalysts. *ACS Catal*. 2021;11(21):13374–13396. doi: 10.1021/acscatal.1c03866

178 Liang R, Hu A, Hatat-Fraile M, Zhou N. Fundamentals on Adsorption, Membrane Filtration, and Advanced Oxidation Processes for Water Treatment. In: Nanotechnology for Water Treatment and Purification. Cham: Springer; 2014:1–45. doi: 10.1007/978-3-319-06578-6_1

179 Yao L, Long Z, Chen Z, Cheng Q, Liao Y, Tian M. Property Characterization and Mechanism Analysis of Polyoxometalates-Functionalized PVDF Membranes by Electrochemical Impedance Spectroscopy. *Membranes*. 2020;10:214. doi: 10.3390/membranes10090214

180 Yao L, Lua SK, Zhang L, Wang R, Dong Z. Dye removal by surfactant encapsulated polyoxometalates. *J Hazard Mater.* 2014;280:428–435. doi: 10.1016/j.jhazmat.2014.08.026

181 Heravi MM, Mirzaei M. Reactivity and stability synergism directed by the electron transfer between polyoxometalates and metal-organic frameworks. *Catal Sci Technol*. 2023;13(14):4162–4172. doi:10.1039/D3CY00569K

182 Du J, Ma Y, Li Y-G. Unraveling photocatalytic electron transfer mechanism in polyoxometalate-encapsulated metal-organic frameworks for high-efficient CO_2 reduction reaction. *Appl Catal B Environ*. 2022;318:121850. doi: 10.1016/j.apcatb.2022.121850

183 Galiano F, Mancuso R, Carraro M, Bundschuh J, Hoinkis J, Bonchio M, et al. A polyoxometalate-based self-cleaning smart material with oxygenic activity for water remediation with membrane technology. *Appl Mater Today.* 2021;23:101002. doi: 10.1016/j.apmt.2021.101002

184 Zhang M-M, Li A-K, Tang M-J, He Q-Y, Peng Y-H, Fan R-J, et al. Constructing polyoxometalates-based electrocatalytic nanofiltration membranes for nitrite removal. *J Membr Sci.* 2024;699:122668. doi: 10.1016/j.memsci.2024.122668

185 Liao Z, Gao T, Zhang J, Wu Q, Shi J, Yang Z, et al. Polyoxometalates decoration combining with solvent activation for enhanced separation performance of nanofiltration membrane. *J Membr Sci.* 2024;706:122964. doi: 10.1016/j.memsci.2024.122964

186 Bonchio M, Carraro M, Scorrano G, Fontananova E, Drioli E. Heterogeneous Photooxidation of Alcohols in Water by Photocatalytic Membranes Incorporating Decatungstate. *Adv Synth Catal.* 2003;345:1119–1126. doi: 10.1002/adsc.200303076

187 Fontananova E, Donato L, Drioli E, Lopez LC, Favia P, d'Agostino R. Heterogenization of Polyoxometalates on the Surface of Plasma-Modified Polymeric Membranes. *Chem Mater.* 2006;18:1561–1568. doi: 10.1021/cm051739g

188 Romanenko I, Lechner M, Wendler F, Hörenz C, Streb C, Schacher FH. POMbranes: polyoxometalate-functionalized block copolymer membranes for oxidation catalysis. *J Mater Chem A.* 2017;5:15789–15796. doi: 10.1039/C7TA03220J

189 Yao L, Zhang L-Z, Wang R, Loh CH, Dong Z-L. Fabrication of catalytic membrane contactors based on polyoxometalates and polyvinylidene fluoride intended for degrading phenol in wastewater under mild conditions. *Sep Purif Technol.* 2013;118:162–169. doi: 10.1016/j.seppur.2013.06.029

190 Yao L, Zhang L, Wang R, Chou S, Dong Z. A new integrated approach for dye removal from wastewater by polyoxometalates functionalized membranes. *J Hazard Mater.* 2016;301:462–470. doi: 10.1016/j.jhazmat.2015.09.027

191 Giannakas AE, Antonopoulou M, Daikopoulos C, Deligiannakis Y, Konstantinou I. Characterization and Catalytic Performance of B-Doped, B-N Co-Doped and B-N-F Tri-Doped TiO2 towards Simultaneous Cr(VI) Reduction and Benzoic Acid Oxidation. *Appl Catal B Environ.* 2016;184:44–54. doi: 10.1016/j.apcatb.2015.11.009

192 McEvoy JG, Zhang Z. Synthesis and Characterization of Magnetically Separable Ag/AgCl-Magnetic Activated Carbon Composites for Visible Light Induced Photocatalytic Detoxification and Disinfection. *Appl Catal B Environ.* 2014;160:267–278. doi: 10.1016/j.apcatb.2013.07.062

DOI: 10.1039/D5EN00964B

193 Gong K, Wang W, Yan J, Han Z. Highly Reduced Molybdophosphate as a Noble-Metal-Free Catalyst for the Reduction of Chromium Using Formic Acid as a Reducing Agent. *J Mater Chem A.* 2015;3(11):6019–6027. doi: 10.1039/C4TA06830K

194 Gong K, Liu Y, Wang W, Fang T, Zhao C, Han Z, Zhai X. Reduced Phosphomolybdates as Molecular Catalysts for Hexavalent Chromium Reduction. *Eur J Inorg Chem*. 2015;32:5351–5356. doi: 10.1002/EJIC.201500883

195 Shi H-F, Yan G, Zhang Y, Tan H-Q, Zhou W-Z, Ma Y-Y, et al. $Ag/Ag_xH_{3-x}PMo_{12}O_{40}$ nanowires with enhanced visible-light-driven photocatalytic performance. *ACS Appl Mater Interfaces.* 2017;9(1):422–30. doi:10.1021/acsami.6b13009

196 Daupor H, Wongnawa S. Urchinlike Ag/AgCl Photocatalyst: Synthesis, Characterization, and Activity. *Appl Catal A Gen.* 2014;473:59–69. doi: 10.1016/J.APCATA.2013.12.036

197 Wang D, Duan Y, Luo Q, Li X, Bao L. Visible Light Photocatalytic Activities of Plasmonic Ag/AgBr Particles Synthesized by a Double Jet Method. *Desalination.* 2011;270(1-3):174–180. doi: 10.1016/J.DESAL.2010.11.042

198 Wan J, Liu E, Fan J, Hu X, Sun L, Tang C, et al. In-situ synthesis of plasmonic Ag/Ag_3PO_4 tetrahedron with exposed {111} facets for high visible-light photocatalytic activity and stability. *Ceram Int*. 2015;41(5):6933–40. doi:10.1016/j.ceramint.2015.01.148

199 Zhao W, Guo Y, Faiz Y, Yuan WT, Sun C, Wang SM, et al. Facile in-suit synthesis of Ag/AgVO3 one-dimensional hybrid nanoribbons with enhanced performance of plasmonic visible-light photocatalysis. *Appl Catal B Environ*. 2015;163:288–97. doi:10.1016/j.apcatb.2014.08.015

200 Zhao X, Zhang Y, Zhao Y, Tan H, Zhao Z, Shi H, et al. $Ag_xH_{3-x}PMo_{12}O_{40}$/Ag nanorods/g-$C_3N_4$ 1D/2D Z-scheme heterojunction for highly efficient visible-light photocatalysis. *Dalton Trans*. 2019;48(19):6484–91. doi:10.1039/C9DT00744J

201 Zhang H, Yang J, Liu Y-Y, Song S-Y, Liu X-L, Ma J-F. Visible Light Photodegradation of Organic Dyes, Reduction of CrVI and Catalytic Oxidative Desulfurization by a Class of Polyoxometalate-Based Inorganic-Organic Hybrid Compounds. *Dyes Pigm.* 2016;133:189–200. doi: 10.1016/j.dyepig.2016.05.051S.

202 Buffet-Bataillon S, Tattevin P, Bonnaure-Mallet M, Jolivet-Gougeon A. Emergence of Resistance to Antibacterial Agents: The Role of Quaternary Ammonium Compounds-a Critical Review. *Int J Antimicrob Agents*. 2012;39(5):381–389. doi: 10.1016/j.ijantimicag.2012.01.011

203 Shakeela K, Rao GR. Thermoreversible, Hydrophobic Ionic Liquids of Keggin-Type Polyanions and Their Application for the Removal of Metal Ions from Water. *ACS Appl Nano Mater.* 2018;1(9):4642–4651. doi: 10.1021/acsanm.8b00920

204 Kitson PJ, Symes MD, Dragone V, Cronin L. Combining 3D Printing and Liquid Handling to Produce User-Friendly Reactionware for Chemical Synthesis and Purification. *Chem Sci.* 2013;4(8):3099–3103. doi: 10.1039/C3SC51253C

205 Ji Y, Ma Y, Ma Y, Asenbauer J, Passerini S, Streb C. Water Decontamination by Polyoxometalate-Functionalized 3D-Printed Hierarchical Porous Devices. *Chem Commun.* 2018;54(24):3018–3021. doi: 10.1039/C8CC00821C

206 Mitchell SG, Streb C, Miras HN, Boyd T, Long D-L, Cronin L. Face-Directed Self-Assembly of an Electronically Active Archimedean Polyoxometalate Architecture. *Nat Chem.* 2010;2:308–312. doi: 10.1038/nchem.581

207 Wang S, Geng X, Zhao Z, Zhang M, Song Y, Sun K, et al. Ammoniated-driven green synthesis of charged polyoxometalate supported ionic liquids for exceptional heavy metal remediation in actual industrial wastewater. *Water Res*. 2025;272:122939. doi:10.1016/j.watres.2024.122939

208 Zou F, Yu R, Li R, Li W. Microwave-assisted Synthesis of HKUST-1 and Functionalized HKUST-1-@ $H_3PW_{12}O_{40}$: Selective Adsorption of Heavy Metal Ions in Water Analyzed with Synchrotron Radiation. *ChemPhysChem*. 2013;14(12):2825–2832. doi: 10.1002/cphc.201300215

209 Zhang H, Xue J, Hu N, Sun J, Ding D, Wang Y, et al. Selective removal of U(VI) from low concentration wastewater by functionalized HKUST-1@$H_3PW_{12}O_{40}$. *J Radioanal Nucl Chem*. 2016;308:865–75. doi:10.1007/s10967-015-4603-6

210 Frost RL, Čejka J, Dickfos MJ. Raman Spectroscopic Study of the Uranyl Minerals Vanmeersscheite $U(OH)_4[(UO_2)_3(PO_4)_2(OH)_2]\cdot 4H_2O$ and Arsenouranylite $Ca(UO_2)[(UO_2)_3(AsO_4)_2(OH)_2]\cdot(OH)_2\cdot 6H_2O$. *Spectrochim Acta A Mol Biomol Spectrosc*. 2009;71(5):1799–1803. doi: 10.1016/j.saa.2008.06.041

211 Shao D, Li Y, Wang X, Hu S, Wen J, Xiong J, et al. Phosphate-functionalized polyethylene with high adsorption of uranium(VI). *ACS Omega*. 2017;2(7):3267–75. doi:10.1021/acsomega.7b00375

212 Han X, Wang Y, Cao X, Dai Y, Liu Y, Dong Z, et al. Adsorptive performance of ship-type nano-cage polyoxometalates for U(VI) in aqueous solution. *Appl Surf Sci*. 2019;484:1035–40. doi:10.1016/j.apsusc.2019.04.121

213 Seino S, Kawahara R, Ogasawara Y, Mizuno N, Uchida S. Reduction-Induced Highly Selective Uptake of Cesium Ions by an Ionic Crystal Based on Silicododecamolybdate. *Angew Chem Int Ed.* 2016;55(12):4055–4059. doi: 10.1002/ange.201511633

214 Hitose S, Uchida S. Rapid Uptake/Release of Cs^+ in Isostructural Redox-Active Porous Ionic Crystals with Large-Molecular-Size and Easily Reducible Dawson-Type Polyoxometalates as Building Blocks. *Inorg Chem.* 2018;57(9):4833–4836. doi: 10.1021/acs.inorgchem.8b00801

215 Liu X, Gong W, Luo J, Zou C, Yang Y, Yang S. Selective adsorption of cationic dyes from aqueous solution by polyoxometalate-based metal-organic framework composite. *Appl Surf Sci.* 2016;362:517–524. doi: 10.1016/j.apsusc.2015.11.151

216 Sabarinathan C, Karuppasamy P, Vijayakumar C, Arumuganathan T. Development of methylene blue removal methodology by adsorption using molecular polyoxometalate: Kinetics, Thermodynamics and Mechanistic Study. *Microchem J.* 2019;146:315–326. doi: 10.1016/j.microc.2019.01.015

217 Bai L, Pan X, Guo R, Linghu X, Shu Y, Wu Y, et al. Sunlight-driven photocatalytic degradation of organic dyes in wastewater by chemically fabricated $ZnO/Cs_4SiW_{12}O_{40}$ nanoheterojunction. *Appl Surf Sci*. 2022;599:153912. doi:10.1016/j.apsusc.2022.153912

218 Wang R, Liu Y, Zuo P, Zhang Z, Lei N, Liu Y. Phthalocyanine-sensitized evolution of hydrogen and degradation of organic pollutants using polyoxometalate photocatalysts. *Environ Sci Pollut Res.* 2020;27:18831–18842. doi: 10.1007/s11356-020-08425-9

219 Yang Z, Gao S, Li H, Cao R. Synthesis and visible light photocatalytic properties of polyoxometalate-thionine composite films immobilized on porous TiO_2 microspheres. *J Colloid Interface Sci.* 2012;375(1):172–179. doi: 10.1016/j.jcis.2012.02.043

220 Qi L, Gong Y, Fang M, Jia Z, Cheng N, Yu L. Surface-Active Ionic-Liquid-Encapsulated Polyoxometalate Nanospheres: Construction, Self-Assembly, Adsorption Behavior, and Application for Dye Removal. *ACS Appl Nano Mater.* 2020;3(1):375–383. doi: 10.1021/acsanm.9b02012

221 Bi B, Xu L, Xu B, Liu X. Heteropoly blue-intercalated layered double hydroxides for cationic dye removal from aqueous media. *Appl Clay Sci.* 2011;54:242–247. doi: 10.1016/j.clay.2011.09.003

222 Lesbani A, Taher T, Rahayu Palapa N, Mohadi R, Rachmat A, Mardiyanto R. Preparation and utilization of Keggin-type polyoxometalate intercalated Ni-Fe layered double hydroxides for enhanced adsorptive removal of cationic dye. *SN Appl Sci.* 2020;2:470. doi: 10.1007/s42452-020-2300-8

223 Lei P, Chen C, Yang J, Ma W, Zhao J, Zang L. Degradation of Dye Pollutants by Immobilized Polyoxometalate with H_2O_2 under Visible-Light Irradiation. *Environ Sci Technol.* 2005;39(21):8466−8474. doi: 10.1021/es050321g

224 Lee C, Keenan CR, Sedlak DL. Polyoxometalate-Enhanced Oxidation of Organic Compounds by Nanoparticulate Zero-Valent Iron and Ferrous Ion in the Presence of Oxygen. *Environ Sci Technol.* 2008;42(13):4921−4926. doi: 10.1021/es800317j

225 Fei B-L, Zhong J-K, Deng N-P, Wang J-H, Liu Q-B, Li Y-G, et al. A novel 3D heteropoly blue type photo-Fenton-like catalyst and its ability to remove dye pollution. *Chemosphere*. 2018;197:241–50. doi:10.1016/j.chemosphere.2018.01.053

226 Grabsi M, Zabat N, Khellaf N, Ismail F. Synthesis of an environmental nano-polyoxometalate $(\alpha_2P_2W_{17}CoO_{61})^{8-}$ as catalyst for dyes degradation: A comparative study oxidation of indigoid and azo dyes. *Environ Nanotechnol Monit Manag*. 2019;12:100269. doi: 10.1016/j.enmm.2019.100269

227 Li L, Sun J-W, Sha J-Q, Li G-M, Yan P-F, Wang C, Yu L. Structure Refinement and Photocatalytic Properties of Porous POMCPs by Selecting the Isomerous PYTTZ. *Dalton Trans.* 2015;44(4):1948−1954. doi: 10.1039/C4DT02960G

228 Shokri A, Fard MS. A critical review in Fenton-like approach for the removal of pollutants in the aqueous environment. *Environmental Challenges*. 2022;7:100534. doi: 10.1016/j.envc.2022.100534

229 An X, Tang Q, Lan H, Liu H, Qu J. Polyoxometalates/TiO_2 Fenton-like photocatalysts with rearranged oxygen vacancies for enhanced synergetic degradation. *Appl Catal B Environ.* 2019;244:407−413. doi: 10.1016/j.apcatb.2018.11.063

230 Orooji Y, Tanhaei B, Ayati A, Tabrizi SH, Alizadeh M, Bamoharram FF, et al. Heterogeneous UV-switchable Au nanoparticles decorated tungstophosphoric acid/TiO_2 for efficient photocatalytic degradation proces. *Chemosphere*. 2021;281:130795. doi:10.1016/j.chemosphere.2021.130795

231 Zhang L, Chen H, Zhao X, Zhai Q, Yin D, Sun Y, et al. The Marriage of Ferrocene and Silicotungstate: An Ingenious Heterogeneous Fenton-like Synergistic Photocatalyst. *Appl Catal B Environ*. 2016;193:47−57. doi: 10.1016/j.apcatb.2016.04.019

232 Wang Q, Liu E, Zhang C, Huang S, Cong Y, Zhang Y. Synthesis of $Cs_3PMo_{12}O_{40}/Bi_2O_3$ Composite with Highly Enhanced Photocatalytic Activity under Visible-Light Irradiation. *J Colloid Interface Sci.* 2018;516:304−311. doi: 10.1016/j.jcis.2018.01.065

233 Samal K, Mahapatra S, Ali MH. Pharmaceutical wastewater as Emerging Contaminants (EC): Treatment technologies, impact on environment and human health. Energy *Nexus.* 2022;6:100076. doi: 10.1016/j.nexus.2022.100076

234 Mishra RK, Mentha SS, Mirsa Y, Dwivedi N. Emerging pollutants of severe environmental concern in water and wastewater: A comprehensive review on current developments and future research. *Water-Energy Nexus*. 2023;6:74−95. doi: 10.1016/j.wen.2023.08.002

235 Wang S, Wang X, Shi X-Y, Meng C-X, Sun C-L, Wu Z-S. A three-dimensional polyoxometalate/graphene aerogel as a highly efficient and recyclable absorbent for oil/water separation. *New Carbon Mater.* 2021;36(1):189−197. doi: 10.1016/S1872-5805(21)60013-6

236 Wang S, Wang X, Shi X-Y, Meng C-X, Sun C-L, Wu Z-S, et al. Emerging contaminants: A One Health perspective. *Innovation.* 2024;4:100612. doi: 10.1016/j.xinn.2024.100612

237 Rubio-Armendáriz C, Alejandro-Vega S, Paz-Montelongo S, Gutiérrez-Fernández ÁJ, Carrascosa-Iruzubieta CJ, Hardisson-de la Torre A. Microplastics as Emerging Food Contaminants: A Challenge for Food Safety. *Int J Environ Res Public Health.* 2022;19(3):1174. doi: 10.3390/ijerph19031174

238 Sousa M, Machado I, Simões LC, Simões M. Biocides as drivers of antibiotic resistance: A critical review of environmental implications and public health risks. *Environ Sci Ecotechnology*. 2025;25:100557. doi: 10.1016/j.ese.2025.100557

239 Caloni S, Durazzano T, Franci G, Marsili L. Sunscreens' UV Filters Risk for Coastal Marine Environment Biodiversity: A Review. *Diversity*. 2021;13:374. doi: 10.3390/d13080374

240 European Commission, Joint Research Centre, Gomez Cortes L, Marinov D, Sanseverino I, Navarro Cuenca A, et al. Selection of substances for the 4th Watch List under the Water Framework Directive. EUR 31148 EN. Luxembourg: Publications Office of the European Union; 2022. ISBN 978-92-76-55020-4. doi:10.2760/01939

241 European Chemicals Bureau, Institute for Health and Consumer Protection (Joint Research Centre). Technical Guidance Document on Risk Assessment in Support of Commission Directive 93/67/EEC on Risk Assessment for New Notified Substances, Commission Regulation (EC) No 1488/94 on Risk Assessment for Existing Substances, Directive 98/8/EC of the European Parliament and of the Council Concerning the Placing of Biocidal Products on the Market. Part III. Luxembourg: European Commission – Joint Research Centre; 2008. https://op.europa.eu/en/publication-detail/-/publication/212940b8-3e55-43f8-8448-ba258d0374bb

242 Boix C, Ibáñez M, Zamora T, Sancho JV, Niessen WMA, Hernández F. Identification of New Omeprazole Metabolites in Wastewaters and Surface Waters. *Sci Total Environ.* 2014;468:706−714. doi: 10.1016/j.scitotenv.2013.08.095

243 Wielens Becker R, Ibáñez M, Cuervo Lumbaque E, Wilde ML, Flores da Rosa T, Hernández F, et al. Investigation of pharmaceuticals and their metabolites in Brazilian hospital wastewater by LC-QTOF MS screening combined with a preliminary exposure and in silico risk assessment. *Sci Total Environ*. 2020;699:134218. doi:10.1016/j.scitotenv.2019.134218

244 Qiu X, Wang R. Polyoxometalate-Based Photocatalytic New Materials for the Treatment of Water Pollutants: Mechanism, Advances, and Challenges. *Catalysts*. 2025;15:613. doi: 10.3390/catal15070613

245 Murmu G, Panigrahi TH, Saha S. Recent advances in the development of polyoxometalates and their composites for the degradation of toxic chemical dyes. *Prog Solid State Chem.* 2024;76:100489. doi: 10.1016/j.progsolidstchem.2024.100489

246 Oliveira M, Antunes W, Mota S, Madureira-Carvalho A, Dinis-Oliveira RJ, Dias da Silva D. An Overview of the Recent Advances in Antimicrobial Resistance. *Microorganisms.* 2024;12:1920. doi: 10.3390/microorganisms12091920

247 Derakhshanrad S, Mirzaei M, Streb C, Amiri A, Ritchie C. Polyoxometalate-Based Frameworks as Adsorbents for Drug of Abuse Extraction from Hair Samples. *Inorg Chem.* 2021;60(3):1472−1479. doi: 10.1021/acs.inorgchem.0c02769

248 Yola ML, Atar N, Eren T, Karimi-Maleh H, Wang S. Sensitive and selective determination of aqueous triclosan based on gold nanoparticles on polyoxometalate/reduced graphene oxide nanohybrid. *RSC Adv.* 2015;5:65953−65962. doi: 10.1039/C5RA07443F

249 Cai J, Zhu G-T, He X-M, Zhang Z, Wang R-Q, Feng Y-Q. Polyoxometalate incorporated polymer monolith microextraction for highly selective extraction of antidepressants in undiluted urine. *Talanta*. 2017;170:252−259. doi: 10.1016/j.talanta.2017.04.020

250 He R, Xue K, Wang J, Yan Y, Peng Y, Yang T, et al. Nitrogen-Deficient g-C_3N_x/POMs Porous Nanosheets with P-N Heterojunctions Capable of the Efficient Photocatalytic Degradation of Ciprofloxacin. *Chemosphere.* 2020;259:127465. doi: 10.1016/j.chemosphere.2020.127465

DOI: 10.1039/D5EN00964B

251 Shi H, Zhao T, Wang J, Wang Y, Chen Z, Liu B, et al. Fabrication of g-C_3N_4/PW_{12}/TiO_2 Composite with Significantly Enhanced Photocatalytic Performance under Visible Light. *J Alloys Compd.* 2021;860:157924. doi: 10.1016/j.jallcom.2020.157924

252 Cheng P, Wang Y, Sarakha M, Mailhot G. Enhancement of the Photocatalytic Activity of Decatungstate, $W_{10}O_{32}^{4-}$, for the Oxidation of Sulfasalazie/Sulfapyridine in the Presence of Hydrogen Peroxide. *J Photochem Photobiol*. 2021;404:112890. doi: 10.1016/j.jphotochem.2020.112890

253 Volin MV, Campbell PL, Connors MA, Woodruff DC, Koch AE. The Effect of Sulfasalazine on Rheumatoid Arthritic Synovial Tissue Chemokine Production. *Exp Mol Pathol*. 2002;73(2):84−92. doi: 10.1006/exmp.2002.2460

254 Wang JL, Xu LE. Advanced Oxidation Processes for Wastewater Treatment: Formation of Hydroxyl Radical and Application. *Crit Rev Environ Sci Technol*. 2012;42(3):251−325. doi: 10.1080/10643389.2010.507698

255 Khan S, Sohail M, Han C, Khan JA, Khan HM, Dionysiou DD. Degradation of Highly Chlorinated Pesticide, Lindane, in Water Using UV/Persulfate: Kinetics and Mechanism, Toxicity Evaluation, and Synergism by H_2O_2. *J Hazard Mater*. 2021;402:123558. doi: 10.1016/j.jhazmat.2020.123558

256 Wang J, Chen Y, Cheng N, Feng L, Gu B-H, Liu Y. Multivalent Supramolecular Self-Assembly between β-Cyclodextrin Derivatives and Polyoxometalate for Photodegradation of Dyes and Antibiotics. *ACS Appl Bio Mater.* 2019;2(12):5898−5904. doi: 10.1021/acsabm.9b00845

257 Li G, Zhang K, Li C, Gao R, Cheng Y, Hou L, et al. Solvent-free method to encapsulate polyoxometalate into metal-organic frameworks as efficient and recyclable photocatalyst for harmful sulfamethazine degrading in water. *Appl Catal B Environ*. 2019;245:753–9. doi:10.1016/j.apcatb.2019.01.012

258 da Silva ES, Sarakha M, Burrows HD, Wong-Wah-Chung P. Decatungstate Anion as an Efficient Photocatalytic Species for the Transformation of the Pesticide 2-(1-Naphthyl) Acetamide in Aqueous Solution. *J Photochem Photobiol A Chem.* 2017;334:61−73. doi: 10.1016/j.jphotochem.2016.10.036

259 Allaoui A, Malouki MA, Wong-Wah-Chung P. Homogeneous Photodegradation Study of 2-Mercaptobenzothiazole Photocatalysed by Sodium Decatungstate Salts: Kinetics and Mechanistic Pathways. *J Photochem Photobiol A Chem.* 2010;212(2−3):153−160. doi: 10.1016/j.jphotochem.2010.04.010

260 Antonaraki S, Triantis TM, Papaconstantinou E, Hiskia A. Photocatalytic Degradation of Lindane by Polyoxometalates: Intermediates and Mechanistic Aspects. *Catal Today.* 2010;151(1−2):119−124. doi: 10.1016/j.cattod.2010.02.017

261 Martinetto Y, Pégot B, Roch-Marchal C, Cottyn-Boitte B, Floquet S. Designing Functional Polyoxometalate-Based Ionic Liquid Crystals and Ionic Liquids. *Eur J Inorg Chem*. 2020;(3):228−247. doi: 10.1002/ejic.201900990

262 Majdafshar M, Piryaei M, Abolghasemi MM, Rafiee E. Polyoxometalate-Based Ionic Liquid Coating for Solid Phase Microextraction of Triazole Pesticides in Water Samples. *Sep Sci Technol.* 2019;54(10):1553−1559. doi: 10.1080/01496395.2019.1572625

263 Misra A, Zambrzycki C, Kloker G, Kotyrba A, Anjass MH, Franco Castillo I, et al. Water purification and microplastics removal using magnetic polyoxometalate-supported ionic liquid phases (MagPOM-SILPs). *Angew Chem Int Ed Engl*. 2020;59(4):1601–5. doi:10.1002/anie.201912111

264 The Royal Society. Microplastics in Freshwater and Soil. London: The Royal Society; 2019. ISBN: 978-1-78252-434-2. https://royalsociety.org/-/media/policy/projects/microplastics/microplastics-evidence-synthesis-report.pdf. Accessed September 1, 2025.

265 Ong BC, Lim HK, Tay CY, Lim T-T, Dong Z. Polyoxometalates for bifunctional applications: Catalytic dye degradation and anticancer activity. *Chemosphere*. 2022;286:131869. doi: 10.1016/j.chemosphere.2021.131869

266 Bijelic A, Aureliano M, Rompel A. The antibacterial activity of polyoxometalates: structures, antibiotic effects and future perspectives. *Chem Commun*. 2018;54:1153−1169. doi: 10.1039/C7CC07549A

267 Aureliano M, Gumerova NI, Sciortino G, Garribba E, Rompel A, Crans DC. Polyoxovanadates with emerging biomedical activities. *Coord Chem Rev*. 2021;447:214143. doi: 10.1016/j.ccr.2021.214143

268 Moghadasi M, Abbasi M, Mousavi M, Mirzaei M. Polyoxometalate-based materials in therapeutic and biomedical applications: current status and perspective. *Dalton Trans.* 2025;54:6333−6345. doi: 10.1039/D4DT03428G

269 Zhang H, Li M, Liu Z, Zhang X, Du C. Two Keggin-type polyoxometalates used as adsorbents with high efficiency and selectivity toward antibiotics and heavy metals. *J Mol Struct.* 2022;1267:133604. doi: 10.1016/j.molstruc.2022.133604

270 Pazhooh P, Khoshnavazi R, Bahrami L, Naseri E. Synthesis and Photocatalytic Activity Assessing of the TiO2 Nanocomposites Modified by Some Lanthanide Ions and Tin-Derivative Sandwich-Type Polyoxometalates. *J Iran Chem Soc.* 2018;15(8):1775−1783. doi: 10.1007/s13738-018-1375-2

271 Wang K, He Y, Zhao Y, Ma P, Wang JA. Propionate-Functionalized Polyoxovanadate $K_2[V_{10}O_{16}(OH)_6(CH_3CH_2CO_2)_6]\cdot 20H_2O$: As Catalyst for Degradation of Methylene Blue. *J Mol Struct*. 2019;1195:184−188. doi: 10.1016/j.molstruc.2019.05.130

272 Missina JM, Leme LBP, Postal K, Santana FS, Hughes DL, de Sá EL, et al. Accessing Decavanadate Chemistry with Tris(Hydroxymethyl)Aminomethane, and Evaluation of Methylene Blue Bleaching. *Polyhedron*. 2020;180:114414. doi: 10.1016/j.poly.2020.114414

273 Yang F, Zhu L, Xu Z, Han Y, Lin X, Shi J, et al. Multi-active photocatalysts of biochar-doped g-C_3N_4 incorporated with polyoxometalates for the high-efficient degradation of sulfamethoxazole. *Environ Pollut*. 2024;361:124715. doi:10.1016/j.envpol.2024.124715

274 Song Y, Bo T, Ma J-C, Ma J-F. Highly efficient photoelectrocatalytic degradation for ciprofloxacin with a new polyoxometalate-based metal-organic hybrid/$BiVO_4$ photoanode. *Green Energy Environ*. 2025;10(7):1531−1542. doi: 10.1016/j.gee.2025.01.007

275 Mohammadian N, Firozjaee TT, Abdi J, Moghadasi M, Mirzaei M. PW_{12}/Fe_3O_4/biochar nanocomposite as an efficient adsorbent for metronidazole removal from aqueous solution: Synthesis and optimization. *Surf Interfaces.* 2024;52:104946. doi: 10.1016/j.surfin.2024.104946

276 Nourolahi H, Farhadi S, Malakooti R, Maleki M, Mahmoudi F. Construction of lacunary α-$K_8SiW_{11}O_{39}$ polyoxometalate/MIL-101(Cr) MOF/$CoFe_2O_4$ magnetic nanocomposites for adsorptive removal of toxic azo dyes and antibiotics from wastewater. *CrystEngComm*. 2025;27:1185−1205. doi: 10.1039/D5CE00013K

277 Li J, Yu Z, Zhang J, Liu C, Zhang Q, Shi H, et al. Rapid, massive, and green synthesis of polyoxometalate-based metal-organic frameworks to fabricate POMOF/PAN nanofiber membranes for selective filtration of cationic dyes. *Molecules.* 2024;29:1493. doi:10.3390/molecules29071493

278 Kholdeeva OA, Timofeeva MN, Maksimov GM, Maksimovskaya RI, Neiwert WA, Hill CL. Aerobic Oxidation of Formaldehyde Mediated by a Ce-Containing Polyoxometalate under Mild Conditions. *Inorg Chem*. 2005;44(3):666−672. doi: 10.1021/ic049109o

279 Te M, Fairbridge C, Ring Z. Oxidation Reactivities of Dibenzothiophenes in Polyoxometalate/H2O2 and Formic Acid/H_2O_2 Systems. *Appl Catal A Gen*. 2001;219(1−2):267−280. doi: 10.1016/S0926-860X(01)00699-8

DOI: 10.1039/D5EN00964B

280 Liu Y, Zhang J, Sheng C, Zhang Y, Zhao L. Simultaneous Removal of NO and SO_2 from Coal-Fired Flue Gas by UV/H_2O_2 Advanced Oxidation Process. *Chem Eng J.* 2010;162(3):1006–1011. doi: 10.1016/j.cej.2010.07.009

281 Gamelas JAF, Evtyugina MG, Portugal I, Evtuguin DV. New Polyoxometalate-Functionalized Cellulosic Fibre/Silica Hybrids for Environmental Applications. *RSC Adv.* 2012;2(3):831–839. doi: 10.1039/C1RA00371B

282 Kholdeeva OA, Vanina MP, Timofeeva MN, Maksimovskaya RI, Trubitsina TA, Melgunov MS, et al. Co-containing polyoxometalate-based heterogeneous catalysts for the selective aerobic oxidation of aldehydes under ambient conditions. *J Catal.* 2004;226(2):363–71. doi:10.1016/j.jcat.2004.05.032

283 Eseva E, Akopyan A, Schepina A, Anisimov A, Maximov A. Deep Aerobic Oxidative Desulfurization of Model Fuel by Anderson-Type Polyoxometalate Catalysts. *Catal Commun.* 2021;149:106256. doi: 10.1016/j.catcom.2020.106256

284 Chi M, Zhu Z, Sun L, Su T, Liao W, Deng C, et al. Construction of biomimetic catalysis system coupling polyoxometalates with deep eutectic solvents for selective aerobic oxidation desulfurization. *Appl Catal B Environ.* 2019;259:118089. doi:10.1016/j.apcatb.2019.118089

285 Khan FI, Ghoshal AK. Removal of Volatile Organic Compounds from Polluted Air. *J Loss Prev Process Ind*. 2000;13(6):527–545. doi: 10.1016/S0950-4230(00)00007-3

286 Meng J, Wang X, Yang X, Hu A, Guo Y, Yang Y. Enhanced Gas-Phase Photocatalytic Removal of Aromatics over Direct Z-Scheme-Dictated $H_3PW_{12}O_{40}$/g-C_3N_4 Film-Coated Optical Fibers. *Appl Catal B Environ.* 2019;251:168–180. doi: 10.1016/j.apcatb.2019.03.063

287 Ullah I. Industrial-scale oxidative desulfurization: comprehensive process design and economic study for maritime oil production. Appl Eng. 2025;9(2):64–87. doi:10.11648/j.ae.20250902.12

288 Kanu A, Kuye A, Idikwu J. Comparative study on technologies for crude oil desulfurization: Hydrodesulfurization vs oxidative desulfurization. Int J *Innov Sci Res Technol.* 2025;4(6):1–15. doi:10.5281/zenodo.8108205

289 He J, Guan L, Zhou Y, Shao P, Yao Y, Lu S, et al. One-pot preparation of mesoporous $K_xPMo_{12}O_{40}$ (x = 1, 2, 3, 4) materials for oxidative desulfurization: electrochemically-active surface area (ECSA) determines their activity. *React Chem Eng.* 2020;5(9):1776–82. doi:10.1039/D0RE00213E

290 Ye G, Hu L, Gu Y, Lancelot C, Rives A, Lamonier C, et al. Synthesis of polyoxometalate encapsulated in UiO-66(Zr) with hierarchical porosity and double active sites for oxidation desulfurization of fuel oil at room temperature. *J Mater Chem A.* 2020;8(37):19396–404. doi:10.1039/D0TA04337K

291 Gao Y, Gao R, Zhang G, Zheng Y, Zhao J. Oxidative Desulfurization of Model Fuel in the Presence of Molecular Oxygen over Polyoxometalate Based Catalysts Supported on Carbon Nanotubes. *Fuel.* 2018;224:261–270. doi: 10.1016/j.fuel.2018.03.034

292 Austigard ÅD, Svendsen K, Heldal KK. Hydrogen Sulphide Exposure in Waste Water Treatment. *J Occup Med Toxicol.* 2018;13:10–20. doi: 10.1186/s12995-018-0191-z

293 Badilla GL, Valdez B, Schorr M. Air Quality - New Perspective. London: IntechOpen; 2012. ISBN: 978-953-51-0674-6. doi: 10.5772/2561

294 Habeeb OA, Kanthasamy R, Ali GAM, Sethupathi S, Yunus RBM. Hydrogen Sulfide Emission Sources, Regulations, and Removal Techniques: A Review. *Rev Chem Eng.* 2018;34(6):837–854. doi: 10.1515/revce-2017-0004

295 Yang C, Wang Y, Fan H, de Falco G, Yang S, Shangguan J, et al. Bifunctional ZnO-MgO/activated carbon adsorbents boost H_2S room temperature adsorption and catalytic oxidation. *Appl Catal B Environ*. 2020;266:118674. doi:10.1016/j.apcatb.2020.118674

296 Adib F, Bagreev A, Bandosz TJ. Analysis of the relationship between H_2S removal capacity and surface properties of unimpregnated activated carbons. *Environ Sci Technol.* 2000;34(4):686–692. doi:10.1021/es990341g

297 Huang K, Feng X, Zhang X-M, Wu Y-T, Hu X-B. The ionic liquid-mediated Claus reaction: a highly efficient capture and conversion of hydrogen sulfide. *Green Chem*. 2016;18(7):1859–1863. doi:10.1039/C5GC03016A

298 Holz S, Köster P, Thielert H, Guetta Z, Repke J-U. Investigation of the degradation of chelate complexes in liquid redox desulfurization processes. *Chem Eng Technol.* 2020;43(3):476–483. doi:10.1002/ceat.201900420

299 Ma Y, Liu X, Wang R. Efficient removal of H2S at high temperature using the ionic liquid solutions of $[C_4mim]_3PMo_{12}O_{40}$—an organic polyoxometalate. *J Hazard Mater.* 2017;331:109–116. doi:10.1016/j.jhazmat.2017.02.036

300 Song J, Luo Z, Britt DK, Furukawa H, Yaghi OM, Hardcastle KI, et al. A multiunit catalyst with synergistic stability and reactivity: a polyoxometalate-metal organic framework for aerobic decontamination. *J Am Chem Soc*. 2011;133(42):16839–46. doi:10.1021/ja203695h

301 Muzio LJ, Quartucy GC. Implementing NOx control: research to application. *Prog Energy Combust Sci*. 1997;23(3):233–266. doi:10.1016/S0360-1285(97)00002-6

302 Skalska K, Miller JS, Ledakowicz S. Trends in NO_x abatement: a review. *Sci Total Environ*. 2010;408(19):3976–3989. doi:10.1016/j.scitotenv.2010.06.001

303 Woodrow P. Nitric oxide: some nursing implications. *Intensive Crit Care Nurs*. 1997;13(2):87–92. doi:10.1016/S0964-3397(97)80186-3

304 Scherrer U, Vollenweider L, Delabays A, Savcic M, Eichenberger U, Kleger GR, et al. Inhaled nitric oxide for high-altitude pulmonary edema. *N Engl J Med*. 1996;334(10):624–629. doi:10.1056/NEJM199603073341003

305 Chaloulakou A, Mavroidis I, Gavriil I. Compliance with the annual NO_2 air quality standard in Athens. Required NOx levels and expected health implications. *Atmos Environ.* 2008;42(3):454–465. doi:10.1016/j.atmosenv.2007.09.067

306 Gómez-García MA, Pitchon V, Kiennemann A. Pollution by nitrogen oxides: an approach to NO_x abatement by using sorbing catalytic materials. *Environ Int.* 2005;31(3):445–467. doi:10.1016/j.envint.2004.09.006

307 van Loon GW, Duffy SJ. Environmental chemistry: a global perspective. 2nd ed. Oxford: Oxford University Press; 2005. p.421–424. ISBN:0199274991

308 Qu Y, An J, He Y, Zheng J. An overview of emissions of SO2 and NOx and the long-range transport of oxidized sulfur and nitrogen pollutants in East Asia. *J Environ Sci.* 2016;44:13–25. doi:10.1016/j.jes.2015.08.028

309 Lin F, Wang Z, Zhang Z, He Y, Zhu Y, Shao J, et al. Flue gas treatment with ozone oxidation: an overview on NO_x, organic pollutants, and mercury. *Chem Eng J.* 2020;382:123030. doi:10.1016/j.cej.2019.123030

310 Fan Z, Shi J-W, Gao C, Gao G, Wang B, Wang Y, He C, Niu C. Gd-modified MnOx for the selective catalytic reduction of NO by NH_3: the promoting effect of Gd on the catalytic performance and sulfur resistance. *Chem Eng J.* 2018;348:820–830. doi:10.1016/j.cej.2018.05.038

311 Hao R, Zhang Y, Wang Z, Li Y, Yuan B, Mao X, Zhao Y. An advanced wet method for simultaneous removal of SO2 and NO from coal-fired flue gas by utilizing a complex absorbent. *Chem Eng J.* 2017;307:562–571. doi: 10.1016/j.cej.2016.08.103

312 Zhao Y, Han Y, Zhao Z. Removal of NO from flue gas by a heterogeneous Fenton-like process. *Chem Eng Technol.* 2018;41(11):2203–2211. doi: 10.1002/ceat.201700717

313 Liu Y, Zhang J, Pan J, Tang A. Investigation on the removal of NO from SO_2-containing simulated flue gas by an

View Article Online
DOI: 10.1039/D5EN00964B

ultraviolet/Fenton-like reaction. *Energy Fuels*. 2012;26(9):5430−5436. doi: 10.1021/ef3008568

314 Wang R, Zhang X, Ren Z. Germanium-based polyoxometalates for the adsorption-decomposition of NO_x. *J Hazard Mater.* 2021;402:123494. doi: 10.1016/j.jhazmat.2020.123494

315 Montero-Montoya R, López-Vargas R, Arellano-Aguilar O. Volatile organic compounds in air: sources, distribution, exposure and associated illnesses in children. *Ann Glob Health.* 2018;84(2):225−238. doi: 10.29024/aogh.910

316 Weon S, Choi E, Kim H, Kim JY, Park H-J, Kim S, et al. Active 001 facet exposed TiO_2 nanotubes photocatalyst filter for volatile organic compounds removal: from material development to commercial indoor air cleaner application. *Environ Sci Technol.* 2018;52(16):9330–40. doi:10.1021/acs.est.8b02282

317 Mølhave L. Volatile organic compounds, indoor air quality and health. *Indoor Air.* 1991;1:357−376. doi: 10.1111/j.1600-0668.1991.00001.x

318 Harper M. Sorbent trapping of volatile organic compounds from air. *J Chromatogr A.* 2000;885(1−2):129−151. doi: 10.1016/S0021-9673(00)00363-0

319 Raillard C, Héquet V, Le Cloirec P, Legrand J. Comparison of different TiO_2 photocatalysts for the gas phase oxidation of volatile organic compounds. *Water Sci Technol.* 2004;50(4):241−250. doi: 10.2166/wst.2004.0274

320 Raillard C, Héquet V, Le Cloirec P, Legrand J. Photocatalytic oxidation of volatile organic compounds present in airborne environment adjacent to sewage treatment plants. *Water Sci Technol.* 2004;49(1):111−114. doi: 10.2166/wst.2004.0032

321 Dong P, Xi X, Hou G. Typical non–TiO_2-based visible-light photocatalysts. In: Semiconductor Photocatalysis. London: IntechOpen; 2016. doi: 10.5772/62889

322 Ma F-J, Liu S-X, Liang D-D, Ren G-J, Wei F, Chen Y-G, Su Z-M. Adsorption of volatile organic compounds in porous metal–organic frameworks functionalized by polyoxometalates. *J Solid State Chem*. 2011;184(11):3034−3039. doi: 10.1016/j.jssc.2011.09.002

323 Salthammer T, Mentese S, Marutzky R. Formaldehyde in the indoor environment. *Chem Rev.* 2010;110(4):2536−2572. doi: 10.1021/cr800399g

324 Salthammer T. Formaldehyde in the ambient atmosphere: from an indoor pollutant to an outdoor pollutant? *Angew Chem Int Ed Engl.* 2013;52(12):3320−3327. doi: 10.1002/anie.201205984

325 Kehrer JP. The Haber–Weiss reaction and mechanisms of toxicity. Toxicology. 2000;149(1):43-50. doi: 10.1016/S0300-483X(00)00231-6

326 Gamelas JAF, Oliveira F, Evtyugina MG, Portugal I, Evtuguin DV. Catalytic oxidation of formaldehyde by ruthenium multisubstituted tungstosilicic polyoxometalate supported on cellulose/silica hybrid. *Appl Catal A Gen.* 2016;509:8−16. doi: 10.1016/j.apcata.2015.10.003

327 Huang Y, Wang J, Ma S, Wang R, Wang Y. Enhanced adsorption-oxidation performance of PMo_{12} immobilized onto porous MCM-41 derived from rice husk for H2S at room temperature. *Fuel.* 2023;333:126448. doi: 10.1016/j.fuel.2022.126448

328 Wang R, Zhang L, Wang X. Tuning the redox activity of polyoxometalate by central atom for high-efficient desulfurization. *J Hazard Mater.* 2022;440:129710. doi:10.1016/j.jhazmat.2022.129710

329 Li J, Wang R. Polyoxometalate/ionic liquid desulfurization system for hydrogen sulfide removal from high-temperature gas stream. *Molecules.* 2022;27:6723. doi:10.3390/molecules27196723

330 Li J, Wang R, Dou S. Electrolytic cell–assisted polyoxometalate based redox mediator for H_2S conversion to elemental sulphur and hydrogen. *Chem Eng J.* 2021;404:127090. doi:10.1016/j.cej.2020.127090

331 Rafiee E, Mirnezami F. Keggin-structured polyoxometalate-based ionic liquid salts: thermoregulated catalysts for rapid oxidation of sulfur-based compounds using H_2O_2 and extractive oxidation desulfurization of sulfur-containing model oil. *J Mol Liq.* 2014;199:156−161. doi:10.1016/j.molliq.2014.08.036

332 Wang R. Performance of new liquid redox desulfurization system of heteropoly compound in comparison with that of iron chelate. *Korean J Chem Eng.* 2003;20:659−663. doi:10.1007/BF02706904

333 Wang R. Investigation on a new liquid redox method for H_2S removal and sulfur recovery with heteropoly compound. *Sep Purif Technol.* 2003;31(1):111−121. doi:10.1016/S1383-5866(02)00153-3

334 Wang B, Wang R. Highly-efficient H_2S capture by deep eutectic solvents based on ionic liquid hybridized polyoxometalate: insights into conformational transitions and structure-activity relationships. *J Hazard Mater*. 2025;495:139037. doi:10.1016/j.jhazmat.2025.139037

335 Wang B, Wang R. Medium and high temperature H2S removal via phosphazene polyoxometalate ionic liquids: performance evaluation and mechanism exploration. *Sep Purif Technol.* 2025;357(Part B):130196. doi:10.1016/j.seppur.2024.130196

336 Huang Y, Zuo Q, Yin M, Wang J, Gao B, Song J, et al. Cyclodextrin-assisted high selectivity of imprinted adsorbents loaded on polyoxometalate@UiO-66 for H_2S removal at ambient temperature. *Sep Purif Technol*. 2025;356(Part B):129932. doi:10.1016/j.seppur.2024.129932

337 Liu F, Deng Y, Niu L, Wang S, Wang B, Li M, et al. Study on desulfurization and regeneration performance of nanofluid system based on heteropoly compound/ionic liquid solutions. *Ind Eng Chem Res*. 2024;63(27):12155−12165. doi:10.1021/acs.iecr.4c01242

338 Zhao Y, Qin X, Zhao X, Wang X, Tan H, Sun H, et al. Polyoxometalates-doped Bi_2O_{3-x}/Bi photocatalyst for highly efficient visible-light photodegradation of tetrabromobisphenol A and removal of NO. *Chin J Catal*. 2022;43(3):771−781. doi:10.1016/S1872-2067(21)63843-3

339 Zhang X, Wang R, Zhu H, Chen Y. Performance of NO_x capture with Dawson polyoxometalate $H_6P_2W_{18}O_{62}{\cdot}28H_2O$. *Chem Eng J.* 2020;400:125880. doi:10.1016/j.cej.2020.125880

340 Weng X, Dai X, Zeng Q, Liu Y, Wu Z. DRIFT studies on promotion mechanism of $H_3PW_{12}O_{40}$ in selective catalytic reduction of NO with NH_3. *J Colloid Interface Sci.* 2016;461:9−14. doi:10.1016/j.jcis.2015.09.004

341 Ma F-J, Liu S-X, Ren G-J, Liang D-D, Sha S. A hybrid compound based on porous metal–organic frameworks and polyoxometalates: NO adsorption and decomposition. *Inorg Chem Commun.* 2012;22:174−177. doi:10.1016/j.inoche.2012.05.055

342 Gómez-García MA, Pitchon V, Kiennemann A. Multifunctional catalysts for de-NOx processes: the case of $H_3PW_{12}O_{40}{\cdot}6H_2O$–metal supported on mixed oxides. *Appl Catal B Environ.* 2007;70(1−4):151−159. doi:10.1016/j.apcatb.2005.12.029

343 Hodjati S, Petit C, Pitchon V, Kiennemann A. Removal of NO_x from a lean exhaust gas by absorption on heteropolyacids: reversible sorption of nitrogen oxides in $H_3PW_{12}O_{40}{\cdot}6H_2O$. *J Catal.* 2001;197(2):324−334. doi:10.1006/jcat.2000.3108

344 Bélanger R, Moffat JB. Sorption and reduction of NO2 on microporous ammonium 12-tungstophosphate. Langmuir. 1996;12(9):2230-2238. doi:10.1021/la950952w

345 Lu S, Guo X, Xu X, Han Z, Chen M, Lin B, et al. POM-promoted synergistic catalysis of NO and chlorobenzene over amorphous $MnCeO_x$ catalysts: activation of lattice oxygen, role of acid site, catalytic mechanism. *J Hazard Mater.* 2025;495:138873. doi:10.1016/j.jhazmat.2025.138873

346 Ma M, Zhang R, Shen Y, Zhou X, Zhai Y, Han Y, et al. Mesoporous Ce–Ti catalysts modified by phosphotungstic acid and chitosan for the synergistic catalysis of CVOCs and NO_x. *Catalysts.* 2025;15:119. doi:10.3390/catal15020119

347 Guo W, Luo Z, Lv H, Hill CL. Aerobic oxidation of formaldehyde catalyzed by polyvanadotungstates. *ACS Catal.* 2014;4(4):1154−1161. doi:10.1021/cs5000763

348 Zhou Y, Yue B, Bao R-L, Liu S-X, He H-Y. Catalytic aerobic oxidation of acetaldehyde over Keggin-type molybdovanadophosphoric acid/SBA-15 under ambient condition. *Chin J Chem.* 2006;24(8):1001−1005. doi:10.1002/cjoc.200690187

349 Ammam M. Polyoxometalates: formation, structures, principal properties, main deposition methods and application in sensing. *J Mater Chem A.* 2013;1(21):6291−6312. doi:10.1039/C3TA01663C

350 Khodadadi Dizaji A, Mortaheb HR, Mokhtarani B. Preparation of supported catalyst by adsorption of polyoxometalate on graphene oxide/reduced graphene oxide. *Mater Chem Phys.* 2017;199:424−434. doi:10.1016/j.matchemphys.2017.07.016

351 Putzbach W, Ronkainen N. Immobilization techniques in the fabrication of nanomaterial-based electrochemical biosensors: a review. *Sensors*. 2013;13(4):4811−4840. doi:10.3390/s130404811

352 Johnson KW. Reproducible electrodeposition of biomolecules for the fabrication of miniature electroenzymatic biosensors. *Sens Actuators B Chem.* 1991;5(1−4):85−89. doi:10.1016/0925-4005(91)80225-9

353 Yang M, Kim DS, Yoon JH, Hong SB, Jeong SW, Yoo DE, et al. Nanopillar films with polyoxometalate-doped polyaniline for electrochemical detection of hydrogen peroxide. *Analyst.* 2016;141(4):1319−1324. doi:10.1039/C5AN02134K

354 Pourbeyram S, Moosavifar M, Hasanzadeh V. Electrochemical characterization of the encapsulated polyoxometalates (POMs) into the zeolite. *J Electroanal Chem.* 2014;714−715:19−24. doi:10.1016/j.jelechem.2013.12.014

355 Zasadzinski JA, Viswanathan R, Madsen L, Garnaes J, Schwartz DK. Langmuir–Blodgett films. *Science*. 1994;263(5154):1726−1733. doi:10.1126/science.8134836

356 Ito T, Yashiro H, Yamase T. Regular two-dimensional molecular array of photoluminescent Anderson-type polyoxometalate constructed by Langmuir–Blodgett technique. *Langmuir.* 2006;22(6):2806−2810. doi:10.1021/la052972w

357 Chen W, McCarthy TJ. Layer-by-layer deposition: a tool for polymer surface modification. *Macromolecules*. 1997;30(1):78−86. doi:10.1021/ma961096d

358 Ma H, Peng J, Han Z, Feng Y, Wang E. Preparation and characterization of luminescent nanocomposite film containing polyoxometalate. *Thin Solid Films*. 2004;446(2):161−166. doi:10.1016/j.tsf.2003.09.040

359 Ammam M, Easton EB. Novel organic–inorganic hybrid material based on tris(2,2′-bipyridyl)dichlororuthenium(II) hexahydrate and Dawson-type tungstophosphate $K_7[H_4PW_{18}O_{62}]\cdot 18H_2O$ as a bifunctional hydrogen peroxide electrocatalyst for biosensors. *Sens Actuators B Chem.* 2012;161(1):520−527. doi:10.1016/j.snb.2011.10.070

360 Ammam M, Fransaer J. Ionic liquid–heteropolyacid: Synthesis, characterization, and supercapacitor study of films deposited by electrophoresis. *J Electrochem Soc*. 2011;158(1):A14−A21. doi:10.1149/1.3507254

361 Zhang L, Li C, Li F, Li S, Ma H, Gu F. A sensing platform based on Cu-MOF encapsulated Dawson-type polyoxometalate crystal material for electrochemical detection of xanthine. *Microchim Acta.* 2023;190:24. doi:10.1007/s00604-022-05601-1

362 Shetty SS, Moosa B, Zhang L, Alshankiti B, Baslyman W, Mani V, et al. Polyoxometalate–cyclodextrin supramolecular entities for real-time in situ monitoring of dopamine released from neuroblastoma cells. *Biosens Bioelectron.* 2023;229:115240. doi:10.1016/j.bios.2023.115240.

363 Tian R, Zhang B, Zhao M, Ma Q, Qi Y. Polyoxometalates as promising enzyme mimics for the sensitive detection of hydrogen peroxide by fluorometric method. *Talanta.* 2018;188:332−338. doi:10.1016/j.talanta.2018.05.085

364 Veríssimo MIS, Evtuguin DV, Gomes MTSR. Polyoxometalate functionalized sensors: a review. *Front Chem.* 2022;10:840657. doi:10.3389/fchem.2022.840657

365 Ammam M, Easton EB. Selective determination of ascorbic acid with a novel hybrid material based 1-butyl-3-methylimidazolium tetrafluoroborate ionic liquid and the Dawson type ion $[P_2Mo_{18}O_{62}]^{6-}$ immobilized on glassy carbon. *Electrochim Acta.* 2011;56(7):2847–2855. doi:10.1016/j.electacta.2010.12.072

366 Wang R, Jia D, Cao Y. Facile synthesis and enhanced electrocatalytic activities of organic–inorganic hybrid ionic liquid polyoxometalate nanomaterials by solid-state chemical reaction. *Electrochim Acta.* 2012;72:101–107. doi:10.1016/j.electacta.2012.04.011

367 Liu S, Tang Z, Wang Z, Peng Z, Wang E, Dong S. Oriented polyoxometalate–polycation multilayers on a carbon substrate. *J Mater Chem.* 2000;10(12):2727–2733. doi:10.1039/B004142O

368 Salimi A, Korani A, Hallaj R, Khoshnavazi R, Hadadzadeh H. Immobilization of $[Cu(bpy)_2]Br_2$ complex onto a glassy carbon electrode modified with α-$SiMo^{12}O^{404-}$ and single walled carbon nanotubes: application to nanomolar detection of hydrogen peroxide and bromate. *Anal Chim Acta.* 2009;635(1):63–70. doi:10.1016/j.aca.2009.01.007

369 Wang B, Cheng L, Dong S. Construction of a heteropolyanion-modified electrode by a two-step sol–gel method and its electrocatalytic applications. J *Electroanal Chem.* 2001;516(1–2):17–22. doi:10.1016/S0022-0728(01)00677-5

370 Thangamuthu R, Pan Y-C, Chen S-M. Iodate sensing electrodes based on phosphotungstate-doped-glutaraldehyde-cross-linked poly-L-lysine coatings. *Electroanalysis.* 2010;22(16):1812–1816. doi:10.1002/elan.201000024

371 Ma H, Zhang Z, Pang H, Li S, Chen Y, Zhang W. Fabrication and electrochemical sensing property of a composite film based on a polyoxometalate and palladium nanoparticles. *Electrochim Acta.* 2012;69:379–383. doi:10.1016/j.electacta.2012.03.017

372 Zhu H, Tang W, Ma Y, Wang Y, Tan H, Li Y. Preyssler-type polyoxometalate-based crystalline materials for the electrochemical detection of H_2O_2. *CrystEngComm.* 2021;23(10):2071–2080. doi:10.1039/D1CE00059D

373 Hu YY, Han RX, Mei L, Liu JL, Sun JC, Yang K, Zhao JW. Design principles of MOF-related materials for highly stable metal anodes in secondary metal-based batteries. Mater *Today Energy.* 2021;19:100608. doi:10.1016/j.mtener.2020.100608

374 Wang C, Ying J, Mou H-C, Tian A-X, Wang X-I. Multi-functional photoelectric sensors based on a series of isopolymolybdate-based compounds for detecting different ions. *Inorg Chem Front.* 2020;7(20):3882–3894. doi:10.1039/D0QI00505C

375 Tian A, Yang M, Ni H, Sun N, Yang Y, Fu Y, Ying J. Use of symmetrical and pendant pyrazole derivatives for the construction of two polyoxometalate-based complexes as electrochemical sensors. *Transit Met Chem*. 2018;43:621–633. doi:10.1007/s11243-018-0250-4

376 Yang M, Rong S, Wang X, Ma H, Pang H, Tan L, et al. Preparation and application of Keggin polyoxometalate-based 3D coordination polymer materials as supercapacitors and amperometric sensors. *ChemNanoMat.* 2021;7(3):299–306. doi:10.1002/cnma.202000654

377 Xin X, Hu N, Ma Y, Wang Y, Hou L, Zhang H, et al. Polyoxometalate-based crystalline materials as a highly sensitive electrochemical sensor for detecting trace Cr(VI).

View Article Online
DOI: 10.1039/D5EN00964B

Dalton Trans. 2020;49:4570–4577. doi:10.1039/D0DT00446D

378 Krutovertsev SA, Ivanova OM, Sorokin SI. Sensing properties of polyaniline films doped with Dawson heteropoly compounds. *J Anal Chem.* 2001;56:1057–1060. doi:10.1023/A:1012569127685

379 Khan MI, Aydemir K, Siddiqui MRH, Alwarthan AA, Marshall CL. Oxidative dehydrogenation properties of novel nanostructured polyoxovanadate based materials. *Catal Lett.* 2011;141:538–543. doi:10.1007/s10562-011-0547-9

380 Tess ME, Cox JA. Humidity-independent solid-state amperometric sensor for carbon monoxide based on an electrolyte prepared by sol–gel chemistry. *Anal Chem.* 1998;70(1):187–190. doi:10.1021/ac9708396

381 Ammam M, Easton EB. Advanced NOx gas sensing based on novel hybrid organic–inorganic semiconducting nanomaterial formed between pyrrole and Dawson type polyoxoanion $[P_2Mo_{18}O_{62}]^{6-}$. *J Mater Chem*. 2011;21(22):7886–7891. doi:10.1039/C1JM11244A

382 Wang T, Sun Z, Wang Y, Liu R, Sun M, Xu L. Enhanced photoelectric gas sensing performance of SnO_2 flower-like nanorods modified with polyoxometalate for detection of volatile organic compound at room temperature. *Sens Actuators B Chem.* 2017;246:769–775. doi:10.1016/j.snb.2017.02.108

383 Zhang Q, Wang T, Sun Z, Xi L, Xu L. Performance improvement of photoelectrochemical NO_2 gas sensing at room temperature by $BiVO_4$–polyoxometalate nanocomposite photoanode. *Sens Actuators B Chem.* 2018;272:289–295. doi:10.1016/j.snb.2018.05.169

384 Shi H, Li N, Sun Z, Wang T, Xu L. Interface modification of titanium dioxide nanoparticles by titanium-substituted polyoxometalate doping for improvement of photoconductivity and gas sensing applications. *J Phys Chem Solids.* 2018;120:57–63. doi:10.1016/j.jpcs.2018.04.014

385 Tian J, Chen X, Wang T, Pei W, Li F, Li D, et al. Modification of indium oxide nanofibers by polyoxometalate electron acceptor doping for enhancement of gas sensing at room temperature. Sens *Actuators B Chem.* 2021;344:130227. doi:10.1016/j.snb.2021.130227

386 Wang Y, Fu X, Wang T, Li F, Li D, Yang Y, et al. Polyoxometalate electron acceptor incorporated improved properties of Cu2ZnSnS4-based room temperature NO_2 gas sensor. *Sens Actuators B Chem.* 2021;348:130683. doi:10.1016/j.snb.2021.130683

387 Sun X, Lan Q, Geng J, Yu M, Li Y, Li X, et al. Polyoxometalate as electron acceptor in dye/TiO2 films to accelerate room-temperature NO_2 gas sensing. *Sens Actuators B Chem.* 2023;374:132795. doi:10.1016/j.snb.2022.132795

388 Kida T, Kawasaki K, Lemura K, Teshima K, Nagano M. Gas sensing properties of a stabilized zirconia-based sensor with a porous MoO_3 electrode prepared from a molybdenum polyoxometallate–alkylamine hybrid film. *Sens Actuators B Chem.* 2006;119(2):562–9. doi:10.1016/j.snb.2006.01.025

389 Wei H, Zhang J, Shi N, Liu Y, Zhang B, Zhang J, et al. A recyclable polyoxometalate-based supramolecular chemosensor for efficient detection of carbon dioxide. *Chem Sci.* 2015;6:7201–5. doi:10.1039/C5SC02020D

390 Guo Y, Gong Y, Qi L, Gao Y, Yu L. A polyoxometalate-based supramolecular chemosensor for rapid detection of hydrogen sulfide with dual signals. *J Colloid Interface Sci.* 2017;485:280–7. doi:10.1016/j.jcis.2016.09.047

391 Bezdek MJ, Luo S-XL, Liu RY, He Q, Swager TM. Trace hydrogen sulfide sensing inspired by polyoxometalate-mediated aerobic oxidation. *ACS Cent Sci*. 2021;7(9):1572–80. doi:10.1021/acscentsci.1c00746

392 Liu S, Volkmer D, Kurth DG. Smart polyoxometalate-based nitrogen monoxide sensors. *Anal Chem*. 2004;76(15):4579–82. doi:10.1021/ac0495283

393 Cai L-X, Chen L, Sun X-Q, Geng J, Liu C-C, Wang Y, et al. Ultra-sensitive triethylamine gas sensors based on polyoxometalate-assisted synthesis of $ZnWO_4$/ZnO hetero-structured nanofibers. *Sens Actuators B Chem*. 2022;370:132422. doi:10.1016/j.snb.2022.132422

394 Tian J, Jiang B, Shao H, Wang Y, Wang T, Li F, et al. A new strategy to one-step construct polyoxometalate/semiconductor one-dimensional tandem heterojunctions toward optimized conductometric sensing performances of ethanol gas. *Sens Actuators B Chem.* 2023;374:132797. doi:10.1016/j.snb.2022.132797

395 Chen L, Cai L-X, Geng J, Liu C-C, Wang Y, Guo Z. Polyoxometalate-assisted in situ growth of $ZnMoO_4$ on ZnO nanofibers for the selective detection of ppb-level acetone. *Sens Actuators B Chem.* 2022;369:132354. doi:10.1016/j.snb.2022.132354

396 Ren Y, Xie W, Li Y, Ma J, Li J, Liu Y, et al. Noble metal nanoparticles decorated metal oxide semiconducting nanowire arrays interwoven into 3D mesoporous superstructures for low-temperature gas sensing. *ACS Cent Sci.* 2021;7(11):1885–97. doi:10.1021/acscentsci.1c00912

397 Zhang X-Z, Zhu W-J, Yang Z-X, Feng Y, Fan L-L, Gao G-G, et al. Ultrasensitive photochromic and Raman dual response to ethylenediamine gas through polyoxometalate–viologen crystalline hybrid. *J Mater Chem C.* 2022;10(41):15451–7. doi:10.1039/D2TC03053E

398 Wang C, Ying J, Zhang X, Zhang B, Tian A, Zhang Y. POM-based compounds as capacitor materials and their photoelectric-sensing properties toward inorganic ions. *J Coord Chem.* 2021;74(14):2315–26. doi:10.1080/00958972.2021.1952998

399 Tian A-X, Yang M-L, Sun N, Fu Y-B, Ying J. A series of pH-dependent POM-based compounds as photocatalysts and electrochemical sensors. *Polyhedron.* 2018;155:337–50. doi:10.1016/j.poly.2018.08.065

400 Zhang X, Zhang Y, Ying J, Zhang B, Wang C, Tian A. A series of POM-based compounds constructed by piperazine and morpholine derivatives: characterization, selective photocatalytic and electrochemical/fluorescence sensing properties. *J Solid State Chem.* 2021;295:121888. doi:10.1016/j.jssc.2020.121888

401 Wang C, Zhou M, Ma Y, Tan H, Wang Y, Li Y. Hybridized polyoxometalate-based metal–organic framework with ketjenblack for the nonenzymatic detection of H_2O_2. *Asian J Chem.* 2018;13(16):2054–9. doi:10.1002/asia.201800758

402 Wang X, Li L, Wang X, Zhang Y. Various amide-derived ligands induced five octamolybdate-based metal–organic complexes: synthesis, structure, electrochemical sensing and photocatalytic properties. *CrystEngComm.* 2021;23(30):5176–83. doi:10.1039/D1CE00266J

403 Liang C, Wang X, Yu D, Guo W, Zhang F, Qu F. In-situ immobilization of a polyoxometalate metal-organic framework (NENU-3) on functionalized reduced graphene oxide for hydrazine sensing. *Chin J Chem*. 2021;39(10):2889–97. doi:10.1002/cjoc.202100314

404 Liu Q-Q, Wang X-L, Lin H-Y, Chang Z-H, Zhang Y-C, Tian Y, et al. Two new polyoxometalate-based metal–organic complexes for the detection of trace Cr(VI) and their capacitor performance. *Dalton Trans.* 2021;50(27):9450–6. doi:10.1039/D1DT01247A

405 Zhang Y, Zhang Y, Li L, Chen J, Li P, Huang W. One-step in situ growth of high-density POMOFs films on carbon cloth for the electrochemical detection of bromate. *J Electroanal Chem.* 2020;861:113939. doi:10.1016/j.jelechem.2020.113939

406 Largeot C, Portet C, Chmiola J, Taberna P-L, Gogotsi Y, Simon P. Relation between the ion size and pore size for an electric double-layer capacitor. *J Am Chem Soc.* 2008;130(9):2730–1. doi:10.1021/ja7106178

407 Cuentas-Gallegos AK, Lira-Cantú M, Casañ-Pastor N, Gómez-Romero P. Nanocomposite hybrid molecular materials for application in solid-state electrochemical supercapacitors. *Adv Funct Mater.* 2005;15(7):1125–33. doi:10.1002/adfm.200400326

408 Vaillant J, Lira-Cantu M, Cuentas-Gallegos K, Casañ-Pastor N, Gómez-Romero P. Chemical synthesis of hybrid materials based on PAni and PEDOT with polyoxometalates for electrochemical supercapacitors. *Prog Solid State Chem.* 2006;34(2):147–59. doi:10.1016/j.progsolidstchem.2005.11.015

409 Pope MT, Müller A. Polyoxometalate chemistry: an old field with new dimensions in several disciplines. Angew Chem Int Ed Engl. 1991;30(1):34–48. doi:10.1002/anie.199100341

410 Pope MT. Heteropoly and isopoly oxometalates. New York: Springer-Verlag; 1983. (Inorganic Chemistry Concepts).

411 Pope MT, Müller A, editors. Polyoxometalates: from platonic solids to anti-retroviral activity. Dordrecht: Springer; 1994. doi:10.1007/978-94-011-0920-8

412 Guo Y-G, Hu J-S, Wan L-J. Nanostructured materials for electrochemical energy conversion and storage devices. *Adv Mater.* 2008;20(15):2878–87. doi:10.1002/adma.200800627

413 Sonoyama N, Suganuma Y, Kume T, Quan Z. Lithium intercalation reaction into the Keggin type polyoxomolybdates. *J Power Sources*. 2011;196(16):6822–7. doi:10.1016/j.jpowsour.2010.09.107

414 Chen J-J, Symes MD, Fan S-C, Zheng M-S, Miras HN, Dong Q-F, et al. High-performance polyoxometalate-based cathode materials for rechargeable lithium-ion batteries. *Adv Mater.* 2015;27(31):4649–54. doi:10.1002/adma.201501088

415 Ni E, Uematsu S, Quan Z, Sonoyama N. Improved electrochemical property of nanoparticle polyoxovanadate $K_7NiV_{13}O_{38}$ as cathode material for lithium battery. *J Nanopart Res.* 2013;15(6):1732. doi:10.1007/s11051-013-1732-0

416 Ma D, Liang L, Chen W, Liu H, Song Y-F. Covalently tethered polyoxometalate–pyrene hybrids for noncovalent sidewall functionalization of single-walled carbon nanotubes as high-performance anode material. *Adv Funct Mater.* 2013;23(48):6100–5. doi:10.1002/adfm.201301624

417 Wang S, Li H, Li S, Liu F, Wu D, Feng X, et al. Electrochemical-reduction-assisted assembly of a polyoxometalate/graphene nanocomposite and its enhanced lithium-storage performance. *Chem Eur J.* 2013;19(33):10895–902. doi:10.1002/chem.201300319

418 Xu C, Yang X, Hu C, Zhang J, Yang L, Yin S. One pot synthesis of polyoxometalates@polyaniline/MXene/CNTs quaternary composites with a 3D structure as efficient electrode materials. *Compos Commun.* 2024;34:101814. doi:10.1016/j.coco.2024.101814

419 Mahajan M, Sigla G, Ogale S. Polypyrrole-encapsulates polyoxomolybdate decorated MXene as a functional 2D/3D nanohybrid for a robust and high performance Li-ion battery. *ACS Appl Energy Mater.* 2021;4(5):4541–50. doi:10.1021/acsaem.1c00175

420 Liu Y, Zhou X, Qiu T, Yao R, Yu F, Song T, et al. Co-assembly of polyoxometalates and porphyrins as anode for high-performance lithium-ion batteries. *Adv Mater*. 2024;36(35):2407705. doi:10.1002/adma.202407705

421 Li Q, Xu M, Wang T, Wang H, Sun J, Sha J. Nanohybridization of CoS_2/MoS_2 heterostructure with polyoxometalate on functionalized reduced graphene oxide for high-performance LIBs. *Chem Eur J.* 2022;28(20):e202200207. doi:10.1002/chem.202200207

422 Li M-T, Zhou X-H, Liang Q-M, Chen J, Sun J-W, Yu Y, et al. POMs-based metal-organic frameworks with interpenetrating structures and their carbon nanotube-coated materials for lithium-ion anode applications. *J Solid State Chem.* 2024;337:124787. doi:10.1016/j.jssc.2024.124787

423 Sun S, Cui L, Yu K, Wang M, Lv J, Ge S, et al. 3D porous metal–organic skeleton based on polyoxometalate nanoclusters as an anode in a lithium-ion battery. *ACS Appl Nano Mater.* 2024;7(1):1310–8. doi:10.1021/acsanm.3c05315

424 Liu J-H, Yu M-Y, Pei W-Y, Wang T, Ma J-F. Self-assembly of polyoxometalate-resorcinarene-based inorganic-organic complexes: metal ion effects on the electrochemical performance of lithium ion batteries. *Chem Eur J.* 2021;27(39):10123–33. doi:10.1002/chem.202100780

425 Ullah I, Aldhafeeri TR, Haider A, Wu X, Ullah Z, Chang S, et al. Layered arrangement of polyoxometalate on a metal–organic framework as a high-capacity anode material for sodium-ion batteries. *ACS Appl Energy Mater.* 2025;8(3):1743–51. doi:10.1021/acsaem.4c02904

426 Liu J, Chen Z, Chen S, Zhang B, Wang J, Wang H, et al. "Electron/ion sponge"-like V-based polyoxometalate: toward high-performance cathode for rechargeable sodium ion batteries. *ACS Nano.* 2017;11(7):6911–20. doi:10.1021/acsnano.7b02062

427 Hartung S, Bucher N, Chen H-Y, Al-Oweini R, Sreejith S, Borah P, et al. Vanadium-based polyoxometalate as new material for sodium-ion battery anodes. *J Power Sources.* 2015;288:270–7. doi:10.1016/j.jpowsour.2015.04.009

428 Cao D, Sha Q, Wang J, Li J, Ren J, Shen T, et al. Advanced anode materials for sodium-ion batteries: confining polyoxometalates in flexible metal–organic frameworks by the "breathing effect". *ACS Appl Mater Interfaces.* 2022;14(19):22186–96. doi:10.1021/acsami.2c04077

429 Zhang LL, Zhao XS. Carbon-based materials as supercapacitor electrodes. *Chem Soc Rev.* 2009;38(9):2520–31. doi:10.1039/B813846J

430 Suppes GM, Deore BA, Freund MS. Porous conducting polymer/heteropolyoxometalate hybrid material for electrochemical supercapacitor applications. *Langmuir.* 2008;24(3):1064–9. doi:10.1021/la702837j

431 Vannathan AA, Maity S, Kella T, Shee D, Das PP, Mal SS. In situ vanadophosphomolybdate impregnated into conducting polypyrrole for supercapacitor. *Electrochim Acta.* 2020;364:137286. doi:10.1016/j.electacta.2020.137286

432 Cuentas-Gallegos AK, Martínez-Rosales R, Baibarac M, Gómez-Romero P, Rincón ME. Electrochemical supercapacitors based on novel hybrid materials made of carbon nanotubes and polyoxometalates. *Electrochem Commun.* 2007;9(8):2088–92. doi:10.1016/j.elecom.2007.06.003

433 Skunik M, Chojak M, Rutkowska IA, Kulesza PJ. Improved capacitance characteristics during electrochemical charging of carbon nanotubes modified with polyoxometallate monolayers. *Electrochim Acta.* 2008;53(11):3862–9. doi:10.1016/j.electacta.2007.11.049

434 Ruiz V, Suárez-Guevara J, Gomez-Romero P. Hybrid electrodes based on polyoxometalate–carbon materials for electrochemical supercapacitors. *Electrochem Commun.* 2012;24:35–8. doi:10.1016/j.elecom.2012.08.003

435 Suárez-Guevara J, Ruiz V, Gomez-Romero P. Hybrid energy storage: high voltage aqueous supercapacitors based on activated carbon–phosphotungstate hybrid materials. *J Mater Chem A.* 2014;2(4):1014–21. doi:10.1039/C3TA14455K

436 Mu A, Li J, Chen W, Sang X, Su Z, Wang E. The composite material based on Dawson-type polyoxometalate and activated carbon as the supercapacitor electrode. *Inorg Chem Commun.* 2015;55:149–52. doi:10.1016/j.inoche.2015.03.032

437 Genovese M, Lian K. Polyoxometalate modified pine cone biochar carbon for supercapacitor electrodes. *J Mater Chem A.* 2017;5(8):3939–47. doi:10.1039/C6TA10382K

438 Maity S, Vannathan AA, Kella T, Shee D, Das PP, Mal SS. Electrochemical performance of activated carbon-supported vanadomolybdates electrodes for energy conversion. *Ceram Int.* 2021;47(19):27132–41. doi:10.1016/j.ceramint.2021.06.128

439 Dubal DP, Nagar B, Suarez-Guevara J, Tonti D, Enciso E, Palomino P, et al. Ultrahigh energy density supercapacitors through a double hybrid strategy. *Mater Today Energy.* 2017;5:58–65. doi:10.1016/j.mtener.2017.05.001

DOI: 10.1039/D5EN00964B

440 Suárez-Guevara J, Ruiz V, Gómez-Romero P. Stable graphene–polyoxometalate nanomaterials for application in hybrid supercapacitors. *Phys Chem Chem Phys.* 2014;16(38):20411–4. doi:10.1039/C4CP03321C

441 Qin J, Zhou F, Xiao H, Ren R, Wu Z-S. Mesoporous polypyrrole-based graphene nanosheets anchoring redox polyoxometalate for all-solid-state micro-supercapacitors with enhanced volumetric capacitance. *Sci China Mater.* 2018;61(2):233–42. doi:10.1007/s40843-017-9132-8

442 Maity S, Das PP, Mal SS. Decavanadate-graphene oxide nanocomposite as an electrode material for electrochemical capacitor. *Mater Technol.* 2022;37:1129–39. doi:10.1080/10667857.2021.1924439

443 Maity S, Vannathan AA, Kumar K, Das PP, Mal SS. Enhanced power density of graphene oxide–phosphotetradecavanadate nanohybrid for supercapacitor electrode. *J Mater Eng Perform.* 2021;30:1371–7. doi:10.1007/s11665-020-05349-w

444 Kumari S, Maity S, Vannathan AA, Shee D, Das PP, Mal SS. Improved electrochemical performance of graphene oxide supported vanadomanganate (IV) nanohybrid electrode material for supercapacitors. *Ceram Int.* 2020;46:3028–35. doi:10.1016/j.ceramint.2019.10.002

445 Maity S, Vannathan AA, Chandewar PR, Shee D, Das PP, Mal SS. Vanadomanganate as a synergistic component in high-performance symmetric supercapacitor. *J Alloys Compd.* 2022;899:163239. doi:10.1016/j.jallcom.2021.163239

446 Maity S, JE M, Biradar BR, Chandewar PR, Shee D, Das PP, et al. Polyoxomolybdate–polypyrrole–graphene oxide nanohybrid electrode for high-power symmetric supercapacitors. *Energy Fuels.* 2021;35(22):18824–32. doi:10.1021/acs.energyfuels.1c03300

447 Zhang B-Y, Wu X-S, Wang N-H, Wang X-L, Han X-Q, Su Z-M. Polyoxometalates-based metal-organic frameworks with conjugated acid-base pairs for proton supercapacitors. *Chem Eng J.* 2024;500:157502. doi:10.1016/j.cej.2024.157502

448 Cui L, Wang M, Yu K, Lv J, Zheng X, Zhou B. The phosphomolybdate hybrids based on nanoscale heteropoly blue and metal-organic chain for supercapacitor and dual-functional electrochemical biosensor. *J Energy Storage.* 2023;60:106592. doi:10.1016/j.est.2022.106592

449 Li T, He P, Dong Y-N, Chen W, Wang T, Gong J, et al. Polyoxometalate-based metal-organic framework/polypyrrole composites toward enhanced supercapacitor performance. *Eur J Inorg Chem.* 2021;2021(21):2063–9. doi:10.1002/ejic.202100202

450 Pakulski D, Gorczyński A, Brykczyńska D, Montes-García V, Czepa W, et al. New Anderson-based polyoxometalate covalent organic frameworks as electrodes for energy storage boosted through keto-enol tautomerization. *Angew Chem Int Ed Engl.* 2023;62(32):e202305239. doi:10.1002/anie.202305239

451 Zhang L, Jiang H, Wang C, Yu K, Lv J, Wang C, et al. Improved supercapacitors and water splitting performances of Anderson-type manganese(III)-polyoxomolybdate through assembly with Zn-MOF in a host–guest structure. *J Colloid Interface Sci.* 2024;654:1393–404. doi:10.1016/j.jcis.2023.10.136

452 Chen H-Y, Wee G, Al-Oweini R, Friedl J, Tan KS, Wang Y, et al. Polyoxovanadate as an advanced electrode material for supercapacitors. *ChemPhysChem.* 2014;15(10):2162–9. doi:10.1002/cphc.201400091

453 Hu C, Zhao E, Nitta N, Magasinski A, Berdichevsky G, Yushin G. Aqueous solutions of acidic ionic liquids for enhanced stability of polyoxometalate-carbon supercapacitor electrodes. *J Power Sources.* 2016;326:569–74. doi:10.1016/j.jpowsour.2016.04.036

454 Dubal DP, Chodankar NR, Vinu A, Kim D-H, Gomez-Romero P. Asymmetric supercapacitors based on reduced graphene oxide with different polyoxometalates as positive and negative electrodes. *ChemSusChem.* 2017;10(13):2742–50. doi:10.1002/cssc.201700792

455 Maity S, Neethu B, Kella T, Shee D, Das PP, Mal SS. Activated carbon-supported vanado-nickelate (IV) based hybrid materials for energy application. *J Energy Storage.* 2021;40:102727. doi:10.1016/j.est.2021.102727

View Article Online
DOI: 10.1039/D5EN00964B

Data availability

Data sharing does not apply to this article as no datasets were generated or analyzed during the current study.